

Purification of phosphoric acid by melt crystallization

Dissertation

zur Erlangung des
Doktorgrades der Ingenieurwissenschaften (Dr.-Ing.)

des

Zentrums für Ingenieurwissenschaften

der Martin-Luther-Universität
Halle-Wittenberg,

Vorgelegt von

Mr. M.Sc. Haihao Tang
geb. am 14.04.1988 in Wenzhou, China

Gutacher: 1. Prof. Dr.-Ing. Dr. h. c. Joachim Ulrich
2. Prof. Dr. Marjatta Louhi-Kultanen

Tag der öffentlichen Verteidigung: 09.05.2016

Halle (Saale), den 19.05.2016

Acknowledgement

The start of my thesis was October 2012 at the Chair of Thermal Process Technology at Martin Luther University Halle-Wittenberg. The project was supported by Solvay Fluor GmbH.

I would like to thank Professor Joachim Ulrich for giving me the opportunity to work on this interesting topic. The discussions with him were open and I really enjoyed. He always encourages me to keep trying.

I would also like to thank Dr. Michael Sell and Dr. Plácido García-Juan for the support of the project. They help me to understand how engineers think and how work in industry. It will be very helpful to me when I will work in industry in future.

There are some more people in the company (Solvay Special Chem, BU Electronics) who attended meetings and helped me to finish the whole project, especially Mr. Jorg Dietzel, Dr. Matthias Dabrunz, Dr. Jean-Marie Collard, Mrs. Christina Dengler, Mrs. Josephine Rost, Mrs. Marie Schäfer and Mrs. Joana Kopf.

Further thanks go to Prof. Dr. Marjatta Louhi-Kultanen who is my second assessor.

Thanks also to my student Ahmed Al Maimani who did a very good lab work for me.

I would also like to thank Mr. Gerhard Schütze who helped me to solve mechanical problems. Thanks to Mrs. Claudia Kirchner who is our secretary helped me all the time.

Thanks is of course to all my colleagues Dr. Patrick Frohberg, Dr. Thi Nhat Phuong Nguyen, Felix Eisenbart, Ronny Oswald, Martha Wellner, Muhammad Ahmad, Anne Hartwig, Julia Herfurth, Julia Seidel, Hamid Altaher, Dr. Kristin Wendt, Xiaoxi Yu, Miaomiao Jin and Jiting Huang who gave me helps.

Last but not least, I want to thank my parents who support me all the time for the study abroad.

Thank all of you.

Haihao Tang

Table of Contents

Acknowledgement.....	1
Table of Contents	3
1. Introduction	6
2. Background and Objectives.....	7
2.1 Production of phosphoric acid	7
2.1.1 The dry process	7
2.1.2 The wet process.....	7
2.2 The methods of purification.....	8
2.2.1 Solvent extraction	8
2.2.2 Ion exchange	8
2.2.3 Electroosmosis	9
2.2.4 Crystallization.....	9
2.3 Electronic grade chemicals.....	9
2.3.1 Definitions	9
2.3.2 Standards	10
2.3.3 Markets of phosphoric acid (electronic grade).....	12
2.4 Wash columns	12
2.4.1 Gravity wash column.....	13
2.4.2 Mechanical wash column	13
2.4.3 Hydraulic wash column	14
2.5 Objectives of study	14
3. Theories and Principles	16
3.1 Crystallization	16
3.1.1 $\text{H}_3\text{PO}_4 - \text{H}_2\text{O}$ phase diagram	18
3.1.2 Metastable zone width of $\text{H}_3\text{PO}_4 - \text{H}_2\text{O}$ system.....	19
3.2 Vapor pressure measurement.....	19
3.3 Crystal growth	20
3.3.1 Phosphoric acid hemihydrate crystals	20
3.3.2 Mechanism of crystal growth	21
3.4 Permeability of a crystal bed	21
3.4.1 Porosity of a crystal bed.....	21

3.4.2 Permeability of a crystal bed.....	22
3.4.3 Compressibility of a crystal bed.....	23
3.5 Analysis.....	24
3.5.1 Density measurement.....	24
3.5.2 In-line measurement techniques.....	25
3.5.3 UV-Vis spectrophotometry.....	26
3.5.4 ICP-OES.....	26
4. Materials and Methods.....	28
4.1 The solubility of phosphoric acid in water.....	28
4.2 The vapor pressure of phosphoric acid and water.....	29
4.3 The measurements of crystal growth.....	31
4.3.1 Off-line measurements.....	31
4.3.2 In-line measurements.....	32
4.4 The distribution coefficient of crystallization and post treatments.....	33
4.4.1 Crystallization.....	33
4.4.2 Post treatments.....	34
4.5 The permeability measurements of the crystal bed.....	34
5. Results.....	36
5.1 The solubility of phosphoric acid in water.....	36
5.1.1 Without additives.....	37
5.1.2 With additives.....	39
5.2 The vapor pressure of phosphoric acid and water.....	39
5.3 The measurements of crystal growth.....	41
5.3.1 Off-line measurements.....	41
5.3.2 In-line measurements.....	49
5.4 The distribution coefficient of crystallization and post treatments.....	54
5.4.1 The distribution coefficient of crystallization.....	54
5.4.2 The distribution coefficient of post treatments.....	57
5.4.3 The effects of chelating agents.....	60
5.5 The permeability measurements of the crystal bed.....	63
5.5.1 The porosity of the crystal bed.....	63
5.5.2 The permeability and the compressibility of the crystal bed.....	64

5.6 The mass balance of the pilot plant	66
5.6.1 The calculations of the mass balance of the pilot plant	67
5.6.2 Examples of the pilot plant calculations	71
5.6.3 The optimization of calculations	74
6. Discussion	76
6.1 The solubility of phosphoric acid in water	76
6.2 The vapor pressure of phosphoric acid and water	78
6.3 The measurement of crystal growth rates	79
6.3.1 Off-line measurements	79
6.3.2 In-line measurements	82
6.4 The distribution coefficient of crystallization and post treatments	84
6.4.1 The distribution coefficient of crystallization and post treatments	84
6.4.2 The effects of chelating agents	87
6.5 The permeability measurements of the crystal bed	88
6.6 The optimization of the purification of phosphoric acid	89
6.7 The mass balance of the pilot plant	91
6.8 Outlook	92
7. Summary	93
8. Zusammenfassung	95
9. List of Symbols and Abbreviations	97
10. References	100
Statement of Authorship	109
Curriculum Vitae	111
Publications	113

1. Introduction

Phosphoric acid is an inorganic acid. It is widely used in chemical, food, fertilizer and electronic industries according to its purity (industrial grade, food grade, technical grade and electronic grade). It can be produced by two different processes, the dry process and the wet process [Wah80]. Due to the high energy consumption of the dry process, the wet process is the most often used process to produce phosphoric acid from phosphate ore. However, many impurities such as iron, aluminum, magnesium, fluorine and sulfate remain as impurities in the found products. Electronic grade phosphoric acid can be used to etch circuits and displays in electronic industry. Any impurities may change the properties or destroy the devices. Therefore, an efficient technique of purification is needed. There are several methods to purify and to get a pure phosphoric acid such as solvent extraction [Ahm07], ion exchange [Ell06], electroosmosis [Koo99] and crystallization [Ris25]. Crystallization, as a highly efficient, low cost and environmental friendly method, is therefore considered here as a potential purification step.

Much research has been carried out in the field of the phosphoric acid concerning physical properties of phosphoric acid [Dav69, Jia11], the phase diagram with water [Smi09, Jia12b], the metastable zone width of phosphoric acid with different impurities [Kim06, Ma09a, San10], the growth of the phosphoric acid hemihydrate crystals in a suspension crystallization using FBRM for measurements [Ma09b, Ma10b], suspension melt crystallization of phosphoric acid [Wan12] and modeling of layer melt crystallization [Jia12a].

A typical crystallization process can enrich the purities in the crystals [Pos96] and, furthermore, an efficient post crystallization treatment [Ulr02] such as washing or sweating is needed to further separate the crystalline products from the residual melt which is enriched with the impurities. A wash column, as an established post treatment technique, combines the washing step and the solid-liquid separation. It can give a relatively high throughput with a simple design. According to its driving force, there are three main kinds of wash columns: Gravity wash column, mechanical wash column and hydraulic wash column [Jan94]. The properties of a crystal bed, such as porosity and permeability, are the key parameters for the application of a wash column. These parameters combined with a purity analysis can be used and be optimized in lab scale experiments so that the results can be used to help to optimize processes in industry (decreasing costs).

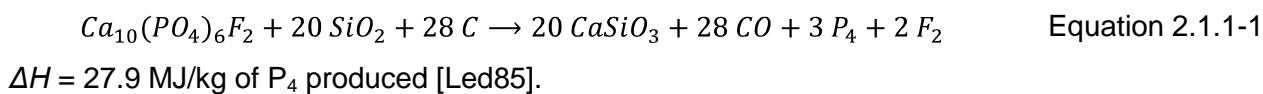
2. Background and Objectives

2.1 Production of phosphoric acid

Phosphoric acid can be produced from phosphate ore via two major process routes: The so-called dry process and the wet process [Wah80]. In the dry process the phosphate ore is reduced to phosphorus and further is burned to phosphorus pentoxide in an electric furnace or in a rotary kiln. Phosphorus pentoxide is absorbed in water and therefore phosphoric acid can be obtained. In the wet process strong mineral acids are used for digestion of the ore. After the digestion phosphoric acid is obtained and purified by other techniques such as electroosmosis and ion exchange.

2.1.1 The dry process

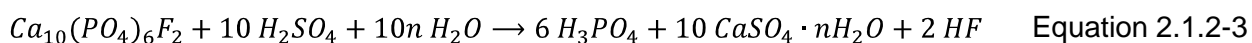
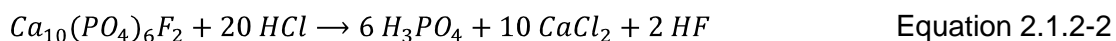
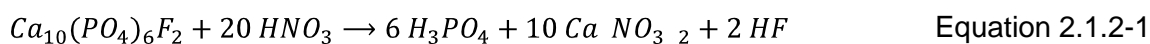
In an electric furnace or a rotary kiln the phosphate ore is burned by addition of silica and carbon at about 1500 °C (see Equation 2.1.1-1).



The obtained phosphorus is further burned to phosphorus pentoxide and absorbed in water or in moderately concentrated phosphoric acid to obtain high concentrated phosphoric acid (> 60 wt% P_2O_5). In this process most impurities from the ore remain in the slag [Wah80]. Therefore the product is clean and highly concentrated. However, due to the high energy consumption ($\Delta H = 27.9 \text{ MJ/kg of } P_4 \text{ produced [Led85]}$) this process is still too expensive to use in the fertilizer industry where costs are the major issue. It can only be used in applications where the product from the wet process is not sufficient pure [Slu87].

2.1.2 The wet process

In the wet process the phosphoric acid can be released from phosphate ore by strong mineral acids, such as nitric acid, hydrochloric acid and sulfuric acid [Slu87] (see Equations 2.1.2-1, 2.1.2-2 and 2.1.2-3).



Sulfuric acid is the only acid which forms an insoluble precipitate ($\text{CaSO}_4 \cdot n\text{H}_2\text{O}$), therefore phosphoric acid can be separated directly by filtration. To the other two acids phosphoric acid needs to be recovered by some special techniques such as solvent extraction [Pho83], ion exchange [Slu87] or cooling crystallization [Ano85, Slu87]. Compared to the dry process the wet process is of low energy consumption and environmental friendly. Although phosphoric acid which is produced in the wet process contains more impurities (compared to the dry process), it can be purified by some techniques (solvent extraction [Ahm07], ion exchange [Eil06], electroosmosis [Koo99] and crystallization [Ros25]) which are similar as the ones in the recovery of phosphoric acid.

2.2 The methods of purification

The main impurities in phosphoric acid which is produced by the wet process are insoluble components and ions (K^+ , Na^+ , Ca^{2+} , Mg^{2+} , Fe^{2+} , Pb^{2+} , Fe^{3+} , Al^{3+} , As^{3+} , Cl^- , SO_4^{2-} , F^-) [Ma10a]. The insoluble components can be separated by filtration or adsorption. The soluble ions can be removed by several different techniques, such as solvent extraction [Ahm07], ion exchange [Eil06], electroosmosis [Koo99] and crystallization [Ros25].

2.2.1 Solvent extraction

Since phosphoric acid is miscible with some organic solvents (isopropanol, tributyl phosphate, butanol and methanol) [Ahm07, Ma10a]. The impurity ions, especially, the cations, can be separated by extraction. However, some anions such as SO_4^{2-} , F^- and SiF_2^- are difficult to be removed. Low energy cost, environmental friendly and high capacity are the advantages of this method.

2.2.2 Ion exchange

Some acidic ion exchange resins can be used for cations exchange during the purification of phosphoric acid [Eil06]. However, to remove different kinds of cations different kinds of resins need to be chosen and the concentration of phosphoric acid should be low enough. Moreover, the resins need to be recycled from the purification process. It takes time and needs some extra devices. Hence, this technique needs to be combined with other techniques to purify phosphoric acid [Ma10a].

2.2.3 Electroosmosis

Koopman [Koo99] studied the purification of phosphoric acid by electroosmosis. It shows that the adsorption speed of phosphate on the anion exchange membrane is much higher than the other anions. Based on this mechanism phosphoric acid can be purified by electroosmosis with different ion exchange membranes. For example, SO_4^{2-} , Fe^{2+} , As^{3+} and Al^{3+} can be removed up to 52.21 %, 96.4 %, 97.95 % and 97.38 %, respectively.

2.2.4 Crystallization

Phosphoric acid hemihydrate crystals can be crystallized from the melt [Ros25]. Most of the impurities can be enriched in the mother liquor. Therefore, after separation a high purity can be reached (up to an electronic grade). If the melt contains high amounts of impurities, recrystallization may be further needed. Some above mentioned techniques can also be used as pretreatments to lower down the impurity content. Compared to the other techniques the crystallization technique is low cost, energy saving and environmental friendly. Therefore, it is not only an ideal technique to purify phosphoric acid, but also to other chemicals.

2.3 Electronic grade chemicals

2.3.1 Definitions

The electronic grade chemicals are used in electronic industry, particularly in semiconductor or microprocessor fabrication. They are:

- Photo resists (resins)
- Etchants (solvents, acids, bases and other chemicals)
- Cleaners (solvents)
- Dopants (high purity metals / non-metals)
- Metallic conductors (Aluminum / copper / silver / gold)
- High purity gases

The main criteria for all these products are the degree of purity. Since most of the products are used for cleaning or etching circuits and semiconductors, any impurities may change the properties of electronic devices. An extremely high purity (ppm or ppb) of product is required.

2.3.2 Standards

Different electronic grade chemicals have different standards. Tables 2.3.2-1 and 2.3.2-2 show

Table 2.3.2-1: Electronic grade standard of hydrogen peroxide [Sol01].

Parameter	unit	Grade 1	Grade 2	Grade 3	Grade 4
		EG-ST*	EG-10	EG-1	Pico
Assay	wt%	30 – 60	30 – 32	30 – 32	30 – 32
Free acid	ppm	0.6 – 40	-	-	-
Stability	g/kg h	-	4	4	4
TOC**	ppm	3 – 30	10	10	10
Cl ⁻	ppb	200 – 1000	200	200	30
NO ₃ ⁻		500 – 3000	400	400	30
SO ₄ ²⁻		200 – 1000	200	200	30
PO ₄ ³⁻		200 – 5000	200	200	30
Al	ppb	10 – 100	10	1	0.1
Sb		10 – 100	10	1	0.1
As		10 – 100	10	1	0.1
Ba		-	10	1	0.1
B		10 – 100	10	1	0.1
Cd		-	10	1	0.1
Ca		10 – 100	10	1	0.1
Cr		10 – 100	10	1	0.1
Cu		10 – 100	10	1	0.1
Fe		10 – 100	10	1	0.1
Pb		10 – 100	10	1	0.1
Li		-	10	1	0.1
Mg		10 – 100	10	1	0.1
Mn		10 – 100	10	1	0.1
Ni		10 – 100	10	1	0.1
K		10 – 100	10	1	0.1
Na		100 – 2000	10	1	0.1
Sn		10 – 100	10	1	0.1
Ti		10 – 100	10	1	0.1
V		-	10	1	0.1
Zn		10 – 100	10	1	0.1

*EG-ST range includes stabilized as well as non-stabilized grades.

**TOC means Total Organic Carbon.

Table 2.3.2-2: Electronic grade standard of phosphoric acid [Sol01].

Parameter	unit	Grade 1	Grade 2	Grade 3
Assay	wt%	74 – 76	79 – 81	79 – 81
		79 – 81	84 – 86	84 – 86
Cl ⁻	ppm	1	1	1
F ⁻		1	1	1
NO ₃ ⁻		5	5	5
SO ₄ ²⁻		12	12	12
Al	ppb	1000	500	50
Sb		10000	3500	1000
As		300	100	50
Ba		-	-	50
B		-	-	50
Cd		-	450	50
Ca		1500	1100	150
Cr		200	200	50
Co		-	50	50
Cu		50	50	50
Fe		2000	700	100
Pb		300	300	50
Li		100	100	50
Mg		200	200	50
Mn		100	100	50
Ni		500	200	50
K		1500	450	150
Na		2500	500	250
Sn		-	-	100
Ti		300	300	50
V		-	-	100
Zn		2000	400	50

the standards of hydrogen peroxide and phosphoric acid which are widely used as etchants in electronic industry [Sol01].

2.3.3 Markets of phosphoric acid (electronic grade)

Phosphoric acid is highly selective in etching Si_3N_4 instead of SiO_2 . In combination with hydrogen peroxide and water, it is used to etch aluminum and InGaAs selective to InP [Sol02]. Besides cleaning and etching electronic grade phosphoric acid can also be used for the production of high purity phosphates [Ouy09]. In the last few years the regional market for phosphoric acid and its phosphate derivatives is mainly dominated by the Asia Pacific region (especially China and India) and this trend is expected to continue in the next years. The markets in the regions such as the Middle East, Africa and Latin America are growing at an astounding rate. Moreover, the North American and European markets are also predicted to generate strong demand for phosphoric acid as these markets are gradually recovering from the economy crisis. In future the global phosphoric acid market is expected to maintain an excellent growth rate [Pho12].

2.4 Wash columns

After a crystallization process the crystals need to be separated from the mixture (solid-liquid separation). It can be achieved by filtration and centrifugation. A different equipment is the so-called wash column which is used for the solid-liquid separation of crystals from their mother liquor. Besides separation it offers functions such as washing, sweating and recrystallization so

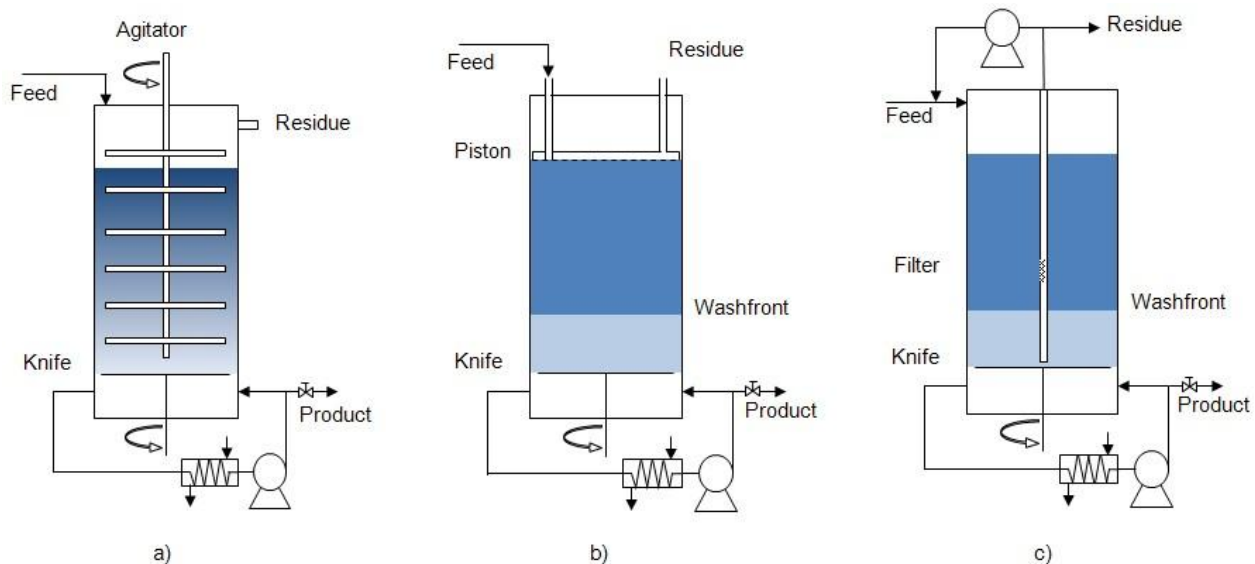


Figure 2.4-1: Wash columns: a) gravity wash column, b) mechanical wash column and c) hydraulic wash column.

Table 2.4-1: Features of forced transport and gravity transport wash columns [Oor00].

	Gravity transport	Forced transport
Capacity [$\text{kg}/\text{m}^2 \text{ h}$]	1000-1500	5000-10000
Residence time of crystals	hours	10 min.
Compressive stress [bar]	negligible	0.5-10
Required crystal size [μm]	>500	100-200
Loss of wash liquid	considerable	negligible
Maximum ΔT [K]	<15	15-20

that a high purity of crystals can be harvested by using small amounts of wash liquid. There are three types of wash columns according to the transportation force of a crystal bed (see Figure 2.4-1): Gravity wash column, mechanical wash column and hydraulic wash column [Jan94]. Table 2.4-1 summarizes the features of three wash columns.

2.4.1 Gravity wash column

In the gravity wash column a crystal bed is transported by gravity. The slurry is fed at the top of the wash column. The crystals settle down into a loosely packed downward moving bed by gravity. The mother liquor leaves the column via an overflow. The packed crystal bed moves down and is molten in a melter. A part of molten product is withdrawn from the bottom and the other part goes back as a reflux to produce a countercurrent washing action. An agitator covers the whole column and slowly stirs the crystal bed to prevent agglomeration. Therefore, there is no washfront comparing the other two types of wash columns. The capacity of gravity wash columns depends on the physical properties of solid and liquid phase, the crystal size distribution and the wall friction, but it does not exceed $1500 \text{ kg}/\text{m}^2 \text{ h}$ for organic compounds [Tak83, Tak84, Jan94].

2.4.2 Mechanical wash column

In the mechanical wash column a dense crystal bed is transported by mechanical force created by a moving piston (see e.g. Sulzer Chemtech Ltd. [Sul01] and GEA Messo PT [Gea01]) or a screw. The slurry is fed at the top of the wash column and is pressed by a piston. The crystals are compressed into a densely packed crystal bed and the mother liquor leaves out through the pores in the piston. At the bottom of the column the crystals are scraped off, suspended in the wash liquid and molten in a melter. Similar to the gravity wash column some part of molten product is withdrawn from the bottom and the other part goes back as a reflux to produce a

countercurrent washing action. The reflux meets the cold crystal bed and recrystallizes. Hence it results in a sharp washfront. The washfront marks a steep temperature gradient and a sharp decrease in the porosity and permeability of the bed. The permeability decreases underneath the washfront improves the washing efficiency and is essential for a stable washing action [Vor72]. The maximum temperature difference which can be overcome between the slurry feed and the molten product is 10-15 K [Jan94]. A larger temperature difference will make the permeability underneath the washfront extremely low and the production capacity will be reduced. The washing action may be hampered. The capacity of mechanical wash column is limited to 10000 kg/m² h [Jan91, Jan94].

2.4.3 Hydraulic wash column

In the hydraulic wash column a dense crystal bed is transported by means of hydraulic force (see e.g. TNO-Thijssen [Tno01]). The mechanism is similarly to the one in the mechanical wash column. However, the mother liquor leaves the wash column via filters which are positioned either in separate filter tubes [Thi83, Thi85, Ark84] or in the wall of the column [Bre80]. The maximum production capacity of hydraulic wash columns will probably be 5000-10000 kg/m² h [Jan94].

2.5 Objectives of study

The aim of the study is to provide all knowledge and data required to design and/or optimize a melt crystallization process to purify phosphoric acid. In order to study the purification process of phosphoric acid via melt crystallization in industry the necessary fundamental background should be prepared in the following chapters. They are:

- Solubility study of phosphoric acid in different pure grade and with different impurity or additives (phase diagrams).
- Vapor pressure measurement of phosphoric acid-water melt at 50, 60 and 70 °C.
- Kinetic study of phosphoric acid hemihydrate crystals of different purity grades and with different impurities or additives. Off-line and in-line techniques should be tested for monitoring the growth rate of the crystals.
- Separation efficiency study of iron via a crystallization process and post treatments. Some chelating agents are extra used for the study of separation efficiency of iron.
- Porosity, permeability and compressibility studies of a crystal bed during filtration.

- Mass balance calculation of a pilot plant based on the data from the lab scale.

All the studies here are based on a lab scale, to clear the mechanisms of the crystallization process and to find an optimized condition for the application of a pilot plant in industry.

3. Theories and Principles

3.1 Crystallization

Crystallization is the process of formation of solid crystals from a liquid (solution crystallization and melt crystallization) or more rarely deposited directly from a gas [Mul97]. The driving force of the process is supersaturation which can be produced by a change of temperature, pressure or composition. Here, in case of a two-component mixture (A and B) the supersaturation of A in B is defined as in Equation 3.1-1.

$$\Delta s = x_A - x_{A,eq} \quad \text{Equation 3.1-1}$$

Where, x_A is the concentration of A in B, [wt%] and $x_{A,eq}$ is the solubility of A in B at the same temperature, [wt%]. The subscript *eq* denotes the equilibrium concentration of A in B, which means the solubility.

In the melt crystallization the supersaturation can be obtained by cooling. Changing the pressure may also change the solubility of the component. However, it is rarely used [Mor97, Toy94, Nag89] and therefore it is not discussed here. The relationship between the composition and the temperature is described in a phase diagram. It also gives limits to temperature and purity during the crystallization process. Figure 3.1-1 shows different types of melt crystallization phase diagrams of organic mixtures [Mat86].

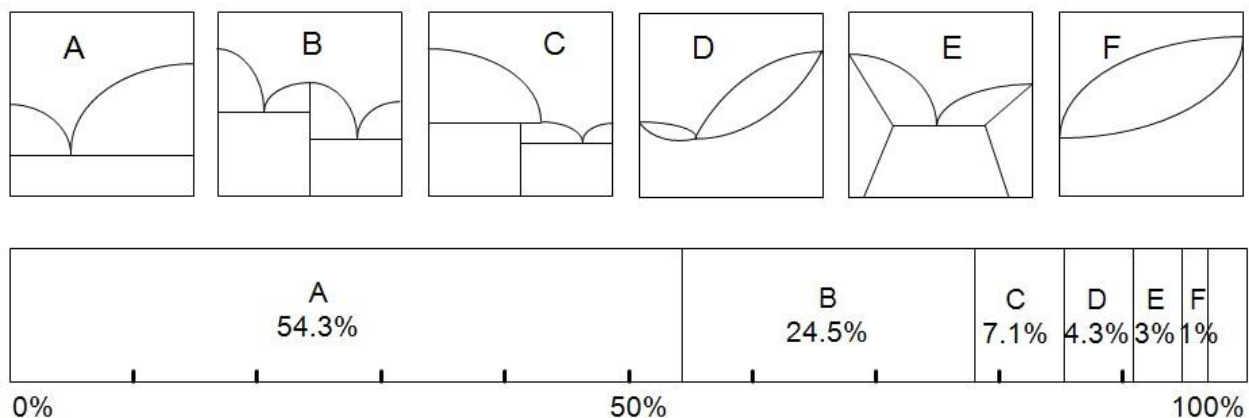


Figure 3.1-1: Different types of melt crystallization phase diagrams [Mat86].

Phase diagrams type A to C are the most common phase diagrams (more than 50%). It has a eutectic point. At this point the mixture crystallizes as a solid from the binary system and the ratio of the two components is a constant. Figure 3.1-2 shows the details of a eutectic binary system with components A and B. In case the component A needs to be crystallized from the

mixture starting from composition x_0 and temperature T_0 . When the temperature is cooled down to T_1 the melt comes to its melting point. From the thermodynamic point of view, when the temperature is cooled down to T_2 the component A crystallizes from the melt and the equilibrium concentration of the component A is x_2 . The solid content x_{solid} (or the yield of solid) can be calculated according to this phase diagram and it is shown in Equation 3.1-2. If the initial concentration x_0 is less than x_E it is impossible to get pure A by cooling. In this case the component B instead of the component A will crystallize from the melt. If the initial concentration x_0 is equal to x_E both A and B will crystallize from the melt and the solid composition is equal to x_E which means no separation.

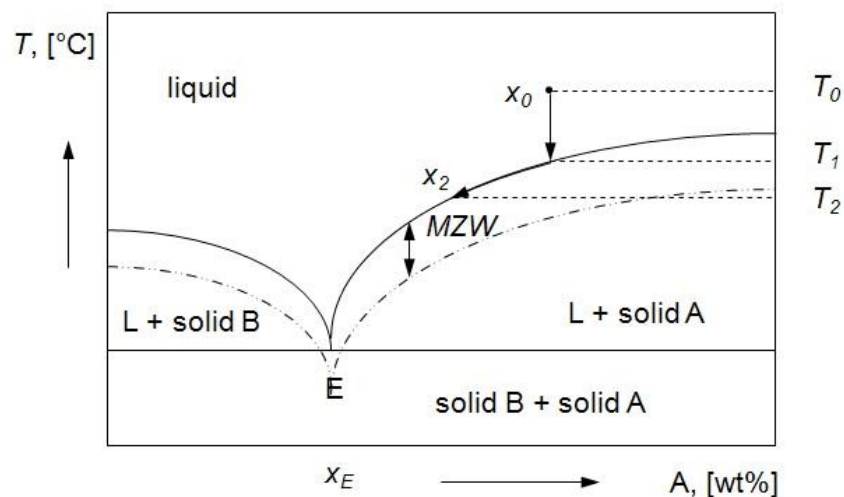


Figure 3.1-2: Principle of a eutectic binary system phase diagram.

$$x_{solid} = \frac{x_0 - x_2}{1 - x_2} \quad \text{Equation 3.1-2}$$

The other phase diagrams (type B and C) can be separated into several phase diagrams which are similar as type A. Phase diagrams type D and F do not have a eutectic point. In principle pure component can be obtained by cooling, however, it takes more steps of the crystallization process to reach a high purity, but it has the potential of a yield up to 100 %, in contrary to the eutectic systems where the eutectic point is the limit for the yield.

When a crystallization process starts it contains two steps: nucleation and crystal growth. There are two types of nucleation: primary nucleation and secondary nucleation [Mul97]. The primary nucleation occurs at a temperature which is lower than the saturation temperature (see Figure 3.1-2). The difference between these two temperatures is called metastable zone width (MZW) of primary nucleation. There are other limits of the MZW which are smaller, due to e.g. the presents of crystals or seed. The MZW is not a constant to a system. It is a kinetic property and

it highly depends on the parameters such as cooling rate, impurities concentrations or presence of crystals with respect to the nucleation line. The other limits of the MZW are fixed by the thermodynamics. When the first nucleus comes the nucleation rate becomes explosive and the nuclei start to grow. The melt starts to desupersaturate. If the temperature of the crystallization process is controlled within the range of the MZW (between the nucleation temperature and the saturation temperature) in the presence of seeds there will be no primary nucleation any more. However, nuclei or seeds can grow under these conditions. Therefore, it is widely used in industry that some seeds crystals are introduced before crystal growth process is started so that due to a low number of crystals bigger crystals can be harvested at the end of the process.

3.1.1 $\text{H}_3\text{PO}_4 - \text{H}_2\text{O}$ phase diagram

Figure 3.1.1-1 shows the phase diagram of H_3PO_4 and H_2O [Jia12b].

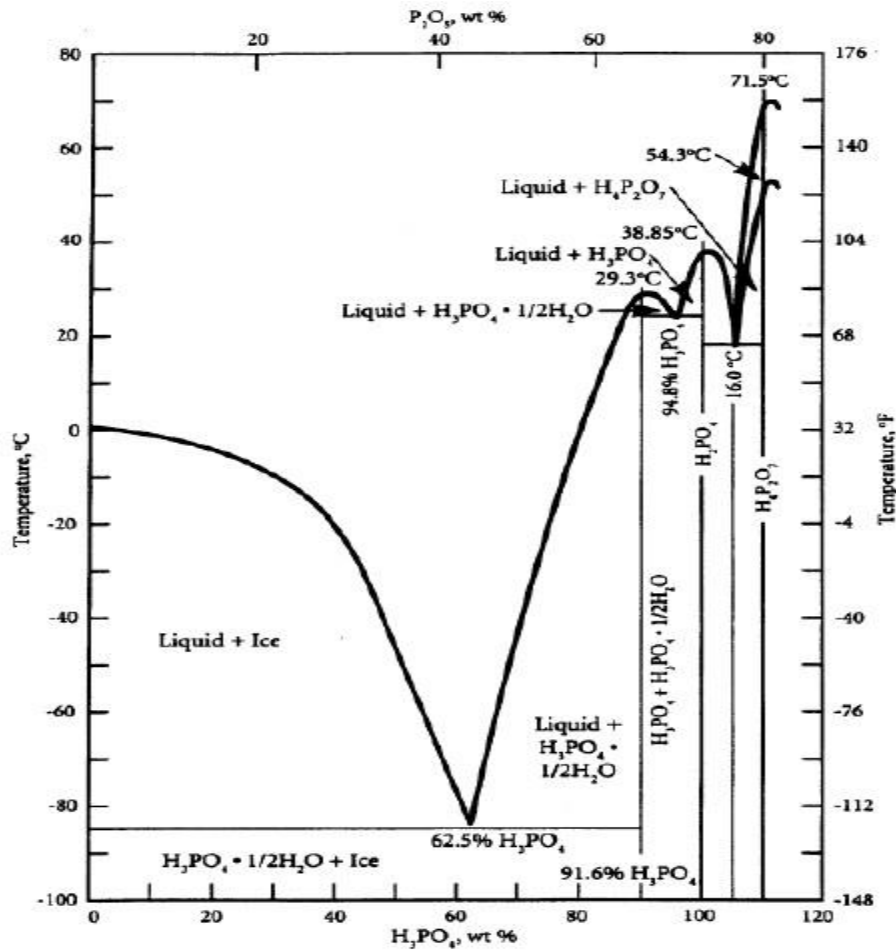


Figure 3.1.1-1: Phase diagram of H_3PO_4 and H_2O [Jia12].

In industry 85 wt% $\text{H}_3\text{PO}_4 - \text{H}_2\text{O}$ melt is widely used for different applications [Sch08]. According to the phase diagram, if 85 wt% of melt is used as a feed of the crystallization process phosphoric acid hemihydrate crystals ($\text{H}_3\text{PO}_4 \cdot 0.5\text{H}_2\text{O}$, 91.6 wt%) can be obtained. A concentration which is higher than 91.6 wt% cannot directly be produced. In this case other techniques, for example evaporation, can be applied.

3.1.2 Metastable zone width of $\text{H}_3\text{PO}_4 - \text{H}_2\text{O}$ system

The $\text{H}_3\text{PO}_4 - \text{H}_2\text{O}$ system has a large MZW (>50 K) [Kim06] (see Figure 3.1.2-1). It is difficult to get $\text{H}_3\text{PO}_4 \cdot 0.5\text{H}_2\text{O}$ crystals without seeding. However, after seeding the MZW decreases to approx. 1-5 K. Hence, giving seeds at a highly supersaturated melt can induce explosive nucleation. Dang *et al.* [Dan07], Ma *et al.* [Ma09b] and Sangwal [San10] also studied the MZW of the $\text{H}_3\text{PO}_4 - \text{H}_2\text{O}$ system with seeding and showed how several impurities, such as Fe^{3+} , Fe^{2+} , Al^{3+} , F^- and SO_4^{2-} , influence the MZW.

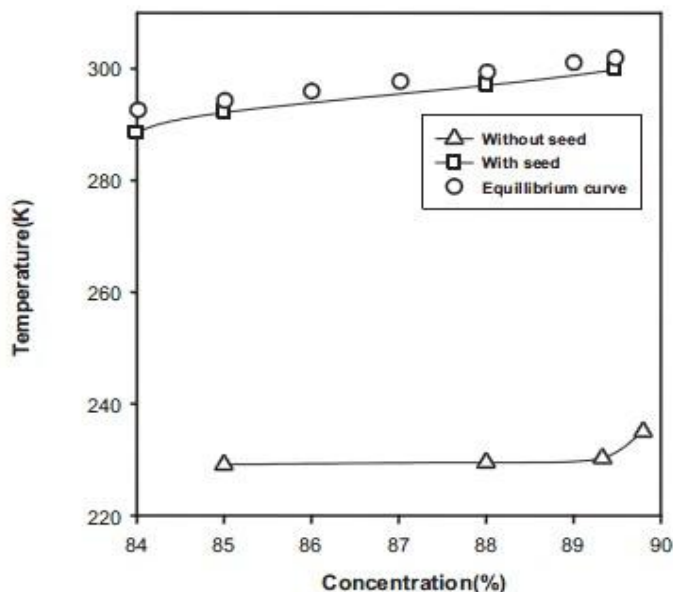


Figure 3.1.2-1: Equilibrium and nucleation curves of $\text{H}_3\text{PO}_4 - \text{H}_2\text{O}$ system without and with seeds [Kim06].

3.2 Vapor pressure measurement

Vapor pressure is defined as the pressure exerted by a vapor in thermodynamic equilibrium with its condensed phases (solid or liquid) at a given temperature in a closed system. To a liquid its vapor pressure can be obtained near the boiling point. During the measurement the substance should completely be in a close system. Therefore, the tube which is shown in Figure 3.2-1 is

used. The liquid at position B and C separates the liquid at position A and the ambient. A vacuum pump gives different pressures so that the liquid at position A can be boiled by changing temperatures. The Clausius-Clapeyron equation [Ken66] (Equation 3.2-1) describes the relationship between the vapor pressure and the temperature. It gives a method that the vapor pressure at a specific temperature can be predicted by measuring the vapor pressures at other temperatures. The details of the vapor pressure measurement are discussed in the Chapter 4.2.

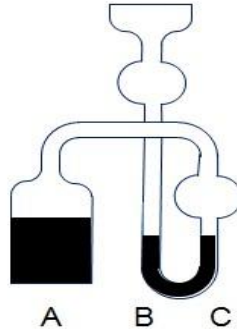


Figure 3.2-1: The tube for the vapor pressure measurements.

$$\ln p = -\frac{\Delta_{vap}H_m}{R} \cdot \frac{1}{T} + C \quad \text{Equation 3.2-1}$$

Where,

p is vapor pressure of the substance, [Pa]

$\Delta_{vap}H_m$ is vaporization enthalpy of the sample, [J/mol]

R is the ideal gas constant, 8.314 [J/(mol•K)]

T is temperature, [K]

C is a constant, [-]

3.3 Crystal growth

3.3.1 Phosphoric acid hemihydrate crystals

The phosphoric acid hemihydrate crystal ($\text{H}_3\text{PO}_4 \cdot 0.5\text{H}_2\text{O}$) is monoclinic ($a = 7.922 \text{ \AA}$, $b = 12.987 \text{ \AA}$, $c = 7.47 \text{ \AA}$, $\alpha = 90^\circ$, $\beta = 109.9^\circ$, $\gamma = 90^\circ$) [Mig69]. The crystal structure and its Miller indices are shown in Figure 3.3.1-1 [Dan10]. The crystal is colorless and highly hygroscopic. The melting point is $29.3 \text{ }^\circ\text{C}$ and the solid density is 1.967 g/cm^3 .

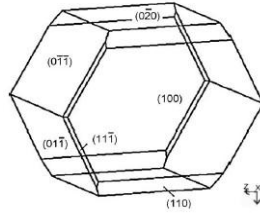


Figure 3.3.1-1: The crystal structure of phosphoric acid hemihydrate [Dan10].

3.3.2 Mechanism of crystal growth

When a supersaturated melt is desupersaturating the crystals start to grow. The growth rate of a specific face or a specific growth direction describes the rate of the growth. To control the growth of crystals the mechanism of the growth needs to be clear. According to McCabe's law, the dependence of the growth rate on the supersaturation in a batch crystallization process is shown as Equation 3.3.2-1.

$$G = k\Delta s^m \quad \text{Equation 3.3.2-1}$$

Where, k is the growth rate constant, [m/s], m is the order of crystal growth, [-], and Δs is the supersaturation of melt, [wt%] [Ngu08]. The exponent m identifies the mechanism of crystal growth. When $m = 1$ the one-dimension crystal growth will be controlled by the diffusion following the gradient concentration. When $m = 2$ the two-dimension crystal growth is controlled by the surface integration from spreading the surface such as spiral growth, volume diffusion-controlled growth and 2D nucleation-mediated growth mechanism. When $m = 3$ the 3D crystal growth is controlled by the poly nuclei growth and the growth takes place by the integration of the nuclei or small particles due to the interaction and attrition [Ngu08, Mul97]. In general the order of crystal growth m is not an integer. Therefore the crystal growth is controlled by both mechanisms. For example, if $m = 1.5$ the crystal growth is controlled by both the diffusion and the surface integration.

3.4 Permeability of a crystal bed

3.4.1 Porosity of a crystal bed

The porosity of a crystal bed is defined as the ratio of the volume of voids to the volume of the crystal bed (see Equation 3.4.1-1).

$$\varepsilon = \frac{\text{volume of voids}}{\text{volume of crystal bed}} = 1 - \frac{\text{volume of crystals}}{\text{volume of crystal bed}} \quad \text{Equation 3.4.1-1}$$

If the density and the mass of the solids or the crystals are known the porosity of the crystal bed ε can easily be calculated.

3.4.2 Permeability of a crystal bed

The permeability, B [m^2], which describes the resistance to flow of a packed bed is defined by Darcy's law:

$$\frac{dp}{dh} = \frac{v\eta}{B} \quad \text{Equation 3.4.2-1}$$

Where, p is the liquid pressure, [Pa]. h is the medium height, [m]. v is the superficial liquid velocity, [m/s]. η is the filtrate viscosity, [Pa*s]. B is the permeability of crystal bed, [m^2].

According to the filtration rate definition:

$$v = \frac{dV}{Adt} = \frac{\Delta p}{\eta(R_c + R_m)} \quad \text{Equation 3.4.2-2}$$

V is the filtrate volume, [m^3], A is the filtration area, [m^2], t is the filtration time, [s], R_c is the resistance of filter cake, [1/m] and, R_m is the resistance of filter medium, [1/m].

$$R_c = \frac{h_c}{B_c}, R_m = \frac{h_m}{B_m} = \frac{h_e}{B_c} \quad \text{Equation 3.4.2-3}$$

B_c is the permeability of filter cake, [m^2] and B_m is the permeability of filter medium, [m^2]. h_c is a filter cake height, [m], h_m is a filter medium height, [m] and h_e is an equivalent filter cake height, [m].

Equation 3.4.2-2 can be rewritten as:

$$\frac{dV}{Adt} = \frac{\Delta p}{\frac{\eta}{B_c}(h_c + h_e)} \quad \text{Equation 3.4.2-4}$$

The filtrate volume V and the height of filter cake h_c can be calculated according to Equations 3.4.2-5 and 3.4.2-6.

$$V = hA(1 - v - v\varepsilon) \quad \text{Equation 3.4.2-5}$$

$$h_c = \frac{v}{1 - \varepsilon} h \quad \text{Equation 3.4.2-6}$$

Where, v is the crystal volume fraction, [%] and ε is the porosity of crystal bed, [%].

$$\frac{A(1-v-v\varepsilon)dh}{Adt} = \frac{\Delta p}{\frac{\eta}{B_c} \left(\frac{v}{1-\varepsilon}h + h_e \right)} \quad \text{Equation 3.4.2-7}$$

It can be rewritten as:

$$\frac{dt}{dh} = kh + C \quad \text{Equation 3.4.2-8}$$

$$k = \frac{\eta}{B_c \Delta p} \cdot \frac{v}{1-\varepsilon} \cdot (1-v-v\varepsilon) \quad \text{Equation 3.4.2-9}$$

$$C = \frac{\eta}{B_c \Delta p} \cdot (1-v-v\varepsilon) h_e \quad \text{Equation 3.4.2-10}$$

Therefore, there is a linear relationship between dt/dh and h . To determine the permeability of the crystal bed, a filtration test is applied [Slu87]. After finding the filtration time t and the suspension heights h under different pressure drops, different slopes k can be obtained and they can be further calculated to find the permeability in respect to the pressure drop.

3.4.3 Compressibility of a crystal bed

A filter cake may be compressed when a pressure is added and its permeability may change. To predict the permeability of crystal bed under another pressure drop, the compressibility of a crystal bed is defined in Equation 3.4.3-1.

$$B_c = B_0 \cdot \Delta p^{-s} \quad \text{Equation 3.4.3-1}$$

B_c shows the real permeability of the crystal bed, [m^2], and B_0 shows the initial permeability of crystal bed which has no effect by pressure drop, [m^2]. Compressibility factor, s ($0 \leq s \leq 1$), [-], describes the compressibility of a crystal bed. When s is close to 0 the crystal bed is incompressible and when s is close to 1 the crystal bed is fully compressible.

The slope k in Equation 3.4.2-8 can be rewritten as:

$$k = \frac{\eta v (1-v-v\varepsilon)}{B_c \Delta p (1-\varepsilon)} = \frac{\eta v (1-v-v\varepsilon)}{B_0 \Delta p^{1-s} (1-\varepsilon)} \quad \text{Equation 3.4.3-2}$$

Equation 3.4.3-2 uses the logarithm on both sides and it is shown in Equation 3.4.3-3.

$$\log k = s - 1 \log \Delta p + C' \quad \text{Equation 3.4.3-3}$$

Where

$$C' = \log \frac{\eta}{B_0} \cdot \frac{v}{1-\varepsilon} \cdot (1-v-v\varepsilon) \quad \text{Equation 3.4.3-4}$$

As it can be seen that, there is a linear relationship between $\log k$ and $\log \Delta p$. From Equation 3.4.3-3, the permeability of crystal bed at any pressure drop can be predicted and the compressibility of the bed can also be known.

3.5 Analysis

3.5.1 Density measurement

The concentration of phosphoric acid-water melt in this thesis is calculated according to its density. The device that is used for the density measurement is METTLER TOLEDO DE40. The mechanism of the density measurement is based on the electromagnetically induced oscillation of a U-shaped glass tube. A magnet is fixed to the U-shaped tube and a so-called transmitter induces the oscillation (see Figure 3.5.1-1). The period of oscillation (or the frequency) is measured by a sensor. Each glass tube vibrates at a so-called characteristic or natural frequency. This changes when the tube is filled with a gas or liquid. The frequency is a function of the mass. When the mass increases, the frequency decreases [Met01]. Equation 3.5.1-1 shows the equation of the density calculation.



Figure 3.5.1-1: U-shaped tube in the density meter (METTLER TOLEDO DE40) [Met01].

$$\rho = \frac{K}{4\pi^2 V_c} T^2 - \frac{m_c}{V_c} \quad \text{Equation 3.5.1-1}$$

Where, K is the measuring cell constant, $[\text{g}\cdot\text{s}^2]$. V_c is the volume of sample (capacity of tube), $[\text{cm}^3]$. T is the period of oscillation, $[\text{s}]$. m_c is the mass of the measuring cell, $[\text{g}]$.

The measuring cell constant K is related to the temperature. Before the measurement K needs to be calibrated with air and water at the same temperature.

3.5.2 In-line measurement techniques

3.5.2.1 FBRM

Focused Beam Reflectance Measurement (FBRM) technique can be used as an in-line measurement technique for the particle size analysis. The device consists of a laser sensor (523 PsyA SSD) and a data acquisition and analysis system (WinORM, Messtechnik Schwartz GmbH). During the measurement the sensor is immersed in the suspension. The laser in the sensor rotates at a fixed high speed so that it scans the particles (see Figure 3.5.2-1) [Hei08]. The signals of reflection are acquired and the so-called arch chord length of the particles is calculated. It represents the size of the particles. The deviations of the arch chord length may represent the shape of the particles [Mos14].

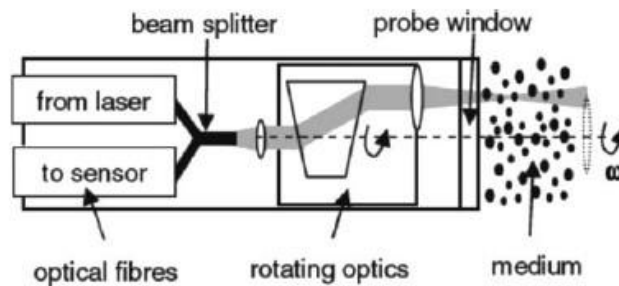


Figure 3.5.2.1-1: Principle of FBRM technique [Hei08].

3.5.2.2 3D ORM

3-Dimension Optical Reflection Measurement (3D ORM) technique is an in-line measurement technique which is similar like FBRM. The device also consists of a laser sensor (APAS 14) and a data acquisition and analysis system (MCSA 1.0.2.32, Sequip S+E GmbH). The difference is that the laser in the sensor does not rotate but the focus of the laser moves back and forth (see Figure 3.5.2.2-1) [Hei08]. It scans particles and measures surface areas of the particles. According to the surface area the software calculates the mean diameter of the particle.

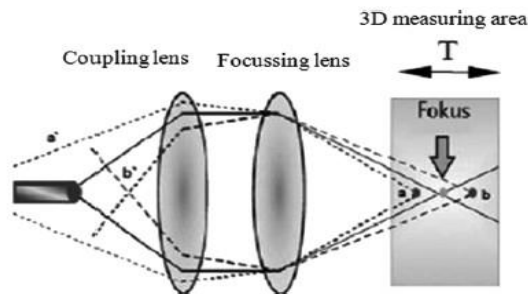


Figure 3.5.2.2-1: Principle of 3D ORM technique [Hei08].

3.5.3 UV-Vis spectrophotometry

Molecules containing π -electrons or non-bonding electrons (n-electrons) can absorb the energy in the form of ultraviolet or visible light to excite these electrons to higher anti-bonding molecular orbitals [Sko03]. The absorbance is related to the concentration of the absorbing substance and the relationship is shown in Equation 3.5.3-1 (Beer-Lambert law).

$$A = \log_{10} \frac{I_0}{I} = \epsilon c L \quad \text{Equation 3.5.3-1}$$

Where, A is the absorbance, [au.]. I_0 is the intensity of the incident light at a given wavelength, [cd]. I is the transmitted intensity, [cd]. ϵ is the extinction coefficient, [au. \cdot L/(mol \cdot cm)]. c is the concentration of the absorbing substance, [mol/L]. L is the path length through the sample, [cm].

Here, the concentration of iron in the phosphoric acid-water melt is analyzed by the method with phenanthroline. The reaction is shown in Figure 3.5.3-1 [For38]. The product has an orange color and it has a maximum absorbance at 510 nm. Before the measurement $(\text{NH}_4)_2\text{Fe}(\text{SO}_4)_2$ is used for the calibration.

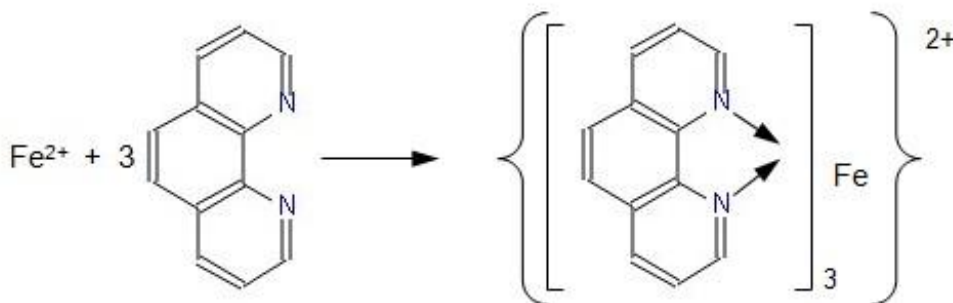


Figure 3.5.3-1: The reaction of iron (II) and phenanthroline [For38].

3.5.4 ICP-OES

Inductively Coupled Plasma-Optical Emission Spectrometry (ICP-OES) is used for the general concentration analysis of metal ions. The mechanism of the measurement is shown in Figure 3.5.4-1 [Roh01]. When plasma energy is given to an analysis sample from outside, the component elements (atoms) are excited. When the excited atoms return to low energy position, emission rays (spectrum rays) are released and the emission rays that correspond to the photon wavelength are measured. The element type is determined based on the position of the photon rays, and the content of each element is determined based on the intensity of the rays [Hit01]. The detection limit of ICP-OES is approx. 1 ppm [Eag01].

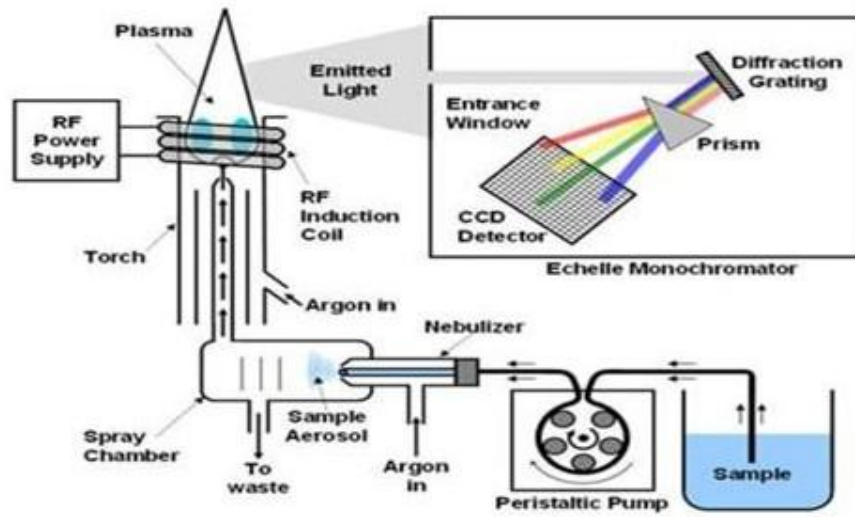


Figure 3.5.4-1: The mechanism of ICP-OES [Roh01].

4. Materials and Methods

4.1 The solubility of phosphoric acid in water

5 mL 85 wt% phosphoric acid was frozen by liquid nitrogen ($-196\text{ }^{\circ}\text{C}$) and later it was stored in a freezer at $-20\text{ }^{\circ}\text{C}$. After 1 day $\text{H}_3\text{PO}_4 \cdot 0.5\text{H}_2\text{O}$ crystals were crystallized according to the phase diagram [Jia12b]. After centrifugation the crystals as seeds were used for inducing the nucleation.

The solubility of H_3PO_4 in water was measured by the isothermal technique. 500 mL $\sim 80\text{ wt}\%$ of H_3PO_4 melt which contains $\sim 80\text{ v/v}\%$ $\text{H}_3\text{PO}_4 \cdot 0.5\text{H}_2\text{O}$ crystals was prepared at $10\text{ }^{\circ}\text{C}$ in a double-walled beaker. The setup is shown in Figure 4.1-1. The supernatant was collected for concentration analysis by a density meter (METTLER TOLEDO DE40). The remaining part was heated ($10.5\text{ }^{\circ}\text{C}$, $\Delta T = 0.5\text{ K}$) for 2 hours with stirring and therefore the crystals were partially dissolved. After that, stirring was stopped and the supernatant was collected again for a concentration analysis by the density meter. These procedure cycles were repeated several times until the temperature reached $29\text{ }^{\circ}\text{C}$. During each cycle, it should be confirmed that there were some crystals in melt. The experiment was repeated two times.

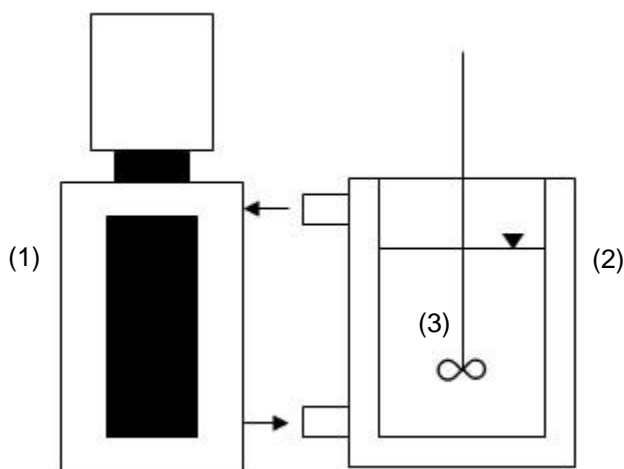


Figure 4.1-1: Solubility measurement (isothermal technique) setup: (1) thermostat, (2) double-walled beaker and (3) mechanical stirrer.

100 ppm B (H_3BO_3 , Merck KGaA), 100-200 ppm Fe^{2+} (Fe powder, Merck KGaA) and 100 ppm Fe^{3+} (Fe_2O_3 , Carl Roth GmbH & Co. KG) as impurity additives, and 1000 ppm ethylenediaminetetraacetic acid (EDTA, Carl Roth GmbH & Co. KG), 1500 ppm etidronic acid (HEDP, Sigma-Aldrich Co.), 1500 ppm diethylenetriamine penta (methylene phosphonic acid)

(DTPMPA, Sigma-Aldrich Co.), 1000 ppm oxalic acid (Carl Roth GmbH & Co. KG), 1500 ppm amino tris (methylene phosphonic acid) (ATMP, Solvay Fluor GmbH) and 1500 ppm pyrophosphoric acid (Sigma-Aldrich Co.) as chelating agent additives were added into H_3PO_4 melt, respectively. The molecular structures of the above-mentioned chelating agents are shown in Figures 4.1-2 to 4.1-7. The solubilities of H_3PO_4 in water with different impurities and chelating agents were measured by the same method which is mentioned above. In addition, the solubilities of two different H_3PO_4 melts (food grade and product grade, from Solvay Fluor GmbH) were also measured by the above-mentioned method.

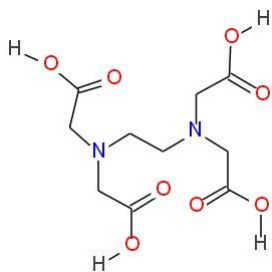


Figure 4.1-2:
Ethylenediaminetetraacetic
acid (EDTA).

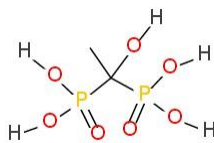


Figure 4.1-3: Etidronic acid
(HEDP).

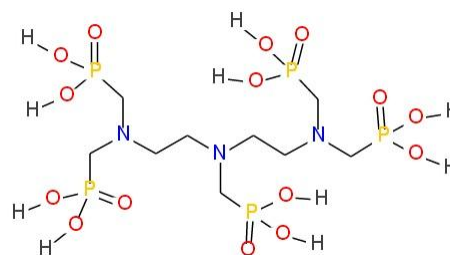


Figure 4.1-4: Diethylenetriamine penta
(methylene phosphonic acid)
(DTPMPA).

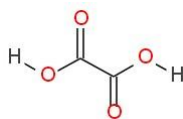


Figure 4.1-5: Oxalic acid
($\text{H}_2\text{C}_2\text{O}_4$).

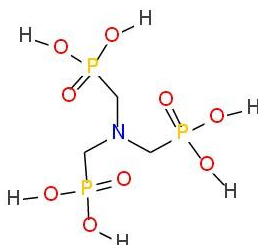


Figure 4.1-6: Amino tris
(methylene phosphonic acid)
(ATMP).

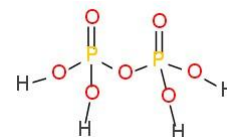


Figure 4.1-7: Pyrophosphoric acid
($\text{H}_4\text{P}_2\text{O}_7$).

4.2 The vapor pressure of phosphoric acid and water

Different concentrations of $\text{H}_3\text{PO}_4 - \text{H}_2\text{O}$ melts (from 80 to 90.92 wt%) were prepared with distilled water. The measurement setup is shown in Figure 4.2-1. A special measurement tube (4) is immersed in a double-walled beaker (2) which is filled with thermal oil. A condenser (6) which is cooled by tap water is connected with the measurement tube (4) and thereafter a U-tube pressure meter (7), a safety bottle (9) and a vacuum pump (10) are connected. By the valve (8), different vacuum degrees can be adjusted.

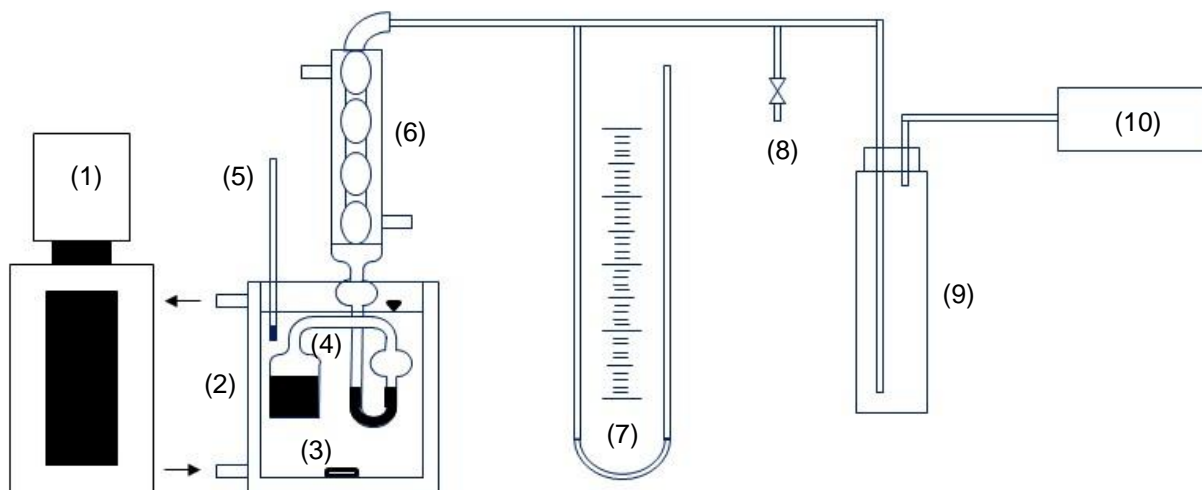


Figure 4.2-1: Setup for vapor pressure measurements: (1) thermostat, (2) double-walled beaker, (3) magnetic stirrer, (4) measurement tube, (5) thermometer, (6) condenser, (7) U-tube pressure meter (filled with mercury), (8) valve, (9) safety bottle and (10) vacuum pump.

A certain amount of the sample (~20 mL) was filled in the measurement tube (4) (shown in Figure 4.2-2) so that all positions (A, B and C) had enough of the sample. The sample on position A is the main part. There was a small amount of sample at positions B and C and it separated the position A and the environment. At a certain degree of the vacuum the sample was heated by a thermostat (1). During this process the sample at position A was evaporated and vapor pressure between position A and positions BC increased. Therefore, the sample level at position C decreased and the level at position B increased. When the temperature reached its boiling point, it was kept boiling for 5 min to ensure that all the inert gases which were between position A and positions BC were removed. Thereafter, the temperature was slowly cooled down (~1 K/min) so that the level at position B decreased and the level at position C increased. The temperature was read when the levels at positions B and C were equal to each other. At this temperature, the vapor pressure of the sample was equal to the value which was shown in the U-tube pressure meter. The valve (8) was further regulated to give another vacuum degree and the previous procedure was repeated so that the vapor pressures of the samples at different temperatures can be obtained.

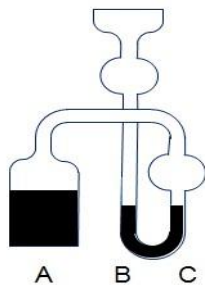


Figure 4.2-2: The tube for the vapor pressure measurements.

4.3 The measurements of crystal growth

4.3.1 Off-line measurements

The off-line measurement of crystal growth was conducted with a temperature controlled cell under a microscope. A saturated $\text{H}_3\text{PO}_4 - \text{H}_2\text{O}$ melt (product grade, Solvay Fluor GmbH) with crystals at $16\text{ }^\circ\text{C}$ was prepared before the crystal growth rate measurements. The setup of the measurement is shown in Figure 4.3.1-1. 3 mL melt with a few crystals was filled into the cell which was connected with a thermostat. The temperature was kept at saturation temperature (in this case $16\text{ }^\circ\text{C}$) for 10 min and was thereafter quickly cooled down (1 K/min) to $14\text{ }^\circ\text{C}$ so that a supersaturated melt ($\Delta s = 0.65\text{ wt\%}$) was obtained. The crystals grew at $14\text{ }^\circ\text{C}$ for 30 min and the growth was recorded through a microscope. Ten crystals were measured under the same conditions. The data were analyzed by the software Analysis 5.0 (Olympus Soft Imaging Solutions).

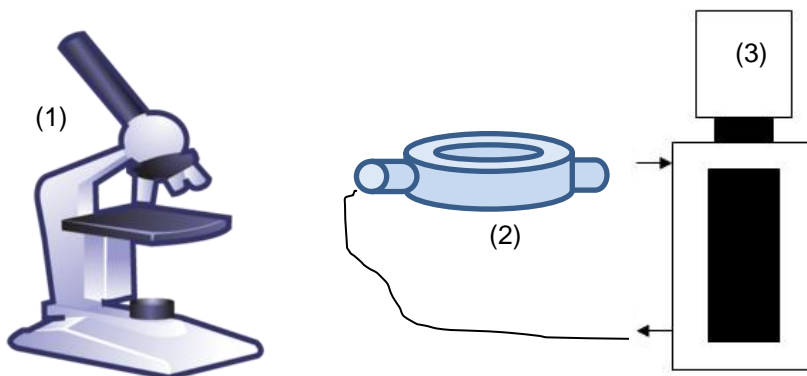


Figure 4.3.1-1: Setup for crystal growth rate measurements: (1) microscope, (2) temperature controlled cell and (3) thermostat.

The experiment was repeated with a food grade of $\text{H}_3\text{PO}_4 - \text{H}_2\text{O}$ melt (Solvay Fluor GmbH) instead of product grade. To the study of impurities 100 ppm B (H_3BO_3 , Merck KGaA), 100-200 ppm Fe^{2+} (Fe powder, Merck KGaA) and 100 ppm Fe^{3+} (Fe_2O_3 , Carl Roth GmbH & Co. KG) were added to the product grade of the sample and the procedure was as same as described before. All the data were also analyzed by the software Analysis 5.0 (Olympus Soft Imaging Solution).

4.3.2 In-line measurements

The in-line measurement of crystal growth was analyzed by an FBRM (Focused Beam Reflectance Measurement) and a 3D ORM (3-Dimension Optical Reflection Measurement) technique. The setup of the experiment is shown in Figure 4.3.2-1. A supersaturated $\text{H}_3\text{PO}_4 - \text{H}_2\text{O}$ melt ($\Delta s = 1.5 \text{ wt}\%$) was stirred at $16.7 \text{ }^\circ\text{C}$ in a double-walled beaker. One sensor each of FBRM (523 PsyA SSD, Messtechnik Schwartz GmbH) and 3D ORM (APAS 14, Sequip S+E GmbH) which each are connected to a computer were immersed in the melt. After stirring for several minutes, the seeds ($\text{H}_3\text{PO}_4 \cdot 0.5\text{H}_2\text{O}$) were added to induce nucleation and crystal growth. The whole process was recorded by the two sensors. Later the experiment was repeated under different supersaturations and all the data were analyzed by the software WinORM (Messtechnik Schwartz GmbH) and MCSA 1.0.2.32 (Sequip S+E GmbH), respectively.

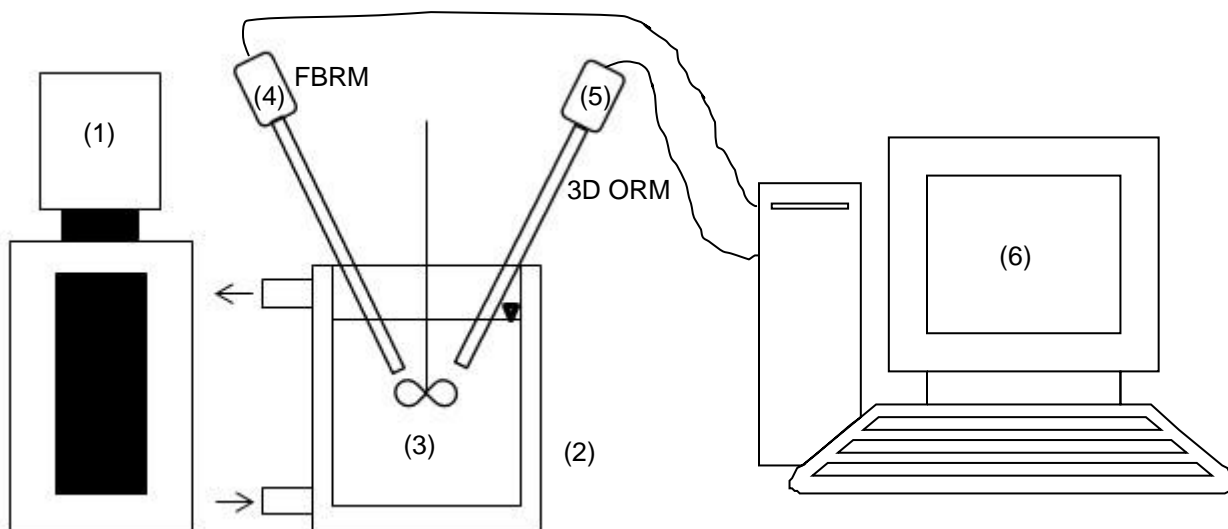


Figure 4.3.2-1: Setup for in-line measurements: (1) thermostat, (2) double-walled beaker, (3) mechanical stirrer, (4) FBRM sensor (523 PsyA SSD), (5) 3D ORM sensor (APAS 14) and (6) computer.

4.4 The distribution coefficient of crystallization and post treatments

4.4.1 Crystallization

Phosphoric acid hemihydrate crystals were crystallized in a double-walled beaker at different conditions of crystallization (different supersaturations and crystallization time). The setup of the experiments is shown in Figure 4.4.1-1. 100 ppm $\text{Fe}(\text{ClO}_4)_3$ ($\text{Fe}(\text{ClO}_4)_3 \cdot x\text{H}_2\text{O}$, Sigma-Aldrich Co.) as an impurity was added to study the efficiency of separation. 150 mL of 85.29 wt% $\text{H}_3\text{PO}_4 - \text{H}_2\text{O}$ melt (Solvay Fluor GmbH) was stirred in the double-walled beaker at 100 rpm. The temperature was set at 17.6, 19.2 and 20.6 °C so that the supersaturations of 1.5, 1 and 0.5 wt% can be obtained, respectively. After adding seeds the suspension was stirred for 2, 1 and 0.5 h at 100 rpm, respectively. Later they were filtrated at the respected temperatures. The samples which were from the initial $\text{H}_3\text{PO}_4 - \text{H}_2\text{O}$ melt with $\text{Fe}(\text{ClO}_4)_3$ additive, the mother liquor and the wet crystals were collected for the iron content analysis by the UV-Vis spectroscopy at 510 nm.

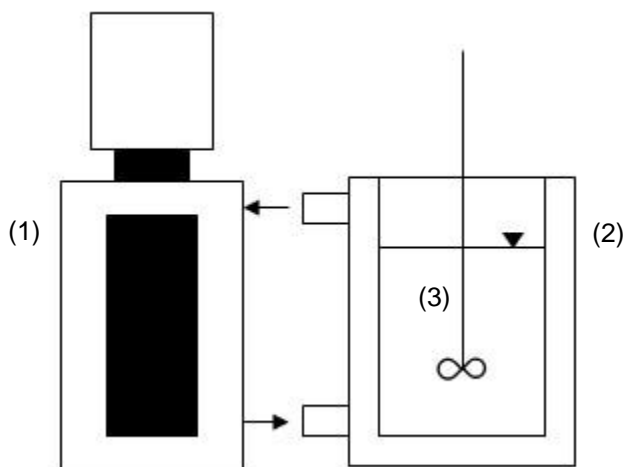


Figure 4.4.1-1: Setup of distribution coefficient measurements of crystallization: (1) thermostat, (2) double-walled beaker and (3) mechanical stirrer.

Additionally, 1000 ppm EDTA (Carl Roth GmbH & Co. KG), 1500 ppm HEDP (Sigma-Aldrich Co.), 1500 ppm DTPMPA (Sigma-Aldrich Co.), 10 ppm oxalic acid ($\text{H}_2\text{C}_2\text{O}_4$, Carl Roth GmbH & Co. KG), 15 ppm ATMP (Cublen, Solvay Fluor GmbH) and 1500 ppm pyrophosphoric acid ($\text{H}_4\text{P}_2\text{O}_7$, Sigma-Aldrich Co.) as chelating agent additives were added into $\text{H}_3\text{PO}_4 - \text{H}_2\text{O}$ melt, respectively. The procedures of the screening tests were the same as mentioned above and they were undertaken at a supersaturation of 1.5 wt% and stirred for 2 h. The samples which were from the initial $\text{H}_3\text{PO}_4 - \text{H}_2\text{O}$ melt with $\text{Fe}(\text{ClO}_4)_3$ and respective chelating agent additives,

the mother liquor and the wet crystals were collected for the iron content analysis by the UV-Vis spectroscopy at 510 nm.

For the iron content analysis by the UV-Vis spectroscopy [Yu06] the standard curve of iron (II) was calibrated by $(\text{NH}_4)_2\text{Fe}(\text{SO}_4)_2$. 1 mL (or 2 g) of sample was diluted to 60 mL by distilled water. The pH of the solution was adjusted to 2 by 3 mol/L HCl and 10 wt% $\text{NH}_3 \cdot \text{H}_2\text{O}$. Later, 2.5 mL of 2 wt% of vitamin C, 10 mL of 0.6 mol/L of NaAc-HAc buffer solution (pH \approx 4.5) and 5 mL of 0.2 wt% of phenanthroline were added, respectively. The volume of the mixture was adjusted to 100 mL by distilled water in a volumetric flask. The mixture has an orange color and it has a maximum absorbance at 510 nm.

4.4.2 Post treatments

The wet crystals which were from the procedures in the Chapter 4.4.1 were further washed or rinsed by the saturated pure $\text{H}_3\text{PO}_4 - \text{H}_2\text{O}$ melt as a washing liquid. The volume of the washing liquid and the washing time were changed in order to study their influences to the efficiency of separation. The feed (the initial $\text{H}_3\text{PO}_4 - \text{H}_2\text{O}$ melt with $\text{Fe}(\text{ClO}_4)_3$) also as a special washing liquid was tested for the efficiency of separation. The iron content in the samples which were treated before and after the washing was analyzed by the UV-Vis spectroscopy at 510 nm.

4.5 The permeability measurements of the crystal bed

A filtration test setup according to the literature [Slu87] is shown in Figure 4.5-1. A thermostated glass tube with a filter is combined with a vacuum flask. A suspension with a certain amount (5 – 40 wt%) of phosphoric acid hemihydrate crystals was prepared before the test. The suspension was filled in a thermostated glass tube under a certain pressure drop and temperature, later the filtration will be started. During the process the height h of the suspension and the respected filtration time t were recorded. When the height of the crystal bed h_c does not change any more the filtration process ends and the height of the crystal bed is recorded. Its porosity can then be calculated. The tests were repeated with the same suspension at least for four different pressure drops and each pressure drop was repeated at least three times.

The crystal size is the main factor that influences the permeability of a crystal bed. In this case, different sizes of phosphoric acid hemihydrate crystals were prepared by different supersaturations and stirring speeds, and they were analyzed by an optical microscope.

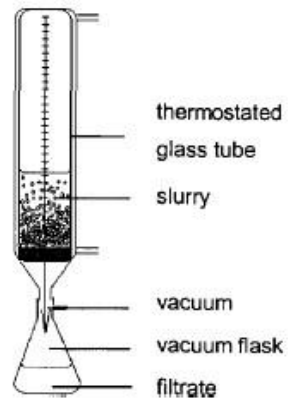


Figure 4.5-1: Setup of filtration tests [Slu87].

5. Results

In this chapter the results of solubility study of phosphoric acid in water without and with additives are shown in Chapter 5.1. The results of vapor pressure measurement of phosphoric acid and water are shown in Chapter 5.2. The measurements of crystal growth via off-line and in-line techniques are shown in Chapter 5.3. The studies of distribution coefficient of crystallization and post treatments are shown in Chapter 5.4. The results of permeability measurements of the crystal bed are shown in Chapter 5.5 and the mass balance calculations of the pilot plant are explained in Chapter 5.6.

5.1 The solubility of phosphoric acid in water

At the beginning, the titration (0.1 mol/L NaOH, phenolphthalein as an indicator) was used to determine the concentration of the $\text{H}_3\text{PO}_4 - \text{H}_2\text{O}$ melt. Due to the fact that the color-change of the ending point is too difficult to recognize, only the highest concentration of the $\text{H}_3\text{PO}_4 - \text{H}_2\text{O}$ melt, for example 90 wt%, was titrated. The other concentrations of the $\text{H}_3\text{PO}_4 - \text{H}_2\text{O}$ melts were diluted from 90 wt% to lower concentrations and their densities were measured by a density meter at 35 °C. The reason to choose 35 °C is that the melting temperature of $\text{H}_3\text{PO}_4 \cdot 0.5\text{H}_2\text{O}$ crystals is approx. 29 °C. In order to avoid any crystallization during the density measurement, the 35 °C was chosen. Figure 5.1-1 shows the relationship between the density and the concentration of $\text{H}_3\text{PO}_4 - \text{H}_2\text{O}$ melt at 35 °C.

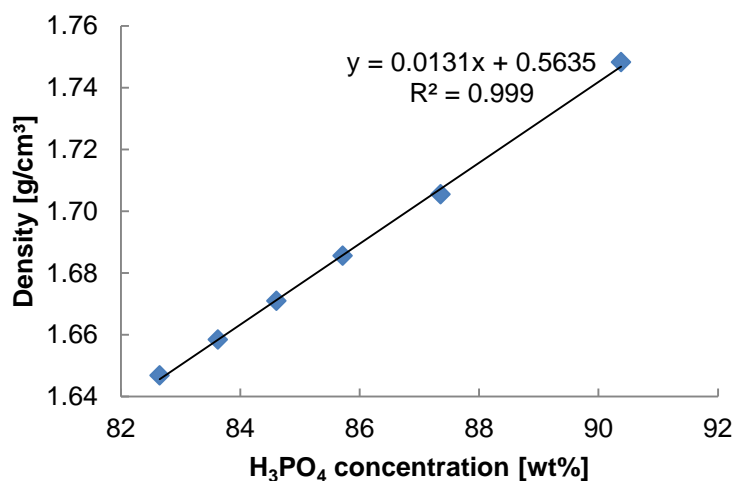


Figure 5.1-1: The density of $\text{H}_3\text{PO}_4 - \text{H}_2\text{O}$ melt vs. its concentration at 35 °C.

Figure 5.1-1 shows that there is a very good linear relationship ($R^2=0.999$) between the density and the concentration of $H_3PO_4 - H_2O$ melt at 35 °C. This relationship is only limited in the concentration range of 80-91 wt%. The used industrial phosphoric acid product, the concentration is usually approx. 85 wt%. During the production by crystallization, the concentration of a mother liquor will not be less than 80 wt% (saturation temperature 5 °C). Therefore, a study of the concentration which is less than 80 wt% is senseless in this case. The curve in Figure 5.1-1 is used as a calibration curve to determine an unknown concentration of a $H_3PO_4 - H_2O$ melt.

5.1.1 Without additives

The solubility of H_3PO_4 in water from the feed sample was measured at first. There were no additional additives in the feed sample, but there were still some impurities within the sample. These impurities, especially, the cations, were analyzed by ICP-OES and they are shown in Table 5.1.1-1.

It can be seen that most cations in the feed, except Sb are less than 1 ppm. To check whether these amounts of impurities have an effect on the solubility change of H_3PO_4 in water, the solubility data of the feed are compared with those from literature [Smi09] and all of them are

Table 5.1.1-1: The concentration of cations in $H_3PO_4 - H_2O$ melts (measured by ICP-OES).

Element [ppm]	Feed	Product grade	Food grade
Al	0.228	0.023	0.083
As	<0.040	0.027	0.121
Ba	<0.005	<0.005	0.011
B	0.023	0.034	4.657
Ca	0.204	0.012	0.081
Cd	<0.005	<0.005	<0.005
Co	<0.030	<0.005	<0.005
Cr	0.118	0.012	0.045
Cu	0.044	<0.005	0.041
Fe	0.425	0.073	0.395
K	0.092	0.012	0.045
Li	<0.005	<0.005	<0.005
Mg	0.022	<0.005	0.036
Mn	0.033	<0.005	<0.005
Na	0.194	0.084	9.569
Ni	0.126	0.009	0.042
Pb	<0.100	<0.005	<0.005
Sr	<0.005	<0.005	<0.005
Sb	3.72	0.165	0.014
Ti	<0.020	<0.005	<0.005
Zn	<0.020	0.007	0.409

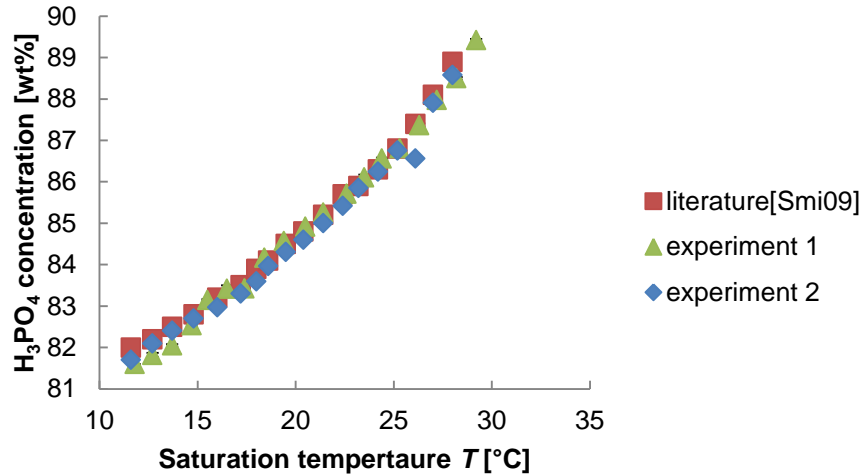


Figure 5.1.1-1: Solubility of H_3PO_4 (feed) in water.

shown in Figure 5.1.1-1. Experiment 2 is the repetition of experiment 1. It can be seen that both experiments match well with the literature data except the part of low concentrations in experiment 1 (< 82 wt%). This may be due to a deviation of an analysis. From this point of view, it can be concluded that the cations in the feed (each cation is less than 1 ppm except Sb) do not change the solubility of H_3PO_4 in water.

Table 5.1.1-1 also gives the content of cations in a product grade and a food grade of H_3PO_4 samples. All the samples are provided by Solvay Fluor GmbH in Bernburg. The H_3PO_4 melt of the food grade has the highest amounts of cations compared to the other two samples. The solubility of the two grade samples are compared with the feed and the literature [Smi09] and the results are shown in Figure 5.1.1-2.

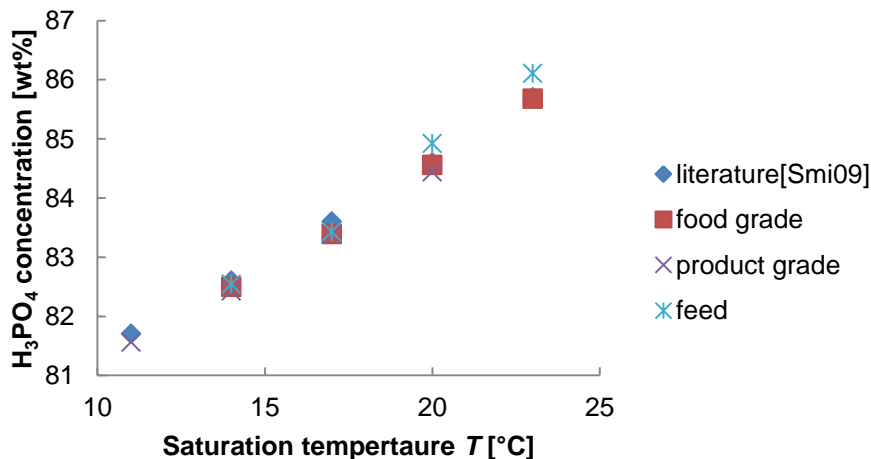


Figure 5.1.1-2: The solubility comparison of different H_3PO_4 samples.

As it can be seen that, most of the points match well with the data which are from the literature [Smi09]. In other words, the cations (low amount) show no influences on the solubility of H_3PO_4 in water.

5.1.2 With additives

The additives were separated into two parts: The impurities and the chelating agents.

To the impurities, 100 ppm B (H_3BO_3), 100-200 ppm Fe^{2+} (Fe powder) and 100 ppm Fe^{3+} (Fe_2O_3) were studied according to the industrial requirements. The solubility data in all three groups show that the three kinds of impurities do not change the solubility of H_3PO_4 in water. These results will further be the preconditions for the crystal growth measurements and it is described in Chapter 5.3.

Six chelating agents: 1000 ppm ethylenediaminetetraacetic acid (EDTA), 1500 ppm etidronic acid (HEDP), 1500 ppm diethylenetriamine penta (methylene phosphonic acid) (DTPMPA), 1000 ppm oxalic acid, 1500 ppm amino tris (methylene phosphonic acid) (ATMP) and 1500 ppm pyrophosphoric acid were studied. All the groups show there is no solubility change of H_3PO_4 in water and these are the preconditions for the chelating agent effect on the separation coefficient in Chapter 5.4.

5.2 The vapor pressure of phosphoric acid and water

For a pure substance the Clausius-Clapeyron equation [Ken66] (Equation 5.2-1) describes the relationship between its vapor pressure and the temperature:

$$\ln p = -\frac{\Delta_{vap}H_m}{R} \cdot \frac{1}{T} + C \quad \text{Equation 5.2-1}$$

Where,

p is vapor pressure of the substance, [Pa]

$\Delta_{vap}H_m$ is vaporization enthalpy of the sample, [J/mol]

R is the ideal gas constant, 8.314 [J/(mol•K)]

T is temperature, [K]

C is a constant, [-]

It can be seen that in case of a pure substance there is a linear relationship between $\ln p$ and $1/T$. To do a study of a mixture the vapor pressure data of $\text{H}_3\text{PO}_4 - \text{H}_2\text{O}$ melt (for example at 87.53 wt%) were drawn with $\ln p \sim 1/T$ and they are shown in Figure 5.2-1. Each measurement was repeated three times (from trial 1 to trial 3). It can clearly be seen that there is a very good linear relationship between $\ln p$ and $1/T$ (see Figure 5.2-1, linear (trial 1), $R^2 = 0.9995$). Ideally, when the two component system starts evaporating the concentrations of the vapor mixtures and their respected solution will change according to the phase diagram. To prove that the concentration changes after measurement have no significant influence on their vapor pressure, each trial sample was analyzed before and after the vapor pressure measurement. Additionally, the sample of the trial 3 was directly used from the trial 2 when the trial 2 was finished and the results are shown in Table 5.2-1.

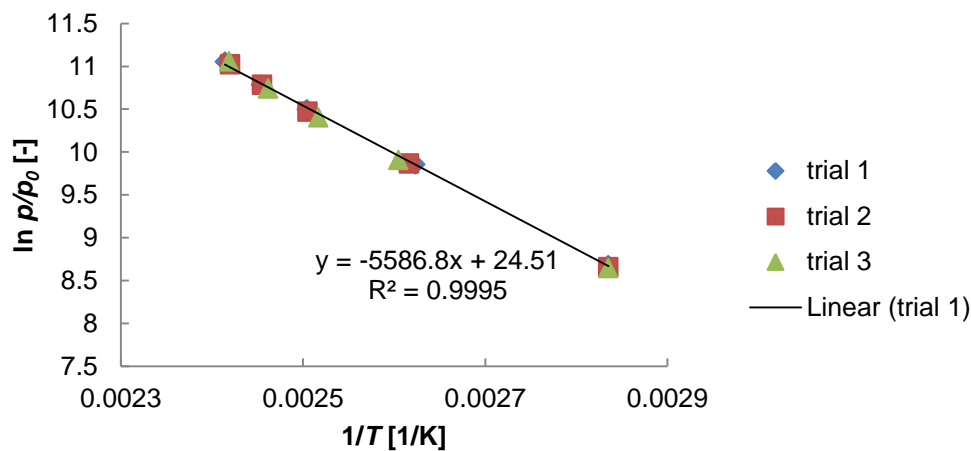


Figure 5.2-1: Vapor pressure vs. temperature of 87.53 wt% $\text{H}_3\text{PO}_4 - \text{H}_2\text{O}$ melt ($p_0 = 1$ Pa).

Table 5.2-1: Concentration analysis of vapor pressure measurement.

Sample	Concentration [wt%]
Before trial 1	87.53±0.03
After trial 1	87.27±0.02
After trial 2 & 3	87.66±0.01

Table 5.2-1 shows that the concentration of each trial sample changed a little due to the evaporation of the melt. However, in Figure 5.2-1 there is no significant change in the vapor pressure of the sample at a certain temperature to be seen. Especially, from the data of trial 3 it can be said that although the sample concentration changed before the measurement (due to trial 2), the vapor pressure from the trial 3 has no significant difference compared to the one from

trial 1. The linear equation can be further used to calculate the vapor pressure at low temperatures such as 50, 60 and 70 °C. Samples of different concentrations were measured in the same way as mentioned before. Their vapor pressures at 50, 60 and 70 °C were calculated by a linear equation and the results are shown in Figure 5.2-2.

It can be seen from Figure 5.2-2 that the vapor pressure which is measured by this method is higher ($\Delta p = \sim 1$ kPa) than the data from literature [Sol13]. There could be a systematic error during the measurement. It can also be seen that in the concentration range of 80 to 91 wt% the vapor pressure of the melt has a linear relationship with its concentration at a constant temperature. The vapor pressure decreases when the concentration is increasing.

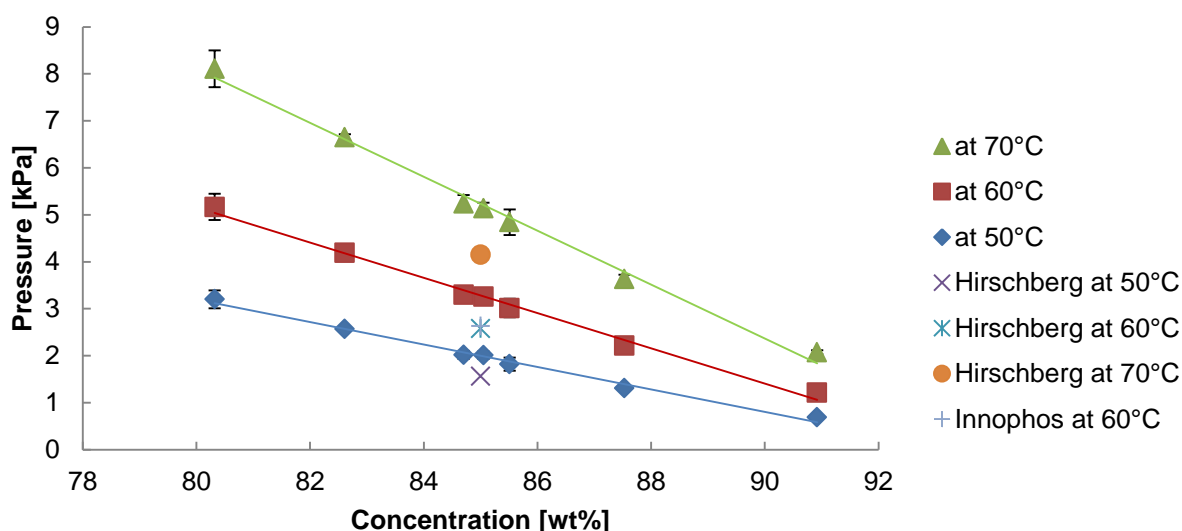


Figure 5.2-2: $\text{H}_3\text{PO}_4 - \text{H}_2\text{O}$ vapor pressure vs. its concentration at different temperatures.

5.3 The measurements of crystal growth

5.3.1 Off-line measurements

5.3.1.1 Crystal growth without additives

At first, the saturated melt of the product grade materials was prepared at 16 °C. When the sample was quickly cooled down to 14 °C ten crystals were recorded by the microscope, respectively. All the growth rates which were measured here are based on the change of the length direction of the crystals. Each crystal grew for 30 min and its growth rate was calculated every 5 min. During the measurement the degree of supersaturation of the mother liquor was

decreasing. Therefore, the growth rate of the crystals in this melt, in principle, was decreasing. The average of growth rates and their deviations were calculated and are shown in Figure 5.3.1.1-1. It can be seen from Figure 5.3.1.1-1 that the growth rate at the beginning was fast (approximately 4.63×10^{-7} m/s). Later, it decreased to 2.57×10^{-7} m/s. The deviations between the individual crystals are very high due to the growth rate dispersion [Jon99, Ulr89]. The growth images of one crystal are shown in Figure 5.3.1.1-2. A $\text{H}_3\text{PO}_4 \cdot 0.5\text{H}_2\text{O}$ crystal has a flat and a hexagonal shape. The two crystals (1-1.5 mm length) in Figure 5.3.1.1-2 were observed from the top and from the side, respectively. After 30 min, a defect in the crystal can clearly be seen which may be resulted from a too fast growth rate.

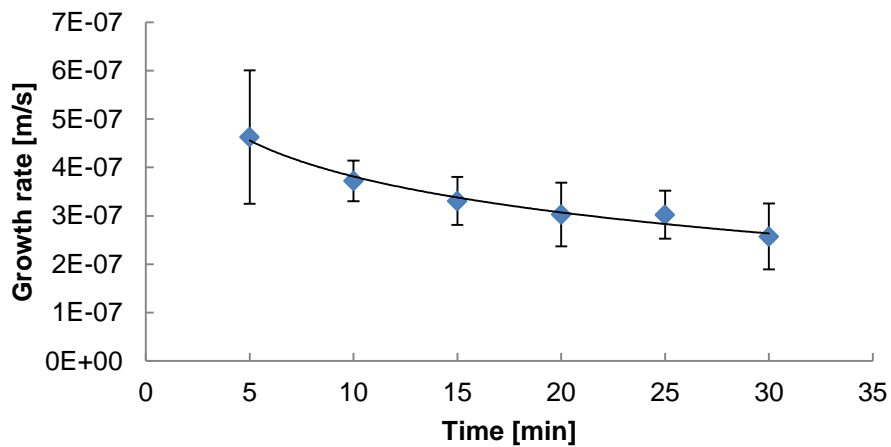


Figure 5.3.1.1-1: The average growth rate of ten crystals at 14 °C.

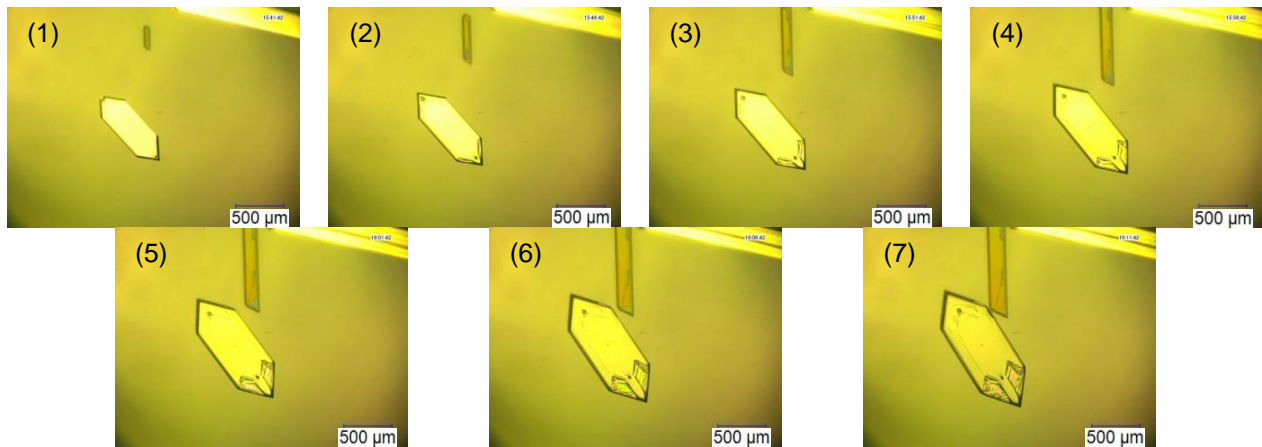


Figure 5.3.1.1-2: Crystal growth after (1) 0 min, (2) 5 min, (3) 10 min, (4) 15 min, (5) 20 min, (6) 25 min, (7) 30 min.

The growth rates under the same supersaturation, but at a temperature level of 9 °C were measured and compared with the one at 14 °C. The results are shown in Figure 5.3.1.1-3. According to the Arrhenius' theory the decrease in temperature will decrease the growth rate. However, in this case the growth rates under the different temperature levels ($\Delta T = 5$ K) makes no significant difference which means the temperature here is not the main factor which can significantly influence the growth rate.

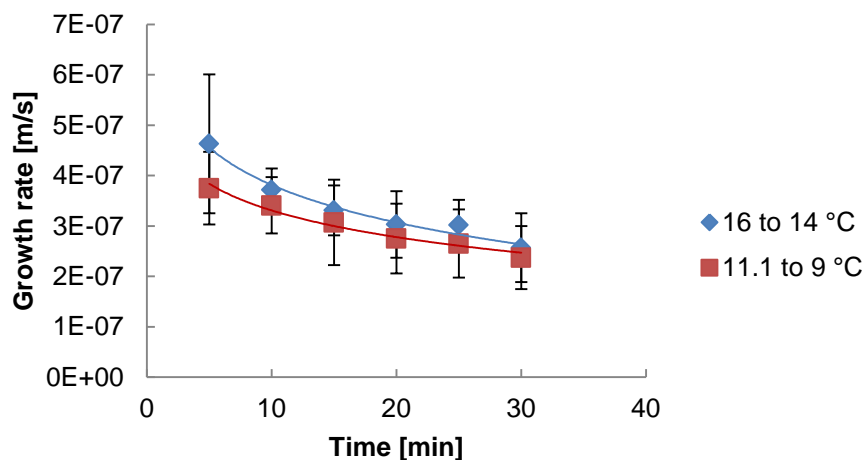


Figure 5.3.1.1-3: The average growth rate of ten crystals at 14 °C and 9 °C.

The growth rates under the different supersaturations were measured and for each supersaturation, ten crystals each were tested. All the crystals grew at 14 °C with their different supersaturations and their growth rates at 15 min were compared with each other. The results are shown in Figure 5.3.1.1-4. It can be seen from Figure 5.3.1.1-4 that the growth rate

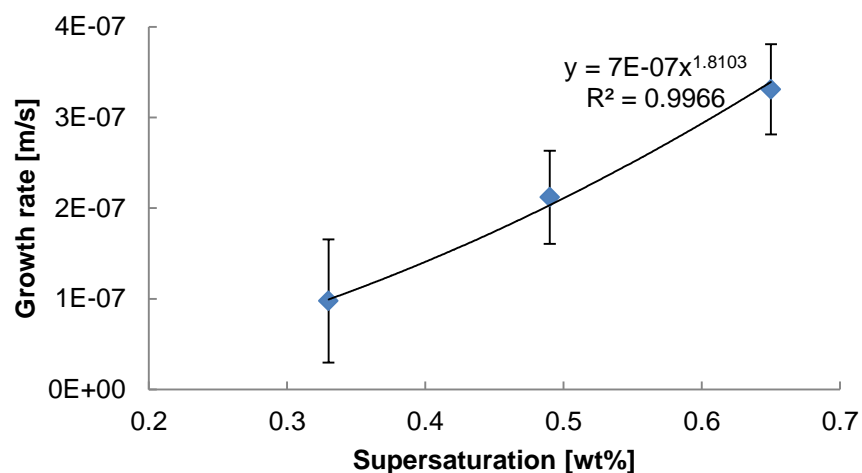


Figure 5.3.1.1-4: $\text{H}_3\text{PO}_4 \cdot 0.5\text{H}_2\text{O}$ crystal growth rates after 15 min under different supersaturations.

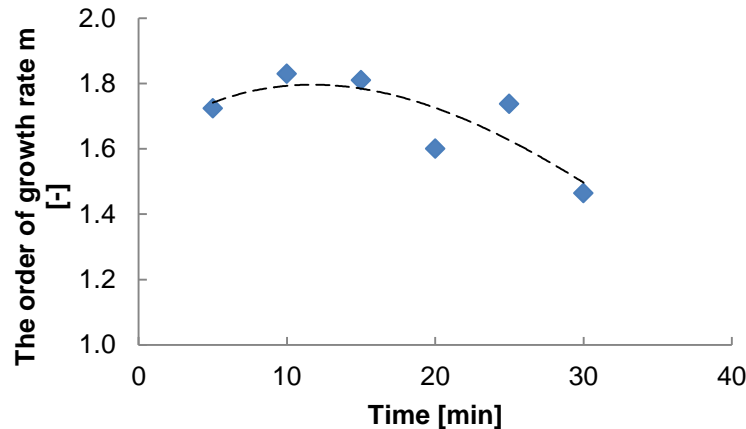


Figure 5.3.1.1-5: The order of growth rate at different growth time points.

increases with increasing supersaturation. This was expected. The order of crystal growth in this case is 1.8. This value is between one and two. It is a one-and-two-dimension growth, so the growth mechanism at this moment is controlled by diffusion and surface-integration.

It needs to be mentioned that the orders of the growth rate at different growth times are different. In Figure 5.3.1.1-5, the order of growth rate changes from 1.4 to 1.8 during the growth of the crystals. However, the mechanism of the growth does not change. In other words the process of the growth in first 30 min is always controlled by diffusion and surface-integration.

Figure 5.3.1.1-6 shows the crystal defects under different supersaturations after 30 min. It can clearly be seen that the lower the supersaturation the less serious the crystal defect become. However, the crystal defects remain in the crystals if they are present from the start. The crystal defect may influence the quality of the crystals. For example impurities can be included in the crystals at the defects or attached on the surface of the crystals due to a larger surface area. It will also increase the difficulty and the time of the post treatments of crystallization process such as sweating or washing to improve the purity of the crystals.

In addition, the growth of the crystals in food grade of $\text{H}_3\text{PO}_4 - \text{H}_2\text{O}$ melts was studied. The curve of the crystal growth and the photos of the crystals are shown in Figures 5.3.1.1-7 and 5.3.1.1-8. The difference between the purities of the food grade and the product grade is already shown in Table 5.1.1-1. Although the average crystal growth rate in food grade liquid is slightly lower than the one in product grade, the deviations are large so that there is at the end of the day no significant difference between the two growth rates. The images in Figure 5.3.1.1-8 show that the shape of some crystals has slightly changed from a hexagonal to a parallelogram.

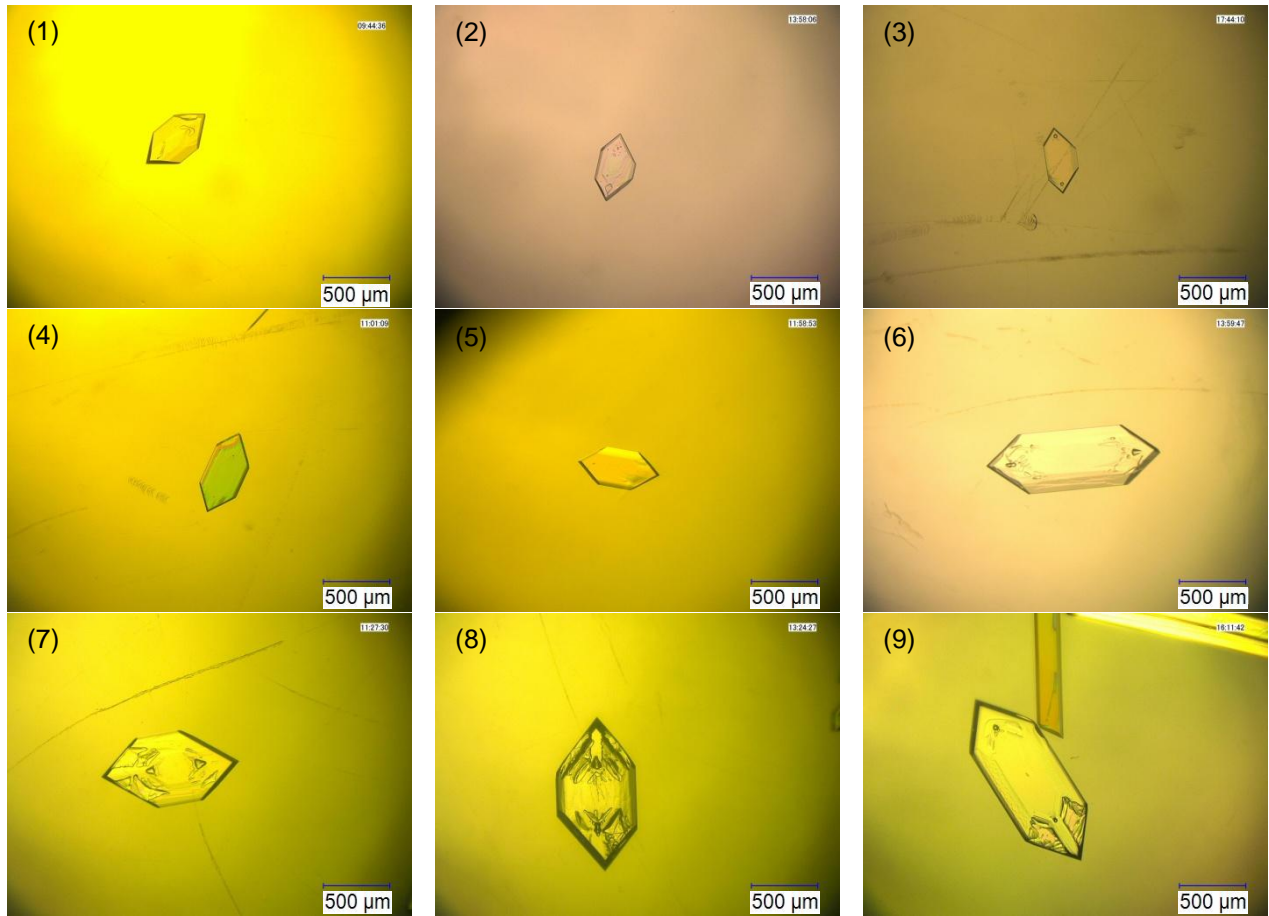


Figure 5.3.1.1-6: $\text{H}_3\text{PO}_4 \cdot 0.5\text{H}_2\text{O}$ crystals after 30 min of growth at a supersaturation of (1), (2), (3) 0.33 wt%, (4), (5), (6) 0.49 wt% and (7), (8), (9) 0.65 wt%.

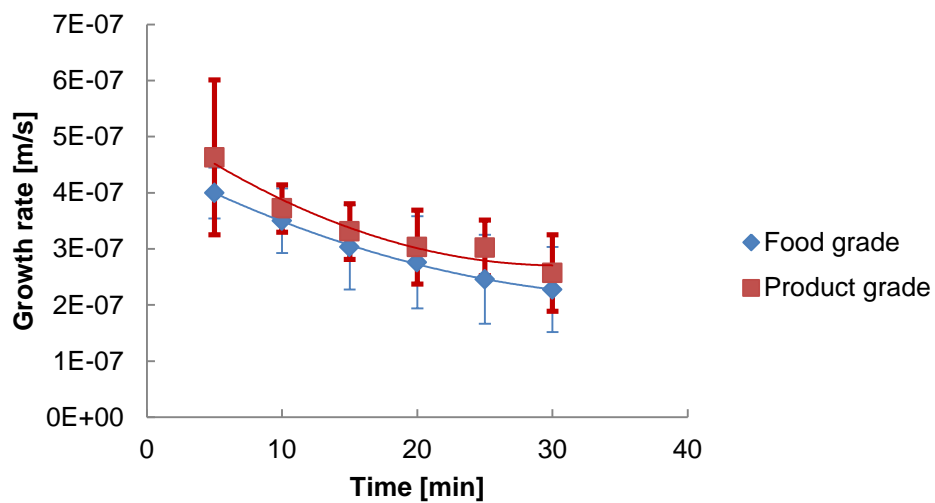


Figure 5.3.1.1-7: Average growth rates of $\text{H}_3\text{PO}_4 \cdot 0.5\text{H}_2\text{O}$ crystals in a food grade and a product grade of $\text{H}_3\text{PO}_4 - \text{H}_2\text{O}$ melt.

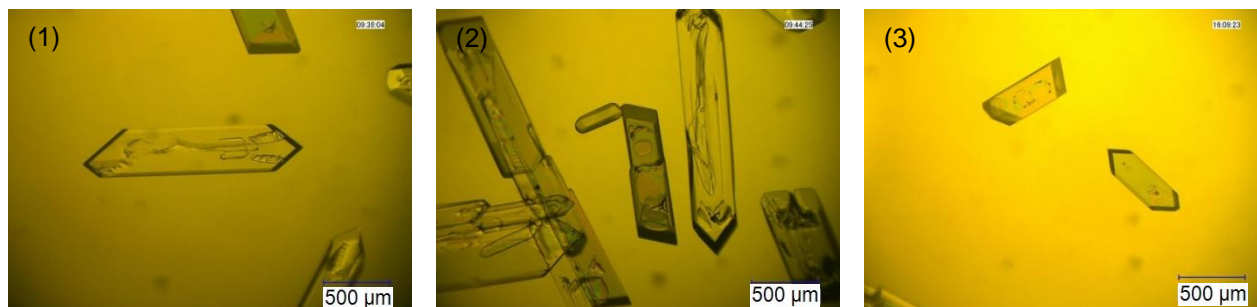


Figure 5.3.1.1-8: $\text{H}_3\text{PO}_4 \cdot 0.5\text{H}_2\text{O}$ crystals in a food grade of $\text{H}_3\text{PO}_4 - \text{H}_2\text{O}$ melt, $\Delta s = 0.65 \text{ wt\%}$.

From Table 5.1.1-1 it can be known that both the concentrations of B and Na in food grade are 100 times higher than the ones in product grade. The changes of the crystal morphology may be due to the concentration increase of these two elements. The effect of impurities will be introduced in Chapters 5.3.1.2-5.3.1.4.

5.3.1.2 The effect of boron

100 ppm B (H_3BO_3) was added into the $\text{H}_3\text{PO}_4 - \text{H}_2\text{O}$ melt in order to see its effect on the growth of $\text{H}_3\text{PO}_4 \cdot 0.5\text{H}_2\text{O}$ crystals. In this case B plays a role of anion in a form of BO_3^{3-} . In the Chapter 5.1.2 it is known that 100 ppm boric acid does not change the solubility of H_3PO_4 in water. Therefore, the growth of the crystals with B can be compared with the one which is without additives at same supersaturation (0.65 wt%) and temperature (14 °C). The $\text{H}_3\text{PO}_4 - \text{H}_2\text{O}$ melt was used here is product grade. The growth rate curves of the crystals and the images of the crystals are shown in Figures 5.3.1.2-1 and 5.3.1.2-2.

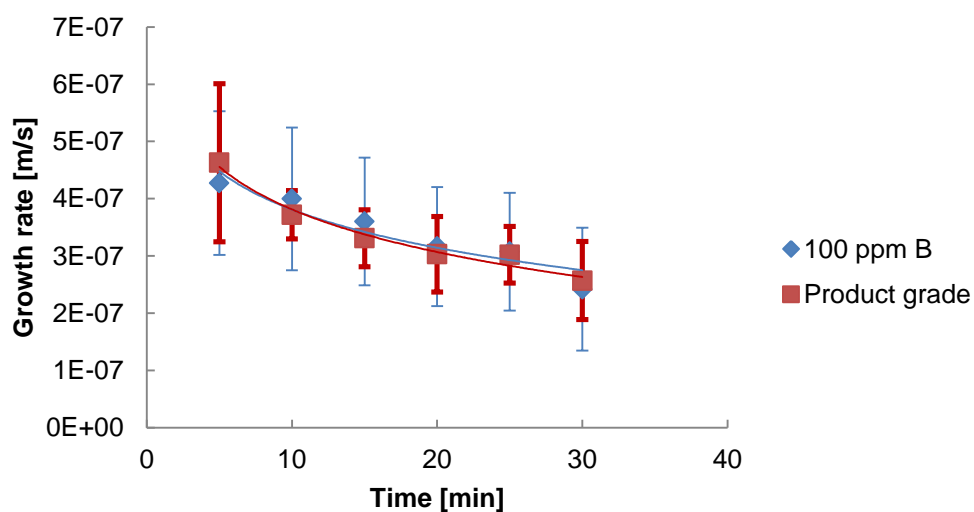


Figure 5.3.1.2-1: Average growth rates of $\text{H}_3\text{PO}_4 \cdot 0.5\text{H}_2\text{O}$ crystals with 100 ppm B in the product grade of $\text{H}_3\text{PO}_4 - \text{H}_2\text{O}$ melt.

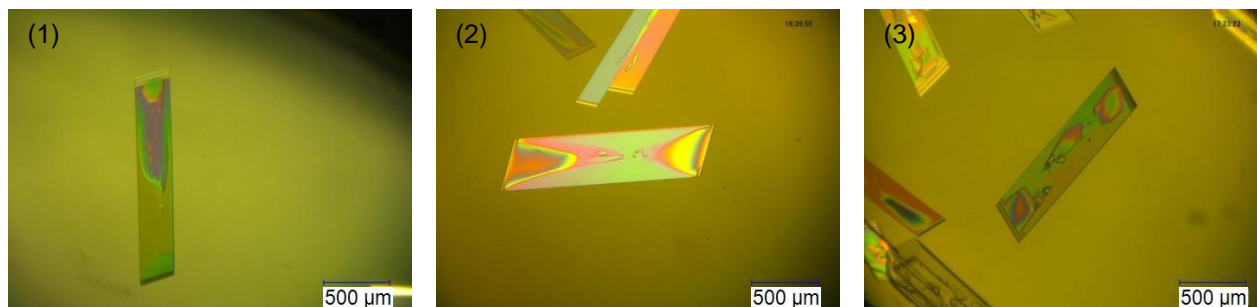


Figure 5.3.1.2-2: $\text{H}_3\text{PO}_4 \cdot 0.5\text{H}_2\text{O}$ crystals in product grade of $\text{H}_3\text{PO}_4 - \text{H}_2\text{O}$ melt with 100 ppm B as an additive, $\Delta s = 0.65$ wt%.

It can be seen that the average growth rate of the crystals with 100 ppm B shows no significant difference to the ones in the product grade melt. But in Figure 5.3.1.2-2 three images show that the shape of the crystals is parallelogram which is different to the one in the product grade. It seems to be that boric acid blocks the face $01\bar{1}$ or $0\bar{1}1$ so that the adjacent face $0\bar{1}\bar{1}$ or 011 can keep growing, respectively. It can also be seen that the crystal defect cannot be avoid during the growth.

5.3.1.3 The effect of iron (II)

100 ppm and 200 ppm Fe^{2+} (Fe powder) was added into the $\text{H}_3\text{PO}_4 - \text{H}_2\text{O}$ melt in order to see its effect on the growth of $\text{H}_3\text{PO}_4 \cdot 0.5\text{H}_2\text{O}$ crystals. In the Chapter 5.1.2 it is shown that 100 ppm and 200 ppm Fe^{2+} do not change the solubility of H_3PO_4 in water. Therefore, the growth of the crystals in the presence of Fe^{2+} can be compared with those experiments which are without additives at same supersaturation (0.65 wt%) and temperature (14 °C). The $\text{H}_3\text{PO}_4 - \text{H}_2\text{O}$ melt used here is product grade and the growth rates of the crystals and the images of the crystals are shown in Figures 5.3.1.3-1 and 5.3.1.3-2, respectively.

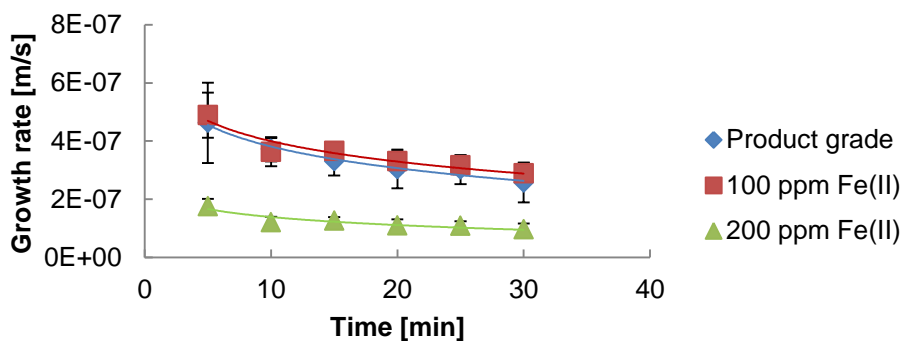


Figure 5.3.1.3-1: Average growth rates of $\text{H}_3\text{PO}_4 \cdot 0.5\text{H}_2\text{O}$ crystals with 100 and 200 ppm Fe^{2+} as an additive in a product grade of $\text{H}_3\text{PO}_4 - \text{H}_2\text{O}$ melt.

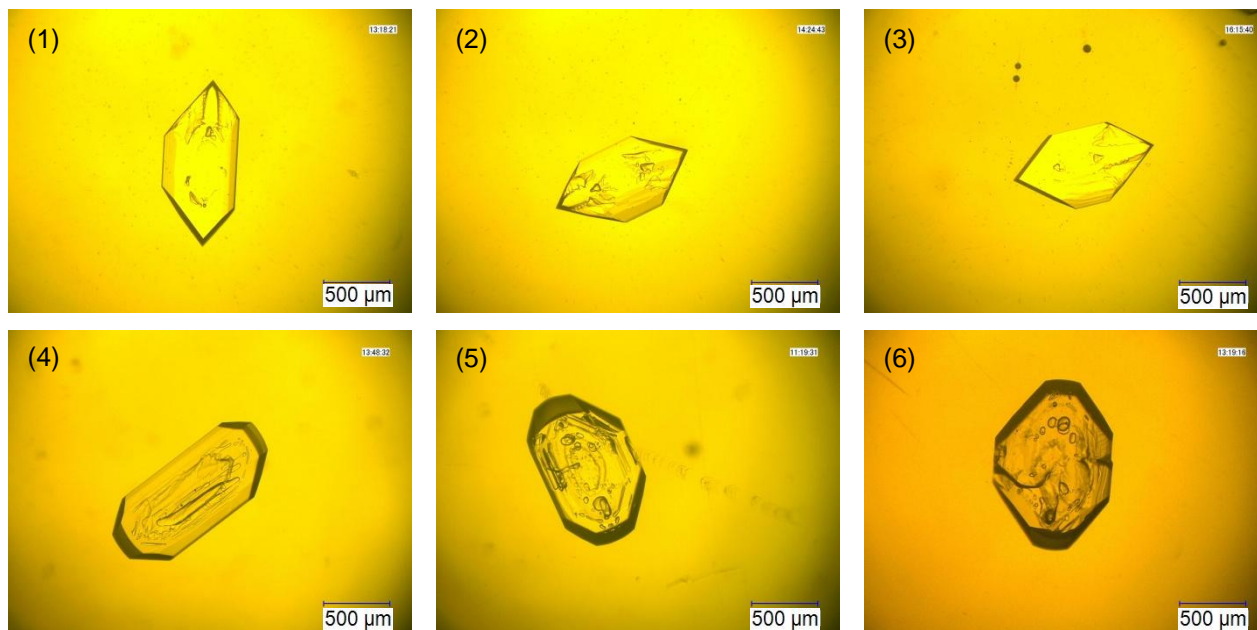


Figure 5.3.1.3-2: $\text{H}_3\text{PO}_4 \cdot 0.5\text{H}_2\text{O}$ crystals in a product grade of $\text{H}_3\text{PO}_4 - \text{H}_2\text{O}$ melt with (1), (2), (3) 100 ppm and (4), (5), (6) 200 ppm Fe^{2+} as an additive, $\Delta s = 0.65$ wt%.

Figure 5.3.1.3-1 shows that although 100 ppm Fe^{2+} has no significant effects on the growth rate, 200 ppm Fe^{2+} slows down the growth of crystals significantly. There would be a limited amount of Fe^{2+} that has no significant effect on the growth of crystals and this value would be no doubt between 100 and 200 ppm. In Figures 5.3.1.3-2 (1), (2), (3), three crystals show no difference to the ones which are from the food grade without additives. Figures 5.3.1.3-2 (4), (5), (6) show some differences. Compared with the ones with 100 ppm B additive (in the Chapter 5.3.1.2) Fe^{2+} blocks the tips of the crystals and they cannot be seen here. It may also be assumed that the vertexes are also two faces.

5.3.1.4 The effect of iron (III)

100 ppm Fe^{3+} (Fe_2O_3) was added into the $\text{H}_3\text{PO}_4 - \text{H}_2\text{O}$ melt in order to see its effect on the growth of $\text{H}_3\text{PO}_4 \cdot 0.5\text{H}_2\text{O}$ crystals. In the Chapter 5.1.2 it is shown that there is no change in the solubility of H_3PO_4 in water with 100 ppm Fe^{3+} as an additive. Therefore, the growth of the crystals with Fe^{3+} can be compared with the ones which are without additives at same supersaturation (0.65 wt%) and temperature (14 °C). The $\text{H}_3\text{PO}_4 - \text{H}_2\text{O}$ melt was used here is product grade and the growth rate data of the crystals and the images of the crystals are shown in Figures 5.3.1.4-1 and 5.3.1.4-2, respectively.

Similarly like the effect of 200 ppm Fe^{2+} , 100 ppm Fe^{3+} also decreases the growth of the crystals (see Figure 5.3.1.4-1). The boundary of faces $01\bar{1}$ and $0\bar{1}1$ are also blocked (see Figure 5.3.1.4-

2). It seems to be that Fe^{3+} does not have only the equivalent effect on the growth of the crystals compared to Fe^{2+} , but also in a lower amount compared to Fe^{2+} . The crystals defects are not clear here due to the slow growth rate.

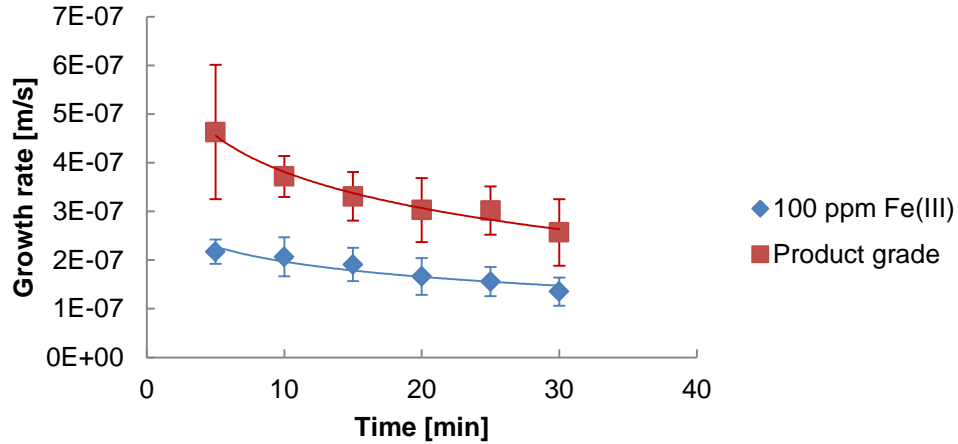


Figure 5.3.1.4-1: Average growth rates of $\text{H}_3\text{PO}_4 \cdot 0.5\text{H}_2\text{O}$ crystals with 100 ppm Fe^{3+} as an additive in a product grade of $\text{H}_3\text{PO}_4 - \text{H}_2\text{O}$ melt.

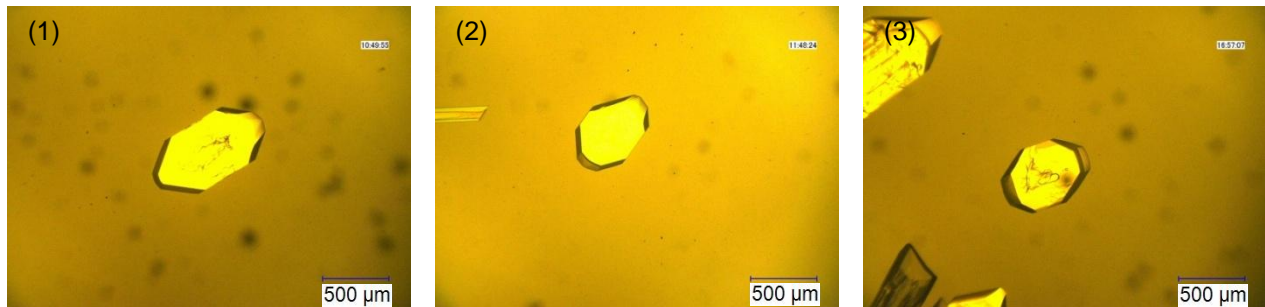


Figure 5.3.1.4-2: $\text{H}_3\text{PO}_4 \cdot 0.5\text{H}_2\text{O}$ crystals in a product grade of $\text{H}_3\text{PO}_4 - \text{H}_2\text{O}$ melt with 100 ppm Fe^{3+} as an additive, $\Delta s = 0.65$ wt%.

5.3.2 In-line measurements

Both FBRM's and 3D ORM's sensors were immersed in $\text{H}_3\text{PO}_4 - \text{H}_2\text{O}$ melt in order to compare their accuracy. During the measurements, it should be assured that the crystals in melt should always pass the sensors.

5.3.2.1 FBRM

The sensor that was used is 523 PsyA SSD and the software for the data analysis is WinORM. The results are shown in Figures 5.3.2.1-1 and 5.3.2.1-2.

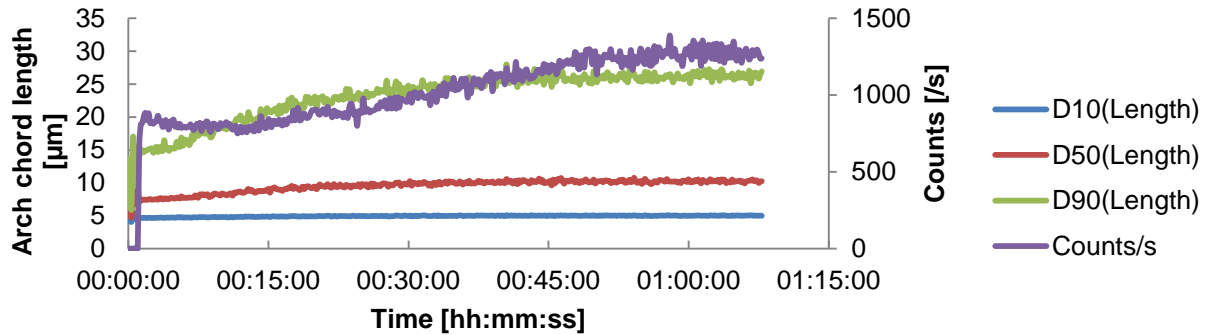


Figure 5.3.2.1-1: The growth rates (arch chord length increase per time) of $\text{H}_3\text{PO}_4 \cdot 0.5\text{H}_2\text{O}$ crystals started with $\Delta s = 1.5$ wt% at 16.7 °C (Data were collected by the FBRM sensor of 523 PsyA SSD and analyzed by the software of WinORM).

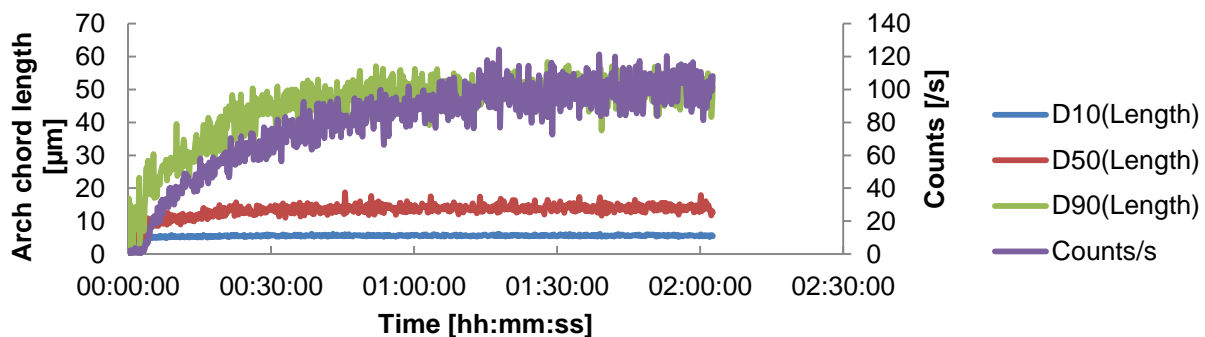


Figure 5.3.2.1-2: The growth rates (arch chord length increase per time) of $\text{H}_3\text{PO}_4 \cdot 0.5\text{H}_2\text{O}$ crystals started with $\Delta s = 0.5$ wt% at 19.8 °C (Data were collected by the FBRM sensor of 523 PsyA SSD and analyzed by the software of WinORM).

Two supersaturations (1.5 wt% and 0.5 wt%) were tested in this case. Each Figure contains four curves: counts, D10, D50 and D90. The counts numbers show how many particles could have been caught by the laser signal. The value of D10, D50 and D90 show how many of the particles in percentage are smaller than this value. For example in Figure 5.3.2.1-1, $D50 = 8$ µm at 15 min. That means there are 50 percent of particles that are smaller than 8 µm. It needs to be mentioned that the particle size which is measured by FBRM is the arch chord length. It does not directly show the original particle size. In addition, D10, D50 and D90 can also be presented based on particle length, surface area or volume.

In the beginning the $\text{H}_3\text{PO}_4 - \text{H}_2\text{O}$ melt was supersaturated. Later the crystallization started when the seeds were introduced at time 0 min. Nucleation appeared immediately after seeding

and the crystals started growing thereafter. During the time the supersaturation was decreasing and after a certain time (30 min) the crystals stopped growing and the mother liquor became saturated. From Figure 5.3.2.1-1 ($\Delta s = 1.5$ wt%) it can be seen that the particle counts immediately increases to 800 counts/s after seeding (few particles, 2 mm). After 2 min it increases slowly up to 1200 counts/s until 1 hour. This may be due to the breakage of the particles, the particle counts slightly increased. D10 and D90 show that most arch chord lengths of the particles are between 5 and 25 μm after 30 min and the median (D50) is approximately 10 μm . All the curves become stable after 1 hour and therefore the parts which are after 1 hour are not shown in Figure 5.3.2.1-1.

Similarly, in Figure 5.3.2.1-2 the particle counts increase to 100 counts/s after 1 hour, but in a slow speed compared to the ones in Figure 5.3.2.1-1. Most arch chord lengths of the particles are between 5 and 50 μm (D10 and D90) and the median (D50) is approximately 13 μm . All the numbers become constants after 1 hour. It shows that after a long time of crystallization at this supersaturation ($\Delta s = 0.5$ wt%) the particle size is bigger than the one at the higher supersaturation ($\Delta s = 1.5$ wt%) where the particles grow slower and the particle numbers at the supersaturation of 0.5 wt% are much less.

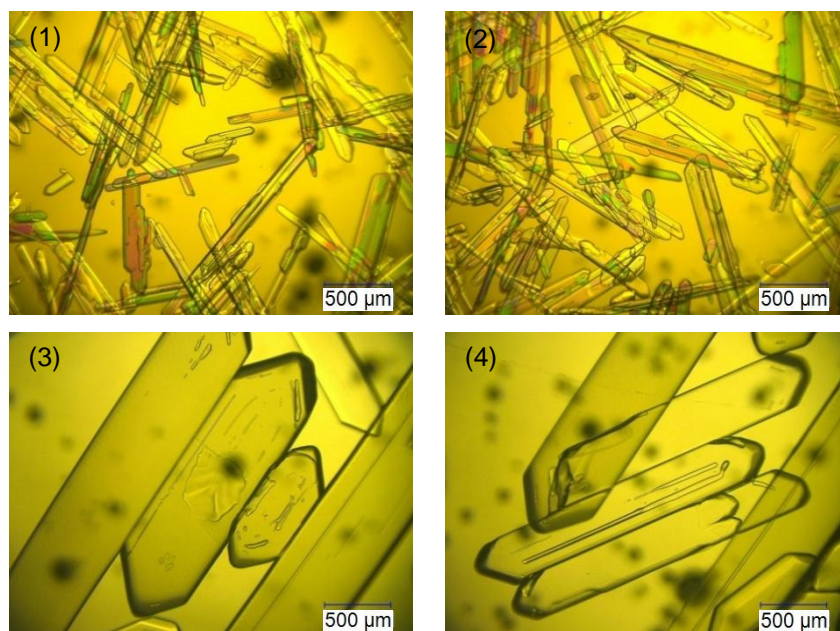


Figure 5.3.2.1-3: $\text{H}_3\text{PO}_4 \cdot 0.5\text{H}_2\text{O}$ crystals under the microscope: (1), (2) at $\Delta s = 1.5$ wt% at 16.7 °C and (3), (4) at $\Delta s = 0.5$ wt% at 19.8 °C.

Before to calculate the growth rate of the crystals, it is necessary to analyze how the arch chord length is related to the real size of the crystals. Figure 5.3.2.1-3 shows the images of the crystals at two different supersaturations under the microscope. The crystals were directly acquired from

the in-line measurement after they reached the equilibrium of the concentration of the liquid phase. It can be seen that, the crystals in Figures 5.3.2.1-3 (1) and (2) are approximately $1000 \times 100 \mu\text{m}$ and the crystals in Figures 5.3.2.1-3 (3) and (4) are approximately $2000 \times 500 \mu\text{m}$. Both sizes in two groups are much higher than the ones given from the analysis of the arch chord length. Therefore, it makes no sense to calculate the growth rate of the crystals according to the results from Figures 5.3.2.1-1 and 5.3.2.1-2.

5.3.2.2 3D ORM

The sensor that was used is APAS 14 and the software for the data analysis is MCSA 1.0.2.32. The measurements were taken at the same time as the FBRM measurements were taken in the same double-walled beaker so that the results can be compared with each other. Figures 5.3.2.2-1 and 5.3.2.2-2 show the results from 3D ORM measurements.

The difference to the FBRM measurement is that 3D ORM laser sensor scans the crystals and the software gives the surface area (as a virtual shape) rather than the arch chord length. Thereafter the related mean diameter will be calculated. In other words, the virtual crystal has the same surface area as the original crystal. If the crystal is cubic or a sphere the mean diameter may be the same as its real diameter. However, to a needle shape or a plate shape the mean diameter is different. From Figure 5.3.2.2-1 ($\Delta s = 1.5 \text{ wt}\%$) it can be seen that after 3 min from the seeding, the mean diameter of most crystals are between 100 and 650 μm (D10 and D90) and the median (D50) is approximately 400 μm . The counts number is approximately 300 counts/s, but with 50 counts/s fluctuation. The system reached its equilibrium after 15 min from the seeding. Similarly, from Figure 5.3.2.2-2 ($\Delta s = 0.5 \text{ wt}\%$), it shows that the mean diameter of

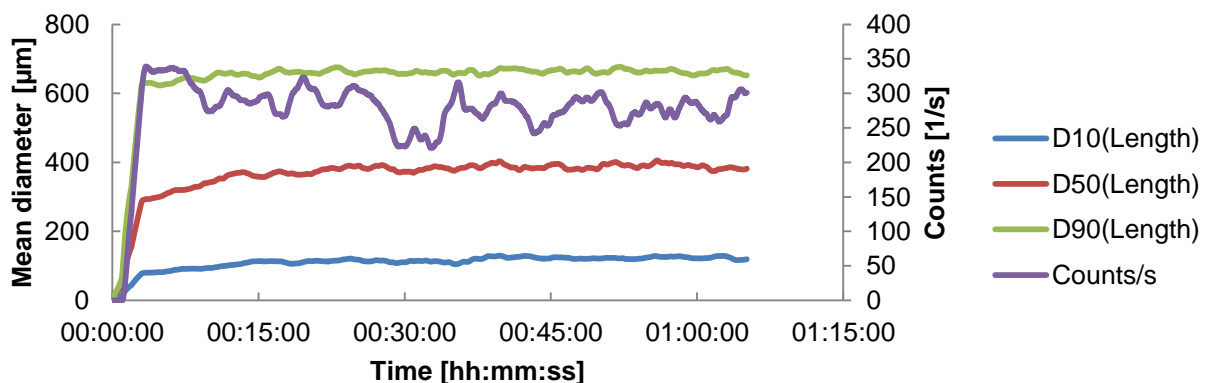


Figure 5.3.2.2-1: The growth rates (mean diameter increase per time) of $\text{H}_3\text{PO}_4 \cdot 0.5\text{H}_2\text{O}$ crystals started with $\Delta s = 1.5 \text{ wt}\%$ at $16.7 \text{ }^\circ\text{C}$ (Data were collected by the 3D ORM sensor of APAS 14 and analyzed by the software of MCSA 1.0.2.32).

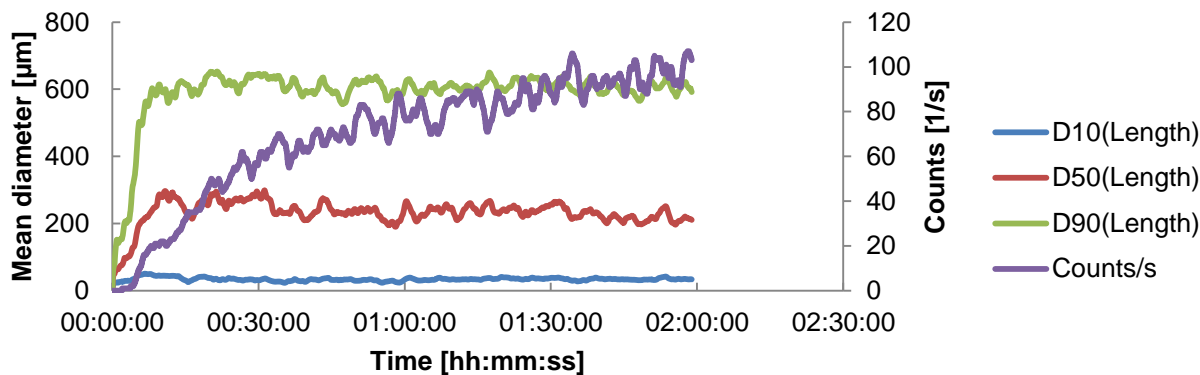


Figure 5.3.2.2-2: The growth rates (mean diameter increase per time) of $\text{H}_3\text{PO}_4 \cdot 0.5\text{H}_2\text{O}$ crystals started with $\Delta s = 0.5 \text{ wt}\%$ at $19.8 \text{ }^\circ\text{C}$ (Data were collected by the 3D ORM sensor of APAS 14 and analyzed by the software of MCSA 1.0.2.32).

most crystals are between 35 and 600 μm (D10 and D90) and the median (D50) is approximately 230 μm . The counts number reached 100 counts/s after 1h30min from the seeding. The mean diameter of the crystals does not change too much after 8 min from the seeding, but the counts number was slowly increasing to 100 count/s after 1h30min. Therefore, the system reached its equilibrium after this time. It can be seen that by the 3D ORM the size of the crystals at a lower supersaturation ($\Delta s = 0.5 \text{ wt}\%$) is smaller than the one at the higher supersaturation ($\Delta s = 1.5 \text{ wt}\%$) and the number of counts is less. These results are slightly different than the ones by the FBRM.

Figure 5.3.2.1-3 already showed the images of the crystals under the microscope. From these images, the surface area of the crystals can be calculated. If the scanned surface area is transferred to a circle, then the mean diameter can easily be calculated. In Figure 5.3.2.1-3 (1), (2) (crystal size: $1000 \times 100 \mu\text{m}$) the mean diameter of the crystals is approximately 360 μm and in Figure 5.3.2.1-3 (3), (4) (crystal size: $2000 \times 500 \mu\text{m}$) the mean diameter of the crystals is approximately 1100 μm . Compared to these two values the mean diameter which were measured at the supersaturation of 1.5 wt% is closer, but not the one at the supersaturation of 0.5 wt%. It could be that at this supersaturation (0.5 wt%) the shape of the crystals is more like a plate. The width is longer than the thickness, and most of the time during the 3D ORM measurement the laser is not perpendicular to the surface of the plates. In other words the scanned surface area is not always $2000 \times 500 \mu\text{m}$. That is why the mean diameter from 3D ORM measurements is smaller than the ones which are from the microscope measurements. At the other supersaturation (1.5 wt%) the width of the crystals is not much longer than the thickness. Therefore, the scanned surface area may not have a too big difference. Additionally, some

sieved NaCl crystals (160-250 μm , cubic) were tested by 3D ORM in order to see whether the mean diameter can be used to describe the growth rates of the crystals. The results show that the mean diameter of NaCl lies in the range of 160-250 μm . Therefore, it is proven that the mean diameter of the $\text{H}_3\text{PO}_4 \cdot 0.5\text{H}_2\text{O}$ crystals which is measured from 3D ORM can be used to monitor the size change of the crystals in melt.

According to Figures 5.3.2.2-1 and 5.3.2.2-2, the growth rate of the crystals after seeding can be calculated. The values are equal to the slopes of the curves which are measured after the seeding and until the curves go into platforms. If the curves of D50 are used the growth rates of the crystals at the supersaturation of 1.5 wt% will be approximately 2.5×10^{-6} m/s and the ones at the supersaturation of 0.5 wt% will be approximately 4.2×10^{-7} m/s. Compared to the growth rates which were measured by the off-line measurement (1.5×10^{-6} m/s at $\Delta s = 1.5$ wt% and 2.0×10^{-7} m/s at $\Delta s = 0.5$ wt%, according to the equation in Figure 5.3.1.1-4), the ones which are from 3D ORM have the same order of magnitude. Due to the high deviation of the growth rates, it can be concluded that the growth rates which were measured by 3D ORM are equal to the ones which were measured by the off-line measurements.

5.4 The distribution coefficient of crystallization and post treatments

5.4.1 The distribution coefficient of crystallization

The distribution coefficient K_d describes the distribution of an element in two different phases. To the distribution coefficient of iron $K_d(\text{Fe})$ it is defined as in Equation 5.4.1-1.

$$K_d \text{ Fe} = \frac{x(\text{Fe}, \text{crystals})}{x(\text{Fe}, \text{feed})} \quad \text{Equation 5.4.1-1}$$

$x(\text{Fe}, \text{crystals})$ is the concentration of iron in crystals, [ppm], and $x(\text{Fe}, \text{feed})$ is the concentration of iron in feed, [ppm]. Since iron is one of impurities in the $\text{H}_3\text{PO}_4 - \text{H}_2\text{O}$ melt, if $K_d(\text{Fe}) = 0$ it shows a perfect separation after the crystallization, and if $K_d(\text{Fe}) = 1$ there is no separation after the crystallization. In this chapter iron as the key element of impurities is studied and all the efficiency of separation tests were based on the change of iron concentration.

Figure 5.4.1-1 shows the relationship of the iron distribution coefficient K_d and the supersaturations of the melt after the crystallization. The retention time of the crystallization was kept for 2 h.

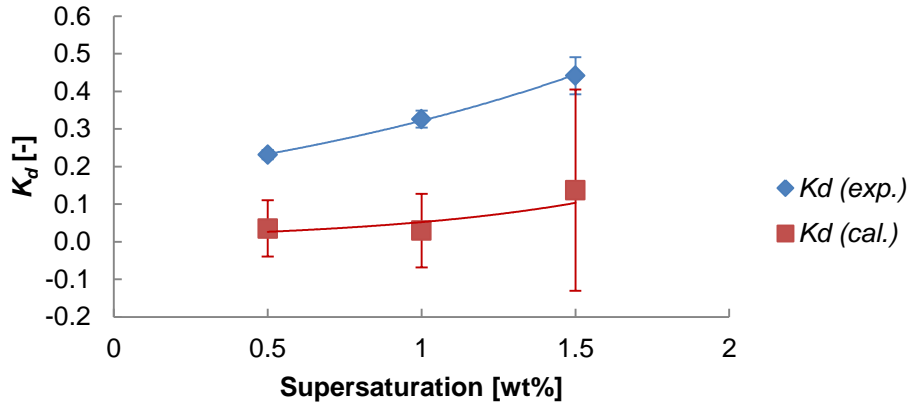


Figure 5.4.1-1: The relationship of the iron distribution coefficient K_d and the supersaturations of the melt after 2 h crystallization.

There are two curves in Figure 5.4.1-1. $K_d(\text{exp.})$ was obtained from the analysis results in the lab. It is defined as in Equation 5.4.1-2. Both the iron concentrations in the crystals and in the feed were measured by the UV-Vis spectroscopy at 510 nm.

$$K_d \text{ exp.} = \frac{x(\text{Fe, exp. in crystals})}{x(\text{Fe, exp. in feed})} \quad \text{Equation 5.4.1-2}$$

$K_d(\text{cal.})$ shows the theoretical concentration of iron in the crystals compared to the one in the feed. Due to the mass balance of iron during crystallization the theoretical concentration of iron in the crystals can be calculated according to Equation 5.4.1-3, and therefore $K_d(\text{cal.})$ can be described in Equation 5.4.1-4.

$$x \text{ Fe, cal. in crystals} = \frac{m \text{ feed} \cdot x \text{ Fe, exp. in feed} - m(\text{ML}) \cdot x(\text{Fe, exp. in ML})}{m(\text{crystals})} \quad \text{Equation 5.4.1-3}$$

$$K_d \text{ cal.} = \frac{x(\text{Fe, cal. in crystals})}{x(\text{Fe, exp. in feed})} \quad \text{Equation 5.4.1-4}$$

$m(\text{feed})$, $m(\text{ML})$ and $m(\text{crystals})$ are the mass of the feed, the mother liquor and the crystals, [kg], respectively.

After crystallization the crystals cannot completely be separated with the mother liquor by a filtration. Since iron is enriched in the mother liquor the concentration of iron from the UV-Vis spectroscopy is, in principle, higher than the value which is from the calculation. This can be proven by Figure 5.4.1-1. $K_d(\text{exp.})$ is higher than $K_d(\text{cal.})$ at the respected supersaturation. The deviations of $K_d(\text{cal.})$ are large. It may give us some information that iron does not distribute homogenously in the mother liquor and in the crystals. Therefore, it might have a slight

difference compared to the mass balance calculation of iron. On the other hand, $K_d(exp.)$ increases when the supersaturation is increasing. It shows that increasing the supersaturation does not give a positive effect on the efficiency of separation. It could be explained that a higher supersaturation gives a faster growth of crystals. If there are some inclusions of iron in the crystals, it cannot diffuse out of the crystals in time. A high supersaturation also leads to a higher number of crystals and smaller crystals if the agitation speed does not change. A high amount of small crystals give large surface areas on which the mother liquor can be attached. Hence, the distribution coefficient K_d is higher than the one with a low supersaturation.

Figure 5.4.1-2 shows the relationship of the distribution coefficient K_d and the time of the crystallization after seeding. The supersaturation was kept at 1 wt% as a constant. In this figure $K_d(exp.)$ and $K_d(cal.)$ have the same meaning as the ones in Figure 5.4.1-1. Similarly, the values of $K_d(exp.)$ are higher than the ones of $K_d(cal.)$ due to the imperfect separation of the mother liquor and the crystals during a filtration. Both $K_d(exp.)$ and $K_d(cal.)$ decrease when the crystallization time is increasing. It shows that a longer time of crystallization can have a better separation of iron. It gives enough time that the iron can diffuse out of the crystals into the mother liquor.

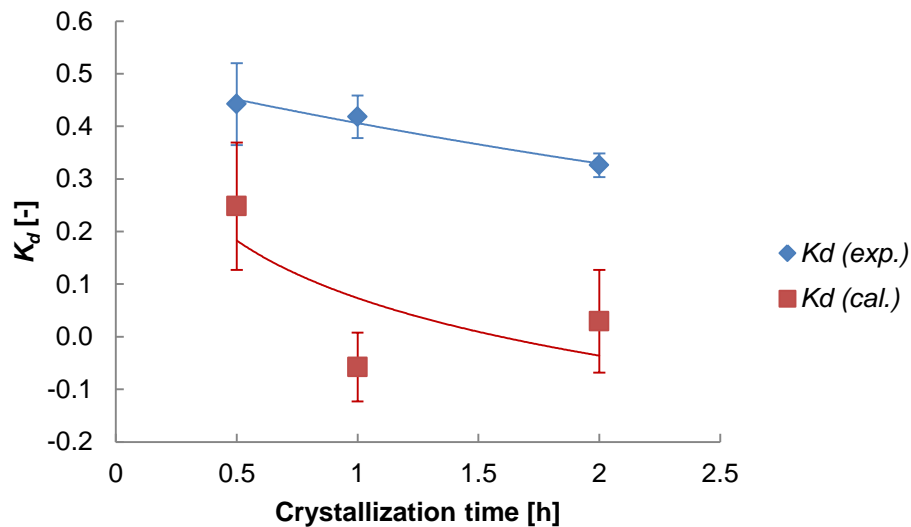


Figure 5.4.1-2: The relationship of the iron distribution coefficient K_d and the retention time of the crystallization after seeding. ($\Delta s = 1$ wt%).

Additionally, after filtration if the concentration of iron in the attached mother liquor on the surface of the crystals is assumed to be the same as the concentration of iron in the mother liquor, the amount of the attached mother liquor can be calculated according to Equation 5.4.1-5:

$$\frac{m(ML, attached)}{m(crystals)} = \frac{K_d \text{ exp.} - K_d(cal.)}{\frac{x(Fe, exp. in ML)}{x(Fe, exp. in feed)} - K_d(exp.)} \times 100\% \quad \text{Equation 5.4.1-5}$$

After calculation there is approximately 30-40 wt% mother liquor which is attached on the surface of the crystals compared to the mass of the crystals.

It needs to be mentioned that all the results which are discussed before are based on the initial concentration of iron of 100 ppm. If the initial concentration of iron in feed decreases to 0.5 ppm both $K_d(exp.)$ and $K_d(cal.)$ will be close to 1 with high deviations. Here, the low concentrations of iron in the samples were analyzed by ICP-OES instead of UV-Vis spectroscopy due to the fact that the UV-Vis spectroscopy does not have enough sensitivity to the low amount of iron. The values of $K_d(exp.)$ and $K_d(cal.)$ may show that there are no separation after the crystallization. This may be because there is a weak interaction between phosphoric acid and iron which is similar to a chelation. The low amount of iron cannot easily be separated by crystallization. Therefore, some chelating agents, for example EDTA, were used so that the iron may be chelated by a chelating agent and further be removed by crystallization. This will be discussed in details in the Chapters 5.4.3 and 6.4.2.

5.4.2 The distribution coefficient of post treatments

After the filtration the crystals were washed by a washing liquid as a step of a post treatment. Here, “washing” means the crystals are immersed in a certain amount of wash liquid with agitation for a certain time. Thereafter, they will be filtrated and the concentration of iron in the crystals will be analyzed by the UV-Vis spectroscopy. The wash liquid can be a saturated pure $H_3PO_4 - H_2O$ melt or the initial feed which is before the crystallization. Therefore, the temperature of washing is the saturation temperature of the wash liquid. The idea that using the feed as a wash liquid is that pure $H_3PO_4 - H_2O$ melt is a part of the product. If it is used as a wash liquid the yield of purification process will decrease. On the surface of the crystals the mother liquor which enriches to high amounts of iron are attached. The concentration of iron here is higher than the one in the feed, and therefore, the feed is chosen as a wash liquid. To compare the efficiency of washing by the two wash liquids, pure $H_3PO_4 - H_2O$ melt and the feed, Figure 5.4.2-1 shows the results.

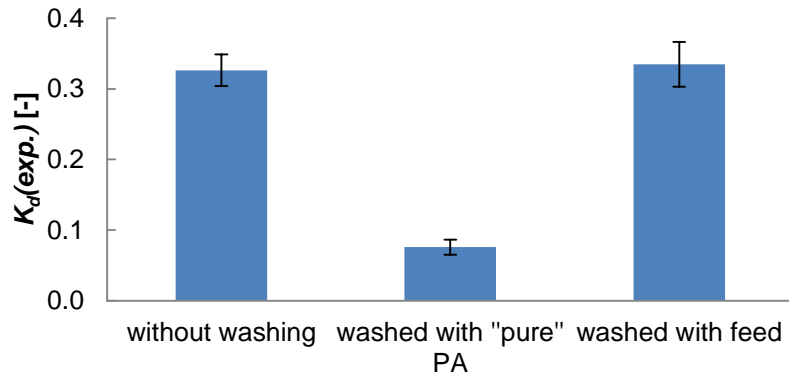


Figure 5.4.2-1: The distribution coefficient K_d after the washing by different wash liquids and without washing ($m(\text{wash liquid}):m(\text{crystals}) = 2:1$, washing time = 30 min).

The crystals which were used here were from the group of crystallization at supersaturation of 1 wt% and the crystallization time of 2 h. The amount of the wash liquid which was used is two times of the mass of the crystals. It needs to be mentioned that although the pure $\text{H}_3\text{PO}_4 - \text{H}_2\text{O}$ melt was used as a wash liquid, it still contains approximately 0.5 ppm iron. It can be seen from Figure 5.4.2-1 that the group which is washed with “pure” PA (phosphoric acid) melt gives a positive effect on the separation of iron. It improves K_d down to less than 0.1 which means the purity of the product was increased by 90 % after the crystallization and washing. The group which is washed with the feed does not show any effects on the separation of iron. It can be concluded that using the feed as a wash liquid to avoid the loss of product is impossible.

To continue the tests of washing by the pure $\text{H}_3\text{PO}_4 - \text{H}_2\text{O}$ melt the time of the washing has changed and the results are shown in Figure 5.4.2-2.

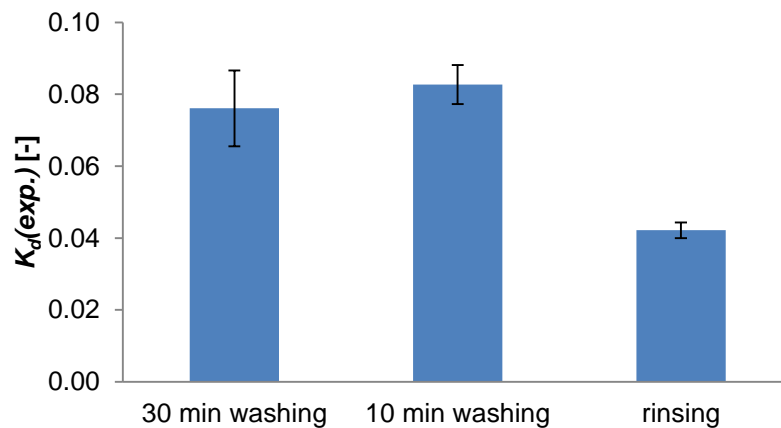


Figure 5.4.2-2: The distribution coefficient K_d after the different time of washing ($m(\text{wash liquid}):m(\text{crystals}) = 2:1$).

There are three groups in Figure 5.4.2-2. “Rinsing” means that the crystals were simply rinsed with the pure $\text{H}_3\text{PO}_4 - \text{H}_2\text{O}$ melt instead of immersing the wash liquid with agitation. The washing time could be set to zero. It can be seen that the group of 30 minutes washing shows a slightly smaller K_d compared to the group of 10 minutes washing. It could be explained that during the washing the iron diffused into the wash liquid and its concentration on the surface of the crystals decreases. The longer the washing time is, the better is the purity of the crystals. Therefore, after the filtration the group of 30 minutes washing has a slightly better separation compared to the group of 10 minutes washing. Compared to these two groups the group of rinsing shows a much better effect on the separation. It significantly improves the K_d to less than 0.05 which means the quality of the material is improved more than 95 % compared to the initial feed. This could be because the attached mother liquor on the surface of the crystals is partially replaced by the wash liquid. In the Chapter 5.4.1 it is calculated that the amount of the attached mother liquor is approximately 30-40 wt% compared to the mass of the crystals. Considered this the K_d obviously decreases after the rinsing and the purity of the wet crystals is improved. Thereafter, the amount of rinsing liquid has changed from 2:1 to 1:1, 1:2 and 1:5 according to the mass of the crystals. The K_d of different groups were analyzed and the results are shown in Figure 5.4.2-3.

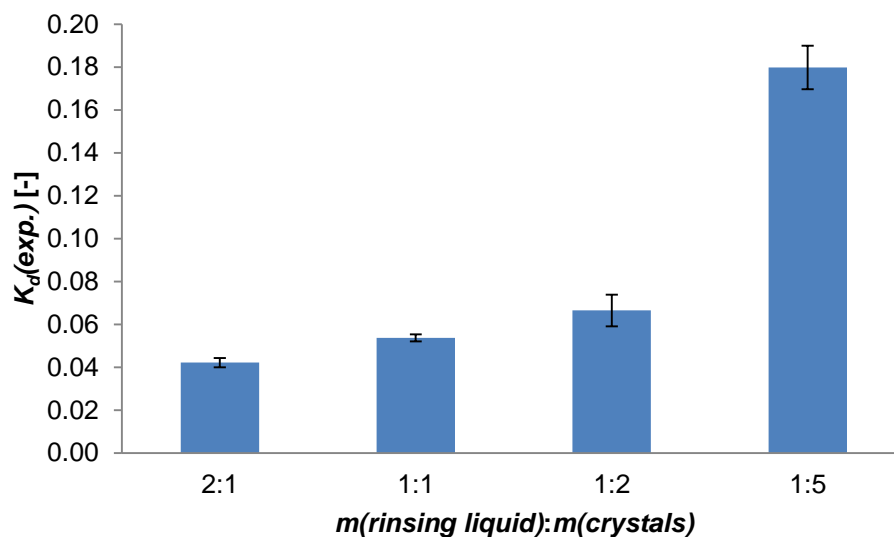


Figure 5.4.2-3: The distribution coefficient K_d after the different amount of rinsing liquid.

It can be seen from Figure 5.4.2-3 that a high amount of rinsing liquid gives a lower K_d which means a better separation. However, due to the fact that the rinsing liquid is a part of the product there will be no output of the product if the ratio of $m(\text{rinsing liquid})/m(\text{crystals})$ is higher than 1. Although the group of 2:1 gives the best K_d of the four groups, it does not make sense during the

production. The more the rinsing liquid is used, the less the product can be obtained. Compared to the result ($K_d(\text{exp.}) = 0.326 \pm 0.022$) of the unwashed wet crystals which were obtained at supersaturation of 1 wt% in Figure 5.4.1-1 the group of the ratio of $m(\text{rinsing liquid})/m(\text{crystals}) = 1:2$ ($K_d(\text{exp.}) = 0.066 \pm 0.007$) improves the purity of the crystals by approximately 80 %. Compared to the $K_d(\text{cal.})$ (0.029 ± 0.098) in Figure 5.4.1-1 at the supersaturation of 1 wt% the $K_d(\text{exp.})$ in the group of 1:2 is closer. In other words rinsing makes effective purification as a way of the post treatments. Combined with the crystallization, it can improve the purity of the material by approximately 93 %.

5.4.3 The effects of chelating agents

Since one of the interested impurities is iron, it can be chelated with many chelating agents such as EDTA and HEDP. Phosphoric acid as a weak chelating agent also has a weak combination with iron. If a stronger chelating agent can combine with the iron instead of phosphoric acid, the complex may be removed after the crystallization. The stability constant $pK(\text{Fe}^{3+})$ evaluates the strength of the combination between a chelating agent and iron. It strongly depends on the pH of the solution. Figure 5.4.3-1 [Sun10] shows the stability constants $pK(\text{Fe}^{3+})$ of some chelating agents at different pH.

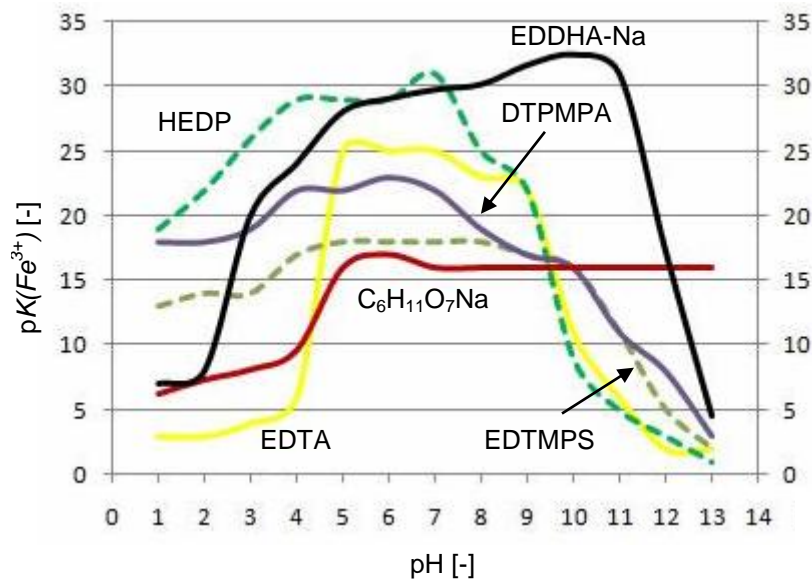


Figure 5.4.3-1: The stability constants $pK(\text{Fe}^{3+})$ of different chelating agents at different pH [Sun10].

It can be seen from Figure 5.4.3-1 that most of the chelating agents have their maximum stability constants between pH 5 and 8. However, an 85 wt% $\text{H}_3\text{PO}_4 - \text{H}_2\text{O}$ melt has a pH of approximately 0 at room temperature. Even though Diallo et al. [Dia13] mentioned in their

research that the reliability of pH measurement in very acid media is not good and sufficiently convincing, it still tells us that at such low pH the stability constants $pK(Fe^{3+})$ of the chelating agents are not high enough compared to their maximum values. Therefore, a series screening tests of chelating agents (1000 ppm EDTA, 1500 ppm HEDP, 1500 ppm DTPMPA, 10 ppm oxalic acid, 15 ppm ATMP (Cublen) and 1500 ppm pyrophosphoric acid) were tested in order to see whether there is a purity improvement after the crystallization. The amounts of the chelating agents are based on 100 ppm iron (EDTA, HEDP, DTPMA and pyrophosphoric acid) and 1 ppm iron (oxalic acid, ATMP and pyrophosphoric acid). After the crystallization the distribution coefficient $K_d(exp.)$ were measured and they are shown in Figures 5.4.3-2 and 5.4.3-3. In Figure 5.4.3-2 the group which has no chelating agent addition is also shown to be compared with the other groups. The crystals in all groups were crystallized at the initial supersaturation of 1.5 wt% for 2 h with agitation.

It can be seen that all $K_d(exp.)$ in Figures 5.4.3-2 and 5.4.3-3 are between 0.5 and 0.6. Considering the deviation of the tests it could be said that all the chelating agents which were tested here do not improve the separation of iron by crystallization. It needs to be mentioned that during the concentration analysis of iron by UV-Vis spectroscopy the color change which was from the group of chelating agents addition was slower than the one which does not contain any chelating agents. It may tell us an information that the iron may be combined with the chelating agents during the crystallization. After separation the chelates distribute as same as the iron only. Therefore, the $K_d(exp.)$ does not show any difference. However, the slow color change which was mentioned before was after the adjustment of pH (to 4.5). It may also show that the iron was not combined with the chelating agents during the crystallization due to the low pH of $H_3PO_4 - H_2O$ melt.

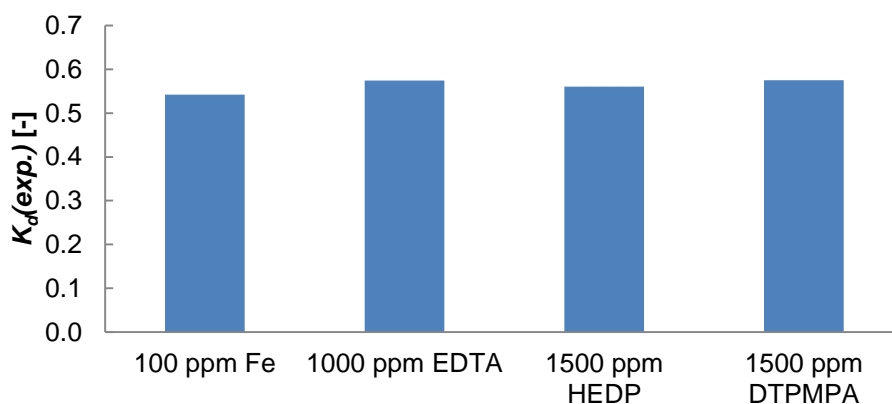


Figure 5.4.3-2: The distribution coefficient $K_d(exp.)$ after the crystallization without and with different chelating agents additives (100 ppm iron in the feed).

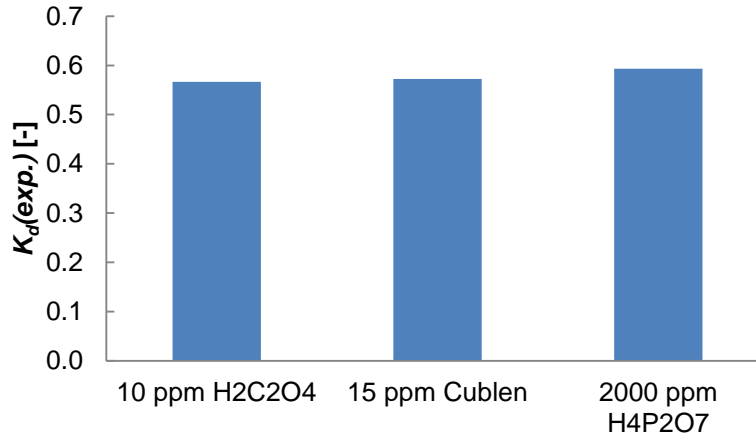


Figure 5.4.3-3: The distribution coefficient $K_d(\text{exp.})$ after the crystallization with different chelating agents additives (1 ppm iron in the feed).

Additionally, Diallo et al. [Dia13] summarized the stability constant pK of iron and phosphoric acid from literatures. In their studies there are four different kinds of chelates between iron and phosphate and they as well as their stability constants are shown in Table 5.4.3-1.

Table 5.4.3-1: The stability constants pK of different combination forms of iron and phosphate [Dia13].

Chelates	pK	Literatures
$\text{Fe}(\text{H}_2\text{PO}_4)_4^-$	9.15	[Ram54]
$\text{Fe}(\text{H}_2\text{PO}_4)_2^{2+}$	3.47-3.61	[Ram54, Gal63, Boh69, Sid73, Wil85]
$\text{Fe}(\text{HPO}_4)_2^-$	13.17	[Fil74]
$\text{Fe}(\text{HPO}_4)^+$	8.13-9.35	[Ram54, Gal63, Boh69, Sid73, Rin67]

In Table 5.4.3-1 the stability constants pK of cations are lower than the ones of anions. In other words the forms of cations, especially, the form of $\text{Fe}(\text{H}_2\text{PO}_4)_2^{2+}$, are not stable in the solution compared to the forms of anions. They will be replaced by the forms of anions, for example $\text{Fe}(\text{HPO}_4)_2^-$ ($pK = 13.17$). All the forms of ions which were analyzed are under the pH of 3 or even below. Therefore, according to the pK s in Figure 5.4.3-1 HEDP ($pK = 25$) and DTPMPA ($pK = 19$) have higher pK s and they can be chelated with the iron instead of phosphate below the pH of 3. However, the $K_d(\text{exp.})$ of HEDP and DTPMPA in Figure 5.4.3-2 show that there are no improvements even though HEDP and DTPMPA are chelated with iron instead of phosphate. The chelates are simply attached on or are included in the crystals during the crystallization process. Thus, adding a chelating agent does not give any positive effects on the process of purification.

5.5 The permeability measurements of the crystal bed

Phosphoric acid hemihydrate crystals are monoclinic crystals and have a needle like shape. During the preparation of the crystals the crystals may have different length due to the crystal breakage or the friction. However, their width does not change. Therefore, to represent a crystal size its width is used.

Three different widths of the crystals are shown in Figure 5.5-1. To prepare different sizes of the crystals different supersaturations and different stirring speeds were used, and they are shown in Table 5.5-1. It can be seen that with a low supersaturation and a slow stirring speed the width of the crystals is big (about 350 μm). The crystals from the three groups were used further for the filtration tests.

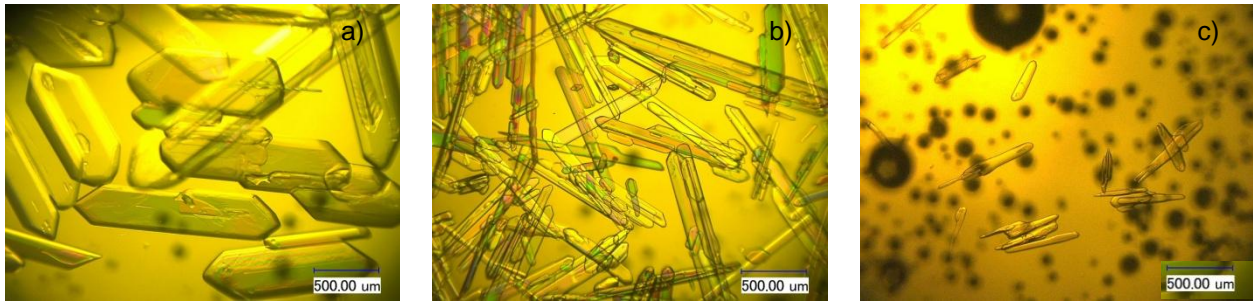


Figure 5.5-1: Phosphoric acid hemihydrate crystals: a) approx. 350 μm , b) approx. 110 μm and c) approx. 90 μm .

Table 5.5-1: Parameters of crystallization that were used for the preparation of $\text{H}_3\text{PO}_4 \cdot 0.5\text{H}_2\text{O}$ crystals.

Group	Supersaturation, [wt%]	Stirring speed, [rpm]	Width of crystals, [μm]
a)	0.5	100	~350
b)	1.5	100	~110
c)	1.5	300	~90

5.5.1 The porosity of the crystal bed

The porosity ε of the crystal bed after filtration is calculated according to Equation 5.5.1-1:

$$\varepsilon = 1 - \frac{m_{crystals}}{\rho_{crystals} h_c A} \times 100\% \quad \text{Equation 5.5.1-1}$$

where, $m_{crystals}$ is the mass of the crystals, [kg], $\rho_{crystals}$ is the density of the crystals, [kg/m^3], h_c is the height of the crystal bed after filtration, [m], and A is the cross section area of the thermostated glass tube, [m^2].

After calculation the porosities of the three groups (a), b) and c)) are listed in Table 5.5.1-1. All the porosities are based on the filtration tests at a pressure drop of 90 kPa (0.9 bar). It can be seen that a crystal bed with small crystals (group c)) has a slightly lower porosity than the other groups. However, it does not decrease much when the size of the crystals decreases. The porosity of a crystal bed may decrease when a high pressure drop is introduced due to the fact that the crystal bed can be compressed. To describe this property the compressibility factor s is introduced and discussed in detail in the Chapter 5.5.2.

Table 5.5.1-1: The properties of the crystal beds.

Group	Crystal bed porosity ϵ [%]	Crystal bed permeability B_c at 3 bar [m^2]	Compressibility factor s [-]
a)	70.8±1.4	$4.71 \times 10^{-10} \pm 3.83 \times 10^{-10}$	0.048±0.591
b)	69.1±0.9	$3.07 \times 10^{-11} \pm 9.92 \times 10^{-12}$	0.194±0.214
c)	68.6±1.4	$3.93 \times 10^{-11} \pm 2.23 \times 10^{-11}$	0.026±0.283

5.5.2 The permeability and the compressibility of the crystal bed

van der Sluis [Slu87] recorded the filtrate volume and the respect filtration time, but in our case the height h of suspension in the thermostated glass tube and the respect filtration time is recorded instead. As an example from group b) Figures 5.5.2-1 and 5.5.2-2 show the linear relationships of $\Delta t/\Delta h \sim h$ and $\log k \sim \log \Delta p$.

According to Equation 3.4.2-8 the line in Figure 5.5.2-1 matches it well ($R^2 = 0.9926$). The slope k can further be used to calculate the permeability B_c of the crystal bed under this pressure drop (90 kPa) according to Equation 3.4-9. To calculate a permeability of the crystal bed at other pressure drops, especially, a high pressure drop which cannot easily be reached in a lab trial, some low pressure drops were tested, and the respected lines and the slopes can be obtained. Thereafter, according to Equation 3.4.3-3 $\log k \sim \log \Delta p$ can be plotted as a linear line ($R^2 = 0.9952$) as shown in Figure 5.5.2-2. The slope of the line in Figure 5.5.2-2 can further be used to calculate the compressibility factor s . All the permeabilities B_c at a pressure drop of 3 bar and the compressibility factors s of the three groups are listed in Table 5.5.1-1.

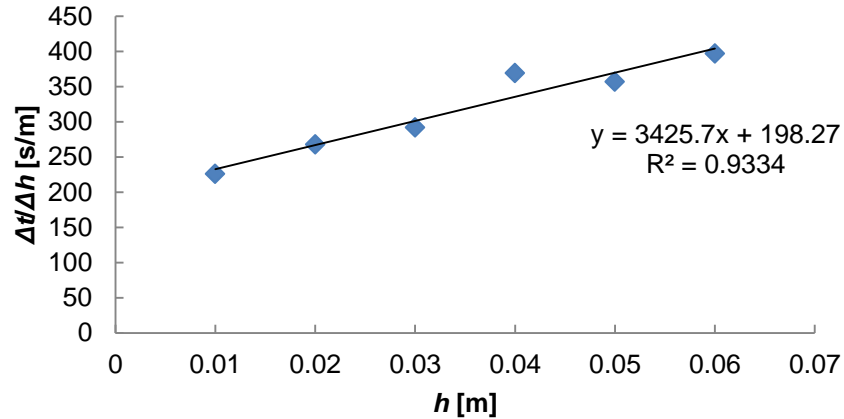


Figure 5.5.2-1: The relationship of $\Delta t/\Delta h$ and the height h of suspension at the pressure drop of 90 kPa (crystals are from group b)).

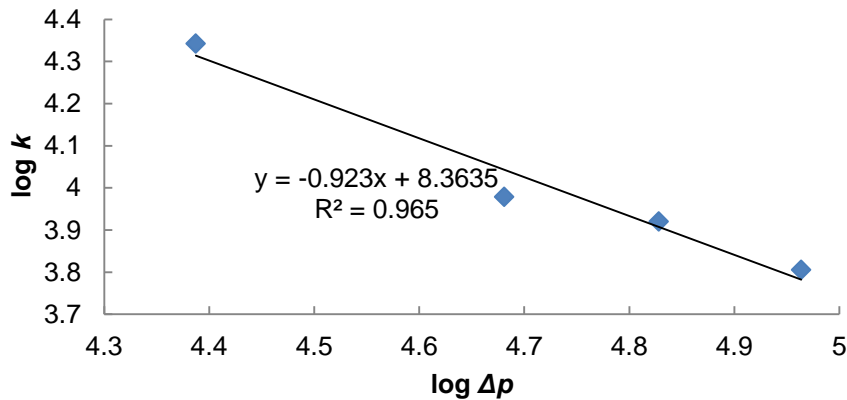


Figure 5.5.2-2: The relationship of log k and log Δp from group b).

As to be seen group a) has a high permeability compared to the other groups. This may be due to the fact that large crystals make bigger pores in the crystal bed. However, in a hydraulic wash column the permeability of a crystal bed should be in a specific range. A too high permeability can decrease the retention time of the crystals and it is not necessary to use a hydraulic wash column. A gravity wash column can be used instead. A too low permeability can increase the difficulty of the operation of the wash column, especially, by increasing the pressure drop of the wash column. van Oord-Knol [Oor00] used two different hydraulic wash columns (TNO-MEP and TNO-Thijssen) in her trials. The TNO-MEP column is an 8 cm diameter hydraulic wash column which needs a permeability of the crystal bed between 1.80×10^{-11} and 7.56×10^{-10} m². The TNO-Thijssen column is a 6 cm hydraulic wash column and it needs a permeability of crystal bed

between 2.6×10^{-11} and 1.2×10^{-10} m². If a pressure drop of 3 bar is used, the permeabilities of the crystal beds in group b) and c) (shown in Table 5.5.1-1) can be used in this two wash columns.

From Table 5.5.1-1 it also can be seen that the three groups have different compressibilities of the crystal beds. The compressibility factors s of group a) and c) are close to 0 (group a): 0.044 and group c): 0.026). In other words their crystal beds are hardly compressible. To prove this the height of the crystal bed can be monitored during the filtration tests using different pressure drops (0-1 bar). The heights of the crystal beds of group a) and c) did not show a significant change. However, the crystal bed height of group b) decreased during increasing pressure drop. Its porosity therefore decreased (approx. 2%). Figure 5.5.2-3 shows the relationship between the permeability B_c of the crystal bed and the pressure drop in group b). It can be seen that a high pressure drop can compress the crystal bed and therefore the permeability decreases. However, the compressibility factor of the crystal bed in group b) is not high ($s = 0.281$), and therefore the crystal bed only can be partially compressed. If a higher pressure drop is introduced, for example $\Delta p = 3$ bar, the permeability of the crystal bed will not decrease too much (see in Table 5.5.1-1).

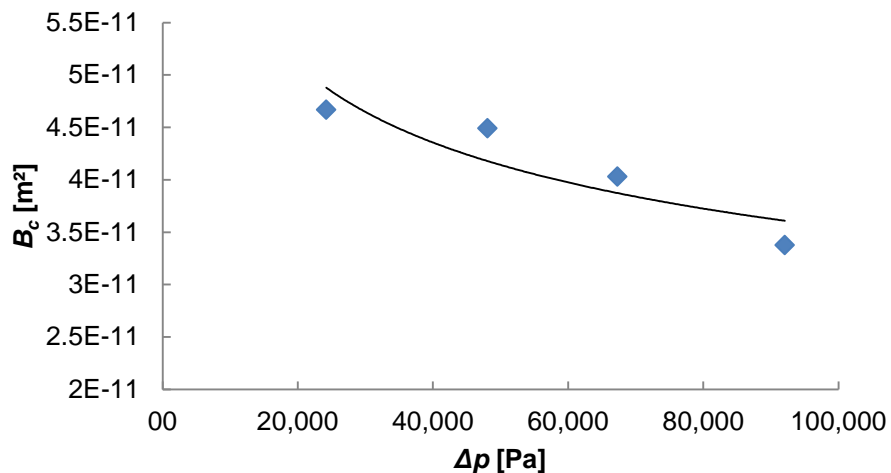


Figure 5.5.2-3: The relationship of permeability B_c and pressure drop Δp in group b).

5.6 The mass balance of the pilot plant

Based on the results of the purification in the lab scale the mass balance calculations of a pilot plant which contains a crystallizer ($V = 1$ m³) and a hydraulic wash column ($\Phi = 55$ cm) are undertaken in this chapter. The flow diagram of a phosphoric acid pilot plant and its mass

balance of the flows are shown in Figure 5.6-1. There are several assumptions for the calculations:

- There is no steering flow between the crystallizer and the hydraulic wash column.
- The temperatures of the mother liquor (outlet and recycle) are equal to the temperature of the crystallization in the crystallizer.
- A solid content in the crystallizer gives a distribution coefficient K_d regardless of the stirring speed and the retention time of the crystallization process.
- There is no heat energy loss in the pilot plant.

Several parameters should be given to start the calculations. They are (see the yellow cells in Figure 5.6-1):

- Flow rates of feed, water input, mother liquor recycle and product output, [kg/h]
- Phosphoric acid concentration of feed, [wt%]
- Temperatures of feed, water input, product output (should be higher than its saturation temperature), [°C]
- Temperature of the crystallization process in the crystallizer, [°C]
- Impurity concentration (Fe^{3+}) in feed, [ppm]

5.6.1 The calculations of the mass balance of the pilot plant

- Feed

Since most of the parameters are given the density of the feed is the only parameter that needs to be calculated. Here is [Jia11]:

$$\rho_{H_3PO_4} = 0.6824 + 1.208 \times 10^{-2} x_{feed} - 1.238 \times 10^{-3} - 3.794 \times 10^{-6} x_{feed} T_{feed}$$

Equation 5.6.1-1

where, $\rho_{H_3PO_4}$ is the density of phosphoric acid, [g/cm³], x_{feed} is the phosphoric acid concentration of feed, [wt%] and T_{feed} is the temperature of feed, [°C].

- Crystallizer

In the crystallizer the equilibrium concentration of mother liquor is equal to the solubility of phosphoric acid in the respected temperature of the crystallization [Smi09]:

Feed	Flow rate =	610	kg/h
	Concentration =	85	wt%
	Temperature =	25	°C
	Density =	1.6864	g/cm ³
Impurity[Fe(III)] =		100	ppm

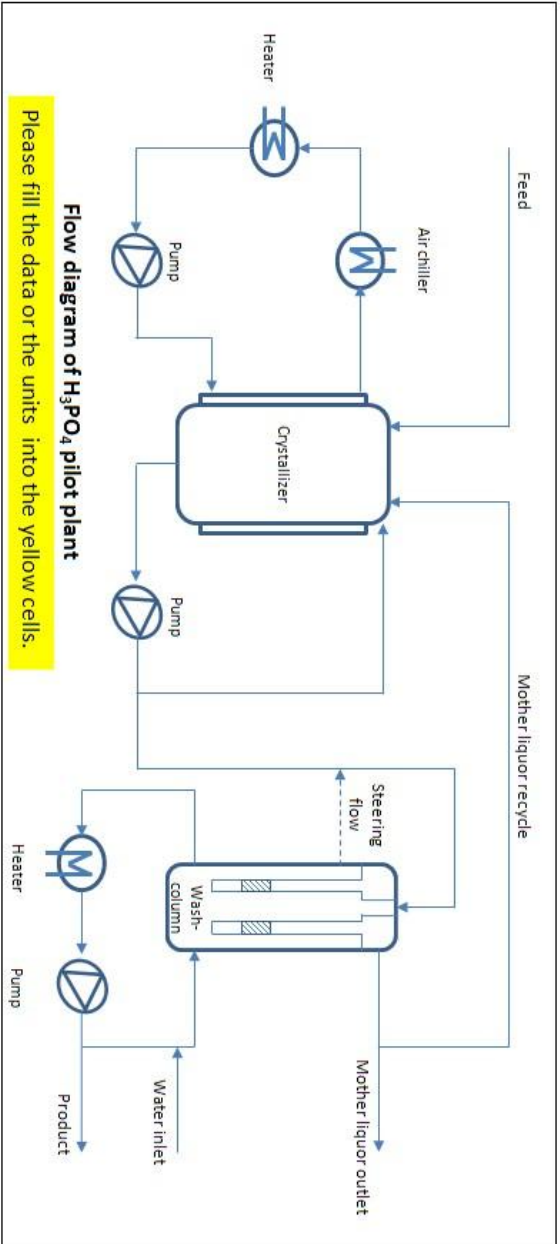
Mother liquor recycle	Flow rate =	170	kg/h
	Concentration =	83.31	wt%
	Temperature =	16	°C
	Density =	1.6741	g/cm ³
Impurity[Fe(III)] =		124.954	ppm

Product loss	Flow rate =	0.76	kg/h
--------------	-------------	------	------

Mother liquor outlet	Flow rate =	486.1	kg/h
	Concentration =	83.31	wt%
	Temperature =	16	°C
	Density =	1.6741	g/cm ³
Impurity[Fe(III)] =		124.954	ppm

Water Inlet	Flow rate =	8.1	kg/h
	Temperature =	25	°C
	Density =	0.9971	g/cm ³

Product	Flow rate =	132	kg/h
	Concentration =	86.01	wt%
	Temperature =	30	°C
	Density =	1.6941	g/cm ³
Impurity[Fe(III)] =		1.968	ppm



Crystallizer	Temperature =	16	°C
	Equilibrium concentration of ML =	83.30	wt%
	Solid content =	15.98	wt%

Figure 5.6-1 : Flow diagram of phosphoric acid pilot plant.

$$x_{ML} = 5.966 \times 10^{-8}T_C^6 - 2.239 \times 10^{-6}T_C^5 + 3.884 \times 10^{-6}T_C^4 + 5.467 \times 10^{-4}T_C^3 - 3.239 \times 10^{-4}T_C^2 + 0.2129T_C + 78.83$$

Equation 5.6.1-2

where, x_{ML} is the equilibrium concentration of the mother liquor in the crystallizer, [wt%] and T_C is the temperature of the crystallization process, [°C].

The solid content is calculated according to Equation 5.6.1-3:

$$x_{solid} = \frac{(x_{feed} - x_{ML}) \cdot m_{feed} \cdot 100}{(m_{feed} + m_{recycle}) \cdot (91.6 - x_{ML})}$$

Equation 5.6.1-3

where, x_{solid} is the solid content, [wt%], m_{feed} and $m_{recycle}$ are the flow rates of feed and mother liquor recycle, [kg/h].

- Water input

The flow rate and the temperature of the water should be given in advance, and its density is calculated according to Equation 5.6.1-4 [Til37]:

$$\rho_{water} = 1 - \frac{(T_{water} + 288.94) \cdot (T_{water} - 3.9863)^2}{508929.2 \cdot (T_{water} + 68.12963)}$$

Equation 5.6.1-4

where, ρ_{water} is the density of water, [g/cm³] and T_{water} is the temperature of water, [°C].

- Mother liquor output, recycle and product

The flow rate of the mother liquor output is based on the mass balance of the flows:

$$m_{output} = m_{feed} + m_{water} - m_{product}$$

Equation 5.6.1-5

where, m_{output} , m_{water} and $m_{product}$ are the flow rates of mother liquor output, water input and product, [kg/h].

To calculate the phosphoric acid concentrations of mother liquor output and recycle:

Assuming

$$m_{product} - m_{water} \leq (m_{feed} + m_{recycle}) \cdot x_{solid}/100$$

Equation 5.6.1-6

It means some part of product goes out from the mother liquor outlet. Therefore,

$$m_{loss} = m_{feed} + m_{recycle} \cdot \frac{x_{solid}}{100} + m_{water} - m_{product}$$

Equation 5.6.1-7

$$x_{product} = \frac{(m_{feed} + m_{recycle}) \cdot x_{solid} \cdot 0.916}{m_{feed} + m_{recycle} \cdot x_{solid}/100 + m_{water}} \quad \text{Equation 5.6.1-8}$$

$$x_{output} = x_{recycle} = \frac{m_{feed} \cdot x_{feed} - m_{product} \cdot x_{product}}{m_{output}} \quad \text{Equation 5.6.1-9}$$

where, m_{loss} is the flow rate of the product which goes out from the mother liquor outlet, [kg/h]. If m_{loss} is negative, it means that some part of the mother liquor goes out with the product.

$$C_{Fe,product} = \frac{m_{feed} \cdot C_{Fe,feed} - m_{output} \cdot C_{Fe,output}}{m_{product}} \quad \text{Equation 5.6.1-10}$$

$$C_{Fe,output} = C_{Fe,recycle}$$

$$= \frac{100 - x_{solid} \cdot m_{feed} - x_{solid} \cdot K_d \cdot m_{feed} \cdot C_{Fe,feed} + C_1}{m_{feed} + m_{recycle} \cdot \frac{100 - x_{solid}}{100} + m_{loss} - 100 - x_{solid} \cdot m_{feed} - x_{solid} \cdot K_d \cdot m_{recycle} - C_2} \quad \text{Equation 5.6.1-11}$$

where

$$C_1 = \frac{[100 - (100 - x_{solid}) \cdot m_{feed} - x_{solid} \cdot K_d] \cdot m_{feed} \cdot C_{Fe,feed} \cdot m_{loss}}{(m_{feed} + m_{recycle}) \cdot x_{solid}} \quad \text{Equation 5.6.1-12}$$

$$C_2 = \frac{[100 - (100 - x_{solid}) \cdot m_{feed} - x_{solid} \cdot K_d] \cdot m_{recycle} \cdot m_{loss}}{(m_{feed} + m_{recycle}) \cdot x_{solid}} \quad \text{Equation 5.6.1-13}$$

$C_{Fe, feed}$, $C_{Fe, output}$, $C_{Fe, recycle}$ and $C_{Fe, product}$ are the iron concentrations in feed, mother liquor output, mother liquor recycle and product, respectively, [ppm].

Otherwise, some part of mother liquor goes out with product.

$$x_{product} = \frac{m_{feed} \cdot x_{feed} - m_{output} \cdot x_{output}}{m_{product}} \quad \text{Equation 5.6.1-14}$$

$$x_{output} = x_{recycle} = x_{ML} \quad \text{Equation 5.6.1-15}$$

$$C_{Fe,product} = \frac{m_{feed} \cdot C_{Fe,feed} - m_{output} \cdot C_{Fe,output}}{m_{product}} \quad \text{Equation 5.6.1-16}$$

$$C_{Fe,output} = C_{Fe,recycle} = \frac{(m_{feed} - \frac{x_{solid} \cdot K_d}{100 - x_{solid}}) \cdot m_{feed} \cdot C_{Fe,feed}}{m_{feed} + m_{recycle} - m_{recycle} \cdot (m_{feed} - \frac{x_{solid} \cdot K_d}{100 - x_{solid}})} \quad \text{Equation 5.6.1-17}$$

5.6.2 Examples of the pilot plant calculations

Two groups were tested for the calculations. The operation conditions and the results of calculations are listed in Figures 5.6.2-1 and 5.6.2-2.

Group 1 has no water input and no mother liquor recycle flow. It can be seen that the solid content in the crystallizer is 17.18 wt%. The concentration of product is 91.2 wt%. The iron concentration in product is approx. 10 ppm (100 ppm as the initial concentration in feed). This is due to the fact that some mother liquor comes out with product. (The flow rate of product loss is - 5.12 kg/h.)

Group 2 has a water input and a mother liquor recycle flow. The solid content in the crystallizer is 16.80 wt%. The concentration of product is 86.01 wt% due to the addition of water. The iron concentration in product is approx. 3 ppm (100 ppm as the initial concentration in feed). The flow rate of product loss is 0.76 kg/h.

It needs to be mentioned that since the impurities are enriched in the mother liquor the product loss should be kept positive so that the mother liquor does not go out with product. During the operations the temperature of the crystallization in the crystallizer, the flow rates of product, mother liquor recycle and water input can be modified so that different concentrations and purities of product can be obtained. Their effects are discussed in Chapter 5.6.3.

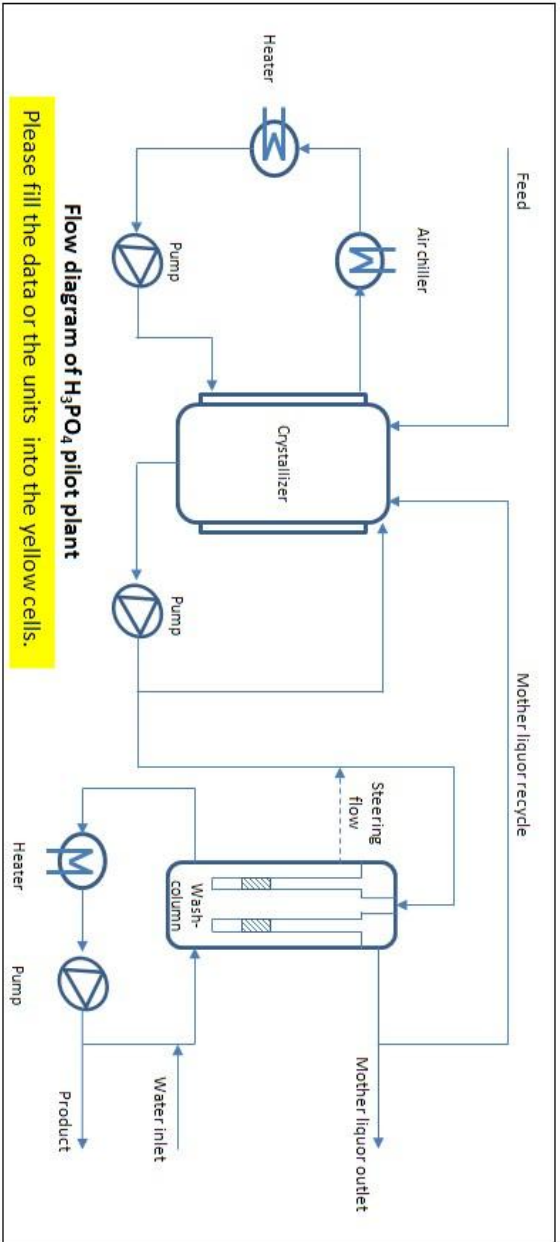
Flow rate =	560	kg/h
Concentration =	85	wt%
Temperature =	25	°C
Density =	1.6864	g/cm ³
Impurity/[Fe(III)] =	100	ppm

Flow rate =	0	kg/h
Concentration =	83.63	wt%
Temperature =	17	°C
Density =	1.6771	g/cm ³
Impurity/[Fe(III)] =	119.833	ppm

Product loss	Flow rate =	-5.12	kg/h
--------------	-------------	-------	------

Flow rate =	458.7	kg/h
Concentration =	83.63	wt%
Temperature =	17	°C
Density =	1.6771	g/cm ³
Impurity/[Fe(III)] =	119.833	ppm

Flow rate =	0	kg/h
Temperature =	25	°C
Density =	0.9971	g/cm ³

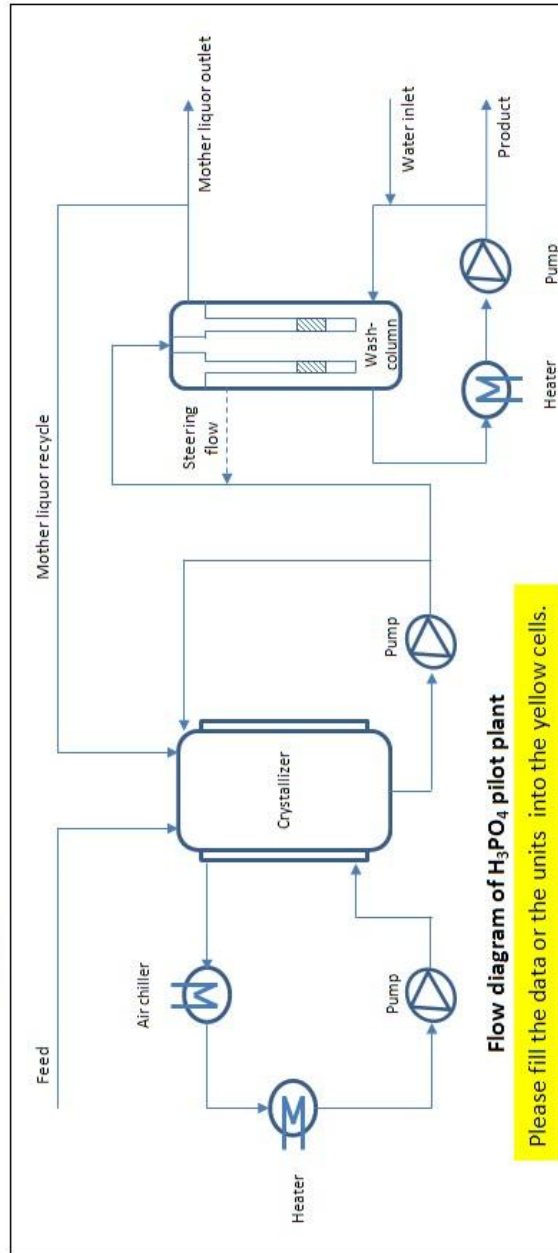


Temperature =	17	°C
Equilibrium concentration of ML =	83.63	wt%
Solid content =	17.18	wt%

Flow rate =	101.3	kg/h
Concentration =	91.20	wt%
Temperature =	30	°C
Density =	1.7574	g/cm ³
Impurity/[Fe(III)] =	10.192	ppm

Figure 5.6-2-1: Flow diagram of phosphoric acid pilot plant.

Feed	Flow rate =	610	kg/h
	Concentration =	85	wt%
	Temperature =	25	°C
	Density =	1.6864	g/cm ³
	Impurity[Fe(III)] =	100	ppm
Mother liquor recycle	Flow rate =	132	kg/h
	Concentration =	83.31	wt%
	Temperature =	16	°C
	Density =	1.6741	g/cm ³
	Impurity[Fe(III)] =	124.531	ppm
Product loss	Flow rate =	0.76	kg/h



Mother liquor outlet	Flow rate =	486.1	kg/h
	Concentration =	83.31	wt%
	Temperature =	16	°C
	Density =	1.6741	g/cm ³
	Impurity[Fe(III)] =	124.531	ppm

Water inlet	Flow rate =	8.1	kg/h
	Temperature =	25	°C
	Density =	0.9971	g/cm ³

Product	Flow rate =	132	kg/h
	Concentration =	86.01	wt%
	Temperature =	30	°C
	Density =	1.6941	g/cm ³
	Impurity[Fe(III)] =	3.528	ppm

Crystallizer	Temperature =	16	°C
	Equilibrium concentration of ML =	83.30	wt%
	Solid content =	16.80	wt%

Figure 5.6.2-2: Flow diagram of phosphoric acid pilot plant.

5.6.3 The optimization of calculations

To find out which parameters have the strongest effect on the impurity (iron) of product the temperature of the crystallization process in the crystallizer, the flow rates of product, mother liquor recycle and water input are varied, respectively. The flow rate, the concentration and the impurity (iron) of feed are fixed as 610 kg/h, 85 wt% and 100 ppm, respectively. The flow rate of product loss is kept zero so that there is no product loss. The results are shown in Figures 5.6.3-1 and 5.6.3-2.

In Figure 5.6.3-1 the temperature of the crystallization process in the crystallizer is changed. Other parameters such as the flow rates of water input and mother liquor recycle are fixed. Since the concentration of feed is fixed the supersaturation is only decided by the temperature of the crystallization process. The flow rate of product is changed so that the product loss is zero. Therefore, the yield of product is changing when the temperature of the crystallization process changes. It can be seen that a low temperature of the crystallization process creates a high yield

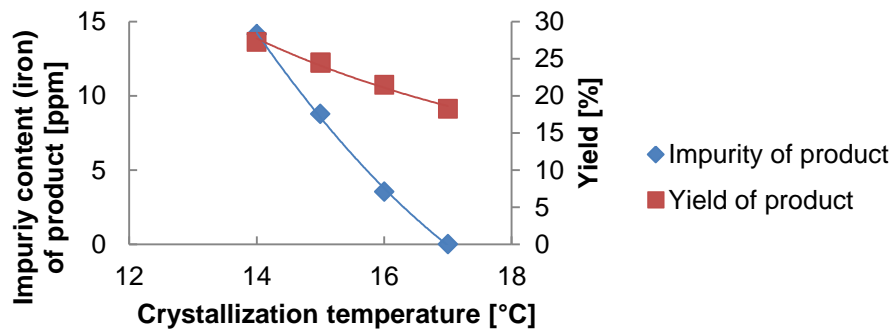


Figure 5.6.3-1: The impurity content (iron) and the yield of product at different temperatures of crystallization. ($m_{water} = 8.1$ kg/h, $m_{recycle} = 132$ kg/h).

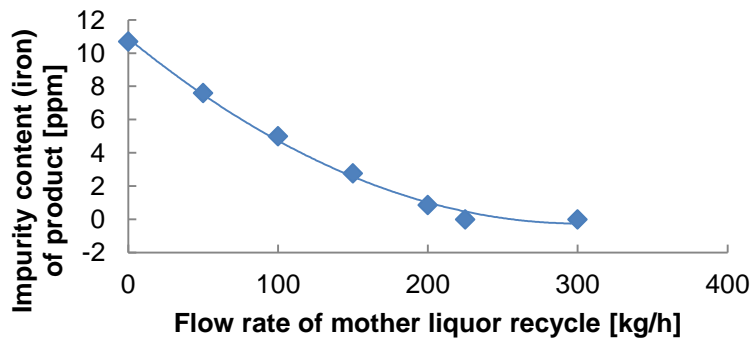


Figure 5.6.3-2: The impurity content (iron) of product with different flow rates of mother liquor recycle. ($m_{water} = 8.1$ kg/h, $T_C = 16$ °C, $m_{product} = 132.76$ kg/h).

of product but a high impurity content. When the temperature of the crystallization process increases to approx. 17 °C the impurity content approaches zero and the yield of product decreases to approx. 18 wt%.

In Figure 5.6.3-2 the flow rate of the mother liquor recycle is changed so that different purities of product can be obtained. It shows that a high flow rate of mother liquor recycle leads to a low impurity content. After approx. 250 kg/h there is no significant decrease of the impurity content in the product. During the change of the flow rate of the mother liquor recycle the yield of product (flow rate of product) does not change, however, the solid content in the crystallizer changes. The higher the flow rate of the mother liquor recycle, the lower is the solid content. Furthermore, the low solid content is helpful for the mass transportation between the crystallizer and the hydraulic wash column.

Additionally, added water can dilute the product into an expected concentration. At the same time it also dilutes the impurity concentration, but only in a small amount (up to 10 %).

6. Discussion

Based on the data in Chapter 5 the experiments and the results are discussed in this Chapter, respectively. They are the discussion of solubility study of phosphoric acid in water in Chapter 6.1, the discussion of the vapor pressure measurement of phosphoric acid and water in Chapter 6.2, the discussion of the measurement of crystal growth via off-line and in-line techniques in Chapter 6.3, the discussion of the distribution coefficient of crystallization and post treatments in Chapter 6.4, the discussion of the permeability measurement of the crystal bed in Chapter 6.5, the optimization of the purification of phosphoric acid in Chapter 6.6, the mass balance discussion of the pilot plant in Chapter 6.7 and the outlook in Chapter 6.8.

6.1 The solubility of phosphoric acid in water

The isothermal technique is a classic method to determine the solubility of substances. During the measurement, the concentration of a melt is changed by adding the substance until it is saturated. The temperature of the whole process is maintained constant. The $\text{H}_3\text{PO}_4 \cdot 0.5\text{H}_2\text{O}$ crystals are highly hygroscopic so that it is not easy to handle them. Therefore, a supersaturated $\text{H}_3\text{PO}_4 - \text{H}_2\text{O}$ melt was prepared in advance and later the melt started to crystallize after adding seeds. When the process reached its equilibrium, the saturated melt and some crystals can be obtained. Other techniques, such as density measurements and titration techniques, can be used to determine the concentration of $\text{H}_3\text{PO}_4 - \text{H}_2\text{O}$ melt. Different saturated concentrations of $\text{H}_3\text{PO}_4 - \text{H}_2\text{O}$ melts can be obtained at different temperatures and a solubility curve can be obtained (as shown in Figures 5.1.1-1 and 5.1.1-2).

Compared to the isothermal technique, the polythermal technique is also a widely used technique to determine the solubility of substances. During the measurement, the temperature is changing until the melt starts to crystallize. In another words, it is the opposite way compared to the isothermal technique to determine the solubility. It includes visual observations, turbidity measurements, focus beam reflectance measurements (FBRM) and calorimetry (e.g. differential scanning calorimetry (DSC)). Especially, DSC measurements can give a relatively precise result with a low amount of the sample. Here it was tried with a $\text{H}_3\text{PO}_4 - \text{H}_2\text{O}$ melt. Unfortunately, the $\text{H}_3\text{PO}_4 \cdot 0.5\text{H}_2\text{O}$ crystals do not nucleate by the cooling down to $-30\text{ }^\circ\text{C}$ and the seeds have to be added during the process. This increases the difficulty of the measurement and therefore, this technique was not used here.

Jiang *et al.* [Jia11] also did a test on the H₃PO₄ density and its concentration. In their research, although the concentration of H₃PO₄ melt can be calculated by an equation (see Equation 6.1-1) from density data at any temperatures, the concentration ranges of H₃PO₄ melt were only from 86 to 102 wt%. In other words, the calibration of the density measurements needs to be done here. The curve in Figure 5.1-1 shows a very good linear relationship and it even can be extrapolated in a small concentration range which is 80 to 90 wt%.

$$w = \frac{\rho - A_0 + A_2T}{A_1 + A_3T} \quad \text{Equation 6.1-1}$$

where,

w is mass fraction of H₃PO₄ melt, [wt%]

ρ is a density of H₃PO₄ melt, [g/cm³]

T is temperature, [°C]

$$A_0 = 0.68235$$

$$A_1 = 1.20811 \times 10^{-2}$$

$$A_2 = 1.2379 \times 10^{-3}$$

$$A_3 = 3.7938 \times 10^{-6}$$

To the solubility measurements, given in Figures 5.1.1-1 and 5.1.1-2 show a very good result that all the cations in three H₃PO₄ samples do not change the solubility of H₃PO₄ in water. The three H₃PO₄ samples are feed, product grade and food grade. Feed is the sample which is before crystallization process (a feed to a crystallizer). The sample of product grade is the one which is after the cleaning process (crystallization and post treatments) and it fits the European standard sales specification (Table 2.3.2-2). It is meaningful that without changing of the solubility of H₃PO₄ in water, the process of the crystallization can follow the solubility curve and therefore, the solid content, yield and the concentration of the mother liquor as well as the temperature range of the process can be predicted at any operation condition. The sample of food grade gives an overview on how much cations are left in the melt and how much cations should be removed according to the standard (Table 2.3.2-2). It has the same solubility data compared to the feed and the product grade and it can be seen that such a low amount of cations (some elements are less than 1 ppm and some are less than 10 ppm) do not affect the solubility of H₃PO₄ in water.

With three additives (100 ppm B, 100-200 ppm Fe^{2+} and 100 ppm Fe^{3+}), all of them were studied in order to see whether there is an effect on the crystal growth (see the Chapters 5.3.1.2, 5.3.1.3 and 5.3.1.4). Before these studies, the additive effects on the solubility of H_3PO_4 in water have to be studied. As expected, none of them showed any effects. Similarly, Dang [Dan07], Ma [Ma09b] and Sangwal [San10] also did some additive studies and some of them show no effects on the solubility of H_3PO_4 in water, but positive effects on the metastable zone width can be noticed. During the crystallization process, the seeds only play the role to induce the nucleation. The whole process is not controlled in the metastable zone. Therefore, here, the additive effects on the metastable zone width were not studied.

Similarly, 6 chelating agents, 1000 ppm ethylenediaminetetraacetic acid (EDTA), 1500 ppm etidronic acid (HEDP), 1500 ppm diethylenetriamine penta (methylene phosphonic acid) (DTPMPA), 1000 ppm oxalic acid, 1500 ppm amino tris (methylene phosphonic acid) (ATMP) and 1500 ppm pyrophosphoric acid, do not show any effects on the solubility of H_3PO_4 in water. These chelating agents were added into the feed, respectively, in order to see whether they can improve the separation efficiency of the iron (see Chapter 5.4). Their amounts (1000-1500 ppm) are calculated based on 100 ppm Fe. Their non-effects on the solubility of H_3PO_4 in water undoubtedly decrease the difficulty of the other studies (such as the study of crystal growth rate and the study of distribution coefficient).

6.2 The vapor pressure of phosphoric acid and water

The special tube (see Figure 4.2-2) provides a method that can be used for the measurement of the vapor pressure. Enough amount of a sample can separate the position A from the environment. During the measurement the liquid level of the positions B and C should be monitored. When the sample is heated it starts to evaporate and the bubbles coming out through the positions B and C. Due to the condenser the gas phase of the sample is cooled down and is condensed. This liquid phase will mix with the sample in the positions B and C. If the sample is a mixture of two components (in this case phosphoric acid and water), the liquid concentration in the positions B and C will change. Therefore, the concentration analyses of the samples are necessary. The results shown in Figure 5.2-1 and Table 5.2-1 already prove that although the concentration of the samples changed after the measurement, the vapor pressure of the mixture does not change much. The relationship between $\ln p$ and $1/T$ is still linear and it fits well the Clausius-Clapeyron equation (Equation 5.2-1). Compared to the data from literature [Sol13] the

results from the experiments are slightly higher. This could be due to the fact that during judging the liquid level of the positions B and C there is a reading delay for the thermometer from our eyes. During the cooling process the temperatures when the liquid level of the positions B and C are equal to each other are slightly lower than the real temperature. Therefore, according to the relationship of $\ln p$ and $1/T$ the vapor pressures at their related concentrations are slightly higher. On the other hand, it is not easy to measure the vapor pressure of the sample at 50 °C. The degree of the vacuum which is from the pump is not reachable. Hence, the data at this temperature are calculated through Equation 5.2-1.

Although the vapor pressure measurements are seen to be not important to the process of crystallization, it is still meaningful to the pre-processes. Before crystallization, the initial concentration of the sample decides its saturation temperature and further decides the operation temperature of a crystallizer. To operate it at a high temperature and to get more crystals the initial concentration of the sample ($\text{H}_3\text{PO}_4 - \text{H}_2\text{O}$ melt) should be high enough. The simplest way to increase the concentration of the melt is evaporation. The water in the $\text{H}_3\text{PO}_4 - \text{H}_2\text{O}$ melt can partially be removed by heating at approx. 160 °C at standard pressure or a lower temperature at vacuum (according to the results in Figure 5.2-2). Thereafter, the crystallization can be started with a concentrated melt. However, the energy cost and an extra device for the evaporation of the melt needs also be considered. It may bring convenience to the next unit operation, but it also increases the costs of the whole process.

6.3 The measurement of crystal growth rates

6.3.1 Off-line measurements

The growth rate of the crystals is an important part of a crystallization process, because it determines the size of the equipment. The crystals should furthermore be controlled at a certain growth rate to achieve a certain size distribution in order to have a solid liquid separation which can go step by step. A too fast growth rate may induce a number of problems, for example agglomeration or many crystals with defects. In case of too fast growth impurities do not have enough time to diffuse out of the boundary layer around the crystals so that they are included in the crystals. The surface of the crystals may be not smooth so that the surface area is increased and the impurities have more opportunities to attach on the surface. In this case, some post treatments such as sweating and washing can efficiently remove part of the impurities. On the other hand, a too slow growth rate may lead to perfect crystals, but the retention time in the

crystallizer needs also to be considered. It indirectly increases the cost, especially, in an industrial scale.

Here, the growth rate of $\text{H}_3\text{PO}_4 \cdot 0.5\text{H}_2\text{O}$ crystals is monitored under the microscope. In a cell, without agitation, the growth of the crystals is mainly controlled by diffusion and therefore the growth rates are, in principle, relatively slow compared to the ones in a stirred crystallizer. However, the growth rates of $\text{H}_3\text{PO}_4 \cdot 0.5\text{H}_2\text{O}$ crystals are still high enough even at a low supersaturation (4.63×10^{-7} m/s at $\Delta s = 0.65$ wt%), (see Figure 5.3.1.1-1). The solid content at this supersaturation is approximately 7 wt% according to the phase diagram (Figure 3.1.1-1). It is much lower than the one at the maximum industrial limit (30-40 wt%). According to the equation in Figure 5.3.1.1-4, the growth rate of the $\text{H}_3\text{PO}_4 \cdot 0.5\text{H}_2\text{O}$ crystals will be approximately 4.3×10^{-6} m/s at a solid content of 30 wt% ($\Delta s = 2.73$ wt%). It is ten times faster than the one at the lower supersaturation (0.65 wt%).

Figure 5.3.1.1-3 shows that the temperature level is not the main factor that changes the growth rate of the crystals significantly. However, it needs to be mentioned that 5 K difference (growing at 14 °C and 9 °C) may not give a strong effect to see how the crystals grow faster or slower. It can only be assumed that the growth rate of the crystals may decrease at low temperature according to Arrhenius' law. Additionally, the viscosity of mother liquor also decreases during the decrease of the temperature. It can also increase the difficulty of diffusion so that the growth rate of the crystals decreases in case the growth is controlled by diffusion. Jiang [Jia12b] measured the viscosity of saturated $\text{H}_3\text{PO}_4 - \text{H}_2\text{O}$ melt. It is shown in Figure 6.3.1-1. It can be seen that the viscosities of the melts which are from 80 to 90 wt% are between 45 and 50 mPa·s. This difference could be neglected during the operations of a crystallization process.

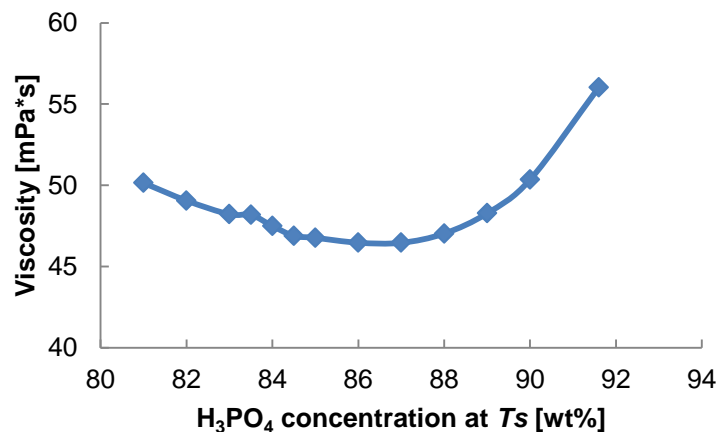


Figure 6.3.1-1: Viscosity of a $\text{H}_3\text{PO}_4 - \text{H}_2\text{O}$ melt at its saturation temperature according to Jiang [Jia12b].

The mechanism of crystal growth is also an important part of this study. According to the order of the growth rate, the growth of crystals is controlled in different ways. If it is close to 1 which means the growth of crystals is controlled by diffusion, changing agitation will be a useful way to change the growth rate. If it is close to 2 that the growth rates of crystals are controlled by surface integration, changing agitation will not work. Adding or removing other chemicals will produce distinguished effects on the growth rate. In reality, the order of the growth rate will not be 1 or 2 and it is always a number which is close to an integer. In other words the growth of crystals is controlled by both mechanisms together. Here, in Figure 5.3.1.1-5 it is shown that the growth orders of $\text{H}_3\text{PO}_4 \cdot 0.5\text{H}_2\text{O}$ crystal is always between 1 and 2 in the first 30 min. Therefore, changing the speed of agitation and adding a specific chemical (additive) will change the rate of the growth. Unfortunately, it is not possible to do an off-line measurement (observation by a microscope) with agitation (which will change to an in-line measurement). Compared to an off-line measurement, an in-line measurement is not possible to monitor the growth of the same crystal all time.

During the growth of crystals its defects cannot be completely avoided. Some impurities with part of mother liquor could be included in the crystals and further they will not be removed by a simple process. The more bubbles or solvent are included in the crystals, the more impurities may be included. Defect may also happen on the surface of the crystals. If the surface of the crystals is not smooth it provides an increased surface area. Therefore, when the surface energy is high it can adsorb more impurities. Figure 5.3.1.1-6 shows that a higher supersaturation gives a serious of defects in the crystals. With these crystals, the post treatments such as sweating and washing are the methods which need to be considered. This is discussed in Chapters 5.4.2 and 6.4.1.

Some impurities sometime may not only be included in the crystals, but they can also change the morphology of the crystals. First of all, to have an overview on this effect, the food grade $\text{H}_3\text{PO}_4 - \text{H}_2\text{O}$ melt was tested. Some crystals grew in this melt and they were monitored under the microscope. All the conditions such as supersaturation and temperature are the same as in the case of the product grade. The results (Figure 5.3.1.1-8) cannot indicate which kind of impurities can change the morphology of the crystals, but it can show us that this change may come from these elements (see Table 5.1.1-1). To test them, some of the elements (B, Fe^{2+} and Fe^{3+}) were picked and further they were added into the product grade of $\text{H}_3\text{PO}_4 - \text{H}_2\text{O}$ melt. The amounts of the additives are 100 and 200 ppm so that they are clearly higher than the other elements and they can be easily analyzed in the lab without high deviations. The substances which were chosen as impurities contain besides the element wanted only, oxygen and

hydrogen. Therefore, H_3BO_3 , Fe powder and Fe_2O_3 as the ideal compounds were added. Since the ICP-OES analysis cannot show the charge of the element, both Fe^{2+} and Fe^{3+} were tested in order to see their differences, respectively. There is also another reason to pick iron. Most materials of the crystallizer and the wash column are stainless steel. The iron may go into the acid melt and may increase its concentration in melt. It is also one of the key elements that should be reduced in all chemicals for electronics. Thus, most of the experiments with impurities here are focused on iron.

Firstly, the morphology of the crystals with B shows a parallelogram and the ones with Fe^{2+} and Fe^{3+} show defects on the tips. It could be deduced that the impurities may be adsorbed on specific faces of the crystals and block the growth of these faces. This could clearly be seen from Figure 5.3.1.2-2 with B. In Figures 5.3.1.3-2 and 5.3.1.4-2 the two tips of the crystal may also be two faces. Without iron these two faces grow with the fastest rate compared to all the others. Hence, there are only two tips can be observed. After the adsorption of iron the growth of the two faces (two tips) slowed down and they appeared in Figures 5.3.1.3-2 and 5.3.1.4-2. Secondly, the growth rates of the lengths also show differences. It did not change in the group of B, but the ones with iron. Ideally, it could be better using different growth rates to show different growth properties of the faces. However, it is not easy to recognize each face, for example the two tips in the case study of the additive iron. In some cases it is not necessary to do a study of all faces. In industry, it is more meaningful to do an overall size study of crystals during growth instead of monitoring each face. To observe a change of the morphology the content of an impurity needs to pass a threshold. An additive lower in amount than this threshold does not change the morphology. This can be seen in the case study of Fe^{2+} . 100 ppm Fe^{2+} does not show any effects on the morphology changing of the crystals, but 200 ppm Fe^{2+} does.

Although some impurities (additives) have specific effects on the growth of crystals they do not have the potential to be used in industry. Due to a property to help to obtain a specific shape of the crystals some impurities (additives) are to be added during the crystallization process. After that the impurities (additives) can be removed or stay with crystals. These impurities (additives) are called "tailor-made" additives and they can be used for control of nucleation, growth shape changes and dissolution of crystals [Lah90].

6.3.2 In-line measurements

The in-line measurement is a very important technique for industrial crystallization. FBRM and 3D ORM can monitor all the steps of crystallization such as nucleation, crystal growth, crystal dissolution, breakage and so on. All the operations can be done in real time so that there will not

be too much loss of products or time. In lab scale the FBRM and the 3D ORM measurements can also mimic a basic process of crystallization. Particle size distribution and growth rate of crystals can be measured by these methods. Although the principles of FBRM and 3D ORM are different both of them are an application of a laser technique. FBRM measures the arch chord length of the crystals and 3D ORM measures the surface area seen from one side of the crystals. In some cases [Mos14, Hel13] they can also show the shape of the particles without help of a microscope.

The accuracy of the in-line measurements is one of the important topics. Both FBRM and 3D ORM do not show the “real” size of the crystals. There are several equations to calculate the real size of the crystals from its arch chord length [Wyn03] or the shade image, but it seriously depends on the shape of the crystals. A needle shaped crystal (for example $\text{H}_3\text{PO}_4 \cdot 0.5\text{H}_2\text{O}$ crystal) is also hardly to be described concerning its size with only one number. Figures 5.3.2.1-1, 5.3.2.1-2, 5.3.2.2-1 and 5.3.2.2-2 also show that none of them shows the real size of the crystals compared to Figure 5.3.2.1-3 which are observed under a microscope. There is also another disadvantage that the in-line measurement cannot trace a single crystal and record its growth. Therefore, it is necessary to combine off-line and in-line measurements.

An improved FBRM technique combined with an in-line camera which is called Particle Vision Measurement (PVM) might be a help. With the help of PVM, the crystals can directly be monitored during the FBRM measurement. The real size and the shape of the crystals can be seen and analyzed by the software. However, this combination (FBRM and PVM) still cannot trace a single crystal, and the resolution to the big crystals (bigger than 1 mm) is not high enough.

On the other hand, 3D ORM as another in-line measurement gives a better result compare to the FBRM here. The mean diameter of the crystals can be represented as the size of the crystals and the growth rate can be calculated according to the slope of the growth curve. Compared to the off-line measurement (microscopy), the growth rate which is measured by 3D ORM is an average growth rate. It does not represent any specific direction of the growth. During the measurement of the crystal growth the in-line measurement also gives a better condition for the mass transfer and heat transfer. Hence, in principle, the growth rate of the crystals which is measured by the in-line measurement may be slightly higher than the one which is measured by the off-line measurement.

The size distribution of the crystals in a melt is also important for the study of crystallization. Since $\text{H}_3\text{PO}_4 \cdot 0.5\text{H}_2\text{O}$ crystals have a needle shape its size distribution is wide. The curves that

are from FBRM and 3D ORM are smoothed. Therefore, the large variation of curves cannot be seen in the figures. If there is a post treatment step, for example a filtration, the size of the crystals should be in a certain range. Therefore, too small or too large sizes of the crystals may have different influences. This is discussed in the Chapter 6.5.

The crystal defects cannot be detected by the FBRM or 3D ORM techniques. The change of the size does not give any information about it. However, the breakage may be detected due to the increasing of the number of counts. Compared to the accuracy of the size, it is not easy to prove how many crystals are seen by the sensors each time. To estimate this the solid content may give a rough contribution. According to the phase diagram of the $\text{H}_3\text{PO}_4 - \text{H}_2\text{O}$ system, in case $\Delta s = 1.5 \text{ wt\%}$ at $16.7 \text{ }^\circ\text{C}$ the solid content is 18.5 wt\% and when $\Delta s = 0.5 \text{ wt\%}$ at $19.8 \text{ }^\circ\text{C}$ the solid content is 7 wt\% . Considered the volume of the crystals at related supersaturation (10 times bigger at $\Delta s = 0.5 \text{ wt\%}$) the number of counts at $\Delta s = 1.5 \text{ wt\%}$ should be at least 20 times higher than the ones at $\Delta s = 0.5 \text{ wt\%}$. From Figures 5.3.2.2-1 and 5.3.2.2-2 it can be seen that there is only a difference of 3 times. Therefore, the accuracy of the count number measurement by 3D ORM is too low for the case of $\text{H}_3\text{PO}_4 \cdot 0.5\text{H}_2\text{O}$ crystals.

Combining in-line and off-line measurements to find out how the crystals grow at different conditions is meaningful. The shape of the crystals, defects and the growth rate of a specific direction or a single face can be analyzed by the off-line measurements (microscopy). The size distribution, particle counts and the overall change of sizes can be analyzed by the in-line measurements (FBRM and 3D ORM). Additionally, nucleation and breakage can also be seen by the in-line measurements. Both techniques are important to the industrial crystallization in terms of process understanding, design and optimization.

6.4 The distribution coefficient of crystallization and post treatments

6.4.1 The distribution coefficient of crystallization and post treatments

The distribution coefficient K_d shows the distribution of an impurity in two different phases, for example in the feed and in the crystals. It shows how much impurity is left in the crystals after a crystallization process. The higher the K_d is, the higher the impurity left in the crystals. When $K_d = 1$ it shows no separation after the crystallization. Vice versa, when $K_d = 0$ the impurity is completely removed from the crystals. In reality, after a crystallization step the crystals cannot be completely separated by a filtration or a centrifugation from the liquid phase which hold the

impurities. Therefore, $K_d(exp.)$ and $K_d(cal.)$ describe the experimental distribution coefficient and the theoretical distribution coefficient, respectively. If the impurity is enriched in the mother liquor the $K_d(exp.)$ should be higher than the $K_d(cal.)$, and vice versa. Some of the crystallization conditions can influence K_d such as the initial supersaturation of the feed, the retention time of the crystallization and the stirring speed. If some fine crystals should be obtained after the crystallization the stirring speed should not be high. Therefore, the initial supersaturation of the feed and the retention time of the crystallization are studied.

To increase the initial supersaturation of the feed can be achieved by increasing the initial concentration of the feed or decreasing the temperature of the crystallization process. Thereafter, the solid content can be increased so that the yield can be increased. In Figure 5.3.2.1-3 the images show the sizes of the crystals under different supersaturations. A high supersaturation with agitation can make crystals smaller. A high supersaturation at growth leads to nonperfect crystal needles which are easily broken by agitation. Therefore, the total surface area is increased. The amount of the attached mother liquor is based on the quantity of the crystals and the surface area of the crystals. Both increasing the quantity and the surface area of the crystals can be obtained by increasing the supersaturation of the feed. In addition, under a high supersaturation the concentration of the mother liquor is high. Therefore, in Figure 5.4.1-1 the $K_d(exp.)$ increases with the increasing of the supersaturation. To the $K_d(cal.)$, due to the large deviations the $K_d(cal.)$ does not show a significant increase. It may prove that the amount of the impurity (iron) within the crystals does not change much with the supersaturation. This also gives information that if an effective post treatment such as washing or rinsing is used the attached mother liquor can be washed away and the purity of the wet crystals may approach to their calculated purity. In other words the distribution coefficient $K_d(exp.)$ will approach to its $K_d(cal.)$.

Additionally, increasing the supersaturation will increase the solid content. A lab scale trial of a crystallization process with approximately 55.6 wt% solid content (supersaturation $\Delta s = 4.5$ wt%) was tested. The test shows that there is a “dead” layer of crystals which is attached to the walls of the crystallizer. The stirrer cannot agitate it. The crystals attached to the walls contain a certain amount of mother liquor which has no movement. Therefore, there may be no separation of the impurities. As an experience the solid content in a crystallizer should not be more than 30 to 40 wt% in industry, otherwise the transportation system may have a problem, especially, it is harmful to the pumps. To solve this problem a process of recrystallization of the mother liquor may be applied, and thus, the cost will increase.

On the other hand, increasing the time of the crystallization with less driving force can also improve the separation of the impurity. In this case, not only the $K_d(exp.)$ decreases with increasing of the crystallization time, but also the $K_d(cal.)$. However, in industry the retention time should always be kept short otherwise it may increase the cost of the operation.

Equation 5.4.1-5 shows a method how the amount of the attached mother liquor can be calculated. In a lab scale crystals out of a crystallizer, due to the fact that after a filtration the crystals still contain some mother liquor (either the mother liquor or the wash liquid). It cannot really be pure. However, in industry when a wash column is used, for example a hydraulic wash column, due to the presence of a wash front the crystals can almost completely be separated from the mother liquor. This was proven by Verdoes *et al.* [Ver02] and Scholz *et al.* [Sch02]. They built a hydraulic wash column in a lab scale and tried with some substances. Many results from them show the crystals can be washed to a very high purity level. They may also give us a potential of the wash columns in crystallization in future.

The efficiency of the post treatments in a lab scale without a wash column can be seen by the experiments and the results shown in Figures 5.4.2-1, 5.4.2-2 and 5.4.2-3. The impurities are enriched in the mother liquor and some of it is attached on the surface of the crystals. Using the feed stream which contains lower concentrations of impurities than the contaminated residue mother liquor as a wash liquid is not efficient for the washing of the crystals. Therefore, the pure saturated melt was used. The washing temperature is decided by the saturation temperature of the wash liquid. The higher the concentration of the wash liquid is used, the higher the temperature for the washing process is.

Washed crystals by the pure melt for a long time (~ 30 min) shows the results that the mother liquor in the wet crystals can be washed away (or be diluted). After the washing and the filtration the new "mother liquor" which contains part of the mother liquor and the wash liquid are attached on the crystals. Therefore, the $K_d(exp.)$ decreases after the washing. When the time of the washing decreases to 10 min the $K_d(exp.)$ does not improve a lot (no significant decrease) until the rinsing is used. As mentioned before washing may dilute the attached mother liquor. However, during the rinsing the wash liquid (rinsing liquid) may represent the attached mother liquor, and therefore, the $K_d(exp.)$ is improved further. A hydraulic wash column washing a crystal bed is more like executing a rinsing process than a washing process due to the fact that the contact time between the crystal bed and the wash liquid is only few seconds.

To optimize the efficiency of rinsing the amount of rinsing liquid is changed from the ratio of 2:1 to 1:5 ($m(rinsing\ liquid):m(crystals)$). The more rinsing liquid is used the more the yield is

decreased, but also may improve the purity of the wet crystals after the rinsing. This ratio is similar to the reflux ratio in a hydraulic wash column. If the reflux ratio is defined as the ratio of reflux/total product, when the reflux ratio = 1 there will be no crystal product any more. However, under this reflux ratio (equal to 1) the purity of the product may ideally be the best. In addition, the results which are from the rinsing trials in the lab scale can only show a tendency how the purity of the crystals changes according to the changes of the ratio of $m(\text{rinsing liquid})/m(\text{crystals})$. To see the rinsing effect in a hydraulic wash column it is necessary to do series trials because the rinsing principle in the hydraulic wash column is more complicated. It can only be said from the Chapter 5.4.2 that the iron as an impurity can be removed up to approximately 95 % after the crystallization and the rinsing in the lab scale. A lower supersaturation of the feed and a higher amount of rinsing liquid can improve the purity of the crystals.

6.4.2 The effects of chelating agents

Six commonly used chelating agents were screened as additives during crystallization. However, none of them showed a positive effect on the separation of irons (as an impurity). One possible reason is that to an acid melt ($\text{H}_3\text{PO}_4 - \text{H}_2\text{O}$ melt) the chelating agents cannot be combined with iron to stable complexes due to the low pK values. Phosphoric acid also has an ability to chelate irons in melt. From Table 5.4.3-1 it can be seen that the $pK(\text{Fe}(\text{HPO}_4)_2^-)$ has the highest number and it is higher than the $pK(\text{Fe}^{3+})$ of some chelating agents except HEDP and DTPMPA. In this case the chelating agents (except HEDP and DTPMPA) act only as an impurity and they can distribute in the mother liquor or even be included in the crystals. Therefore, to separate these parts of chelating agents is troublesome. The other reason is that even though some chelating agents (HEDP and DTPMPA) can chelate the irons, the complex can still be attached on the surface of the crystals or as inclusions. Hence, it turns back to the situations of the low $pK(\text{Fe}^{3+})$ of chelating agents.

Additionally, to the iron content analysis UV-Vis spectroscopy can analyze the content which is higher than 10 ppm. To a low iron concentration (less than 10 ppm) ICP-OES was used. Two techniques gave similar $K_a(\text{exp.})$ s. However, the deviations from the analysis of ICP-OES are relatively higher than the one from UV-Vis spectroscopy. In an industry scale the iron concentration in the feed will not be higher than 1 ppm. The reason for using 100 ppm iron in feed is to differentiate from the other impurities. The concentration of the interested element (iron, here) should be much higher than the concentration of the other impurities. Besides this all the

screenings with 100 ppm iron in the feed only gives the information on how well a process of crystallization separates an impurity.

Although the screening of the chelating agents showed no purity improvement of the crystals, it may contain some information that no matter the iron is chelated or not, it may be isolated from the crystals. If an efficient post treatment is used, the purity of the crystals will be improved.

6.5 The permeability measurements of the crystal bed

Three different sizes of phosphoric acid hemihydrate crystals were tested in order to see the permeability of a crystal bed. The results can be further used to evaluate the possibility that whether a crystal bed can be used in a hydraulic wash column or not. To calculate the permeability of a crystal bed the porosity of the crystal bed was measured first. The results in Table 5.5.1-1 show that the porosities of the crystal beds in three groups are close to 70 %. Such a high porosity can give a relatively high permeability. On the other hand, the pore size of the crystal bed can also influence the permeability of the crystal bed. Bigger pores produce a high permeability. In the three groups examined here the porosities are similar. Therefore, the difference of the permeability of the crystal bed is mainly from the pore size of the crystal bed. Unfortunately, it is not easy to measure the pore size of a crystal bed. Here is a potential for the optimization in future works.

Larger crystals give a higher permeability of the crystal beds. The two groups of the crystal size classes group b) and c) are suitable for the use in a hydraulic wash column operation (permeability range from 1.80×10^{-11} to 7.56×10^{-10} m² and 2.6×10^{-11} and 1.2×10^{-10} m²). A too low permeability cannot allow the filtrate (mother liquor and melt) to pass through the crystal bed and a higher pressure drop should therefore be introduced. A too high permeability will decrease the retention time of the wash liquid in the presence of the crystals in the wash column, especially, at the crystals in the wash section. If the retention time of the crystals in the wash liquid is short the diffusion washing cannot work well. In this case the impurities are included in the crystals they cannot be washed away and therefore the purity of the crystals cannot be very high. A high permeability also causes a high flow rate (both mother liquor and product melt). The mother liquor can be recycled by the steering flow. However, there will be more loss of the product due to the fact that the product cannot be part of the recycle stream as a wash liquid. The loss of the product can hence go back to the crystallizer to be recrystallized. The yield of the product will be

directly decreased. In this case a gravity wash column can be used instead of hydraulic wash column.

Table 5.5.1-1 also shows the compressibility factor s of the crystal beds in the three groups. It shows how difficult a crystal bed can be compressed. If $s = 0$ the crystal bed is incompressible. If $s = 1$ the crystal bed is completely compressible. The compressibility factors of the three groups are close to 0, especially, group a) and c) which show an incompressible property. However, according to their deviations the compressibility of the crystal beds in three groups may show no big difference. When a high pressure drop is applied during filtration the permeability of the crystal bed will decrease but only in a very small amount (~ 2 %).

In an industrial scale a wash column could have the height of a crystal bed of may be up to one meter (depends on the scale of the wash column). Due to the gravity and the driving force (hydraulic force) the permeabilities of the crystal beds at different positions are different. The permeability of the crystal bed which is close to the filter in principle is the minimum. This value should be at the range of the required permeability. However, to measure the permeability of a crystal bed in a lab scale can only lead to an average permeability.

In addition, there are some other parameters which can influence the permeability of crystal beds such as filtrate viscosity and suspension density which changes the height of the crystal bed. A high filtrate viscosity causes a low permeability of the crystal bed. The viscosity of phosphoric acid-water melt changes from 45 mPa*s to 50 mPa*s (according to its concentration from 80 wt% to 90 wt%) at their respected saturation temperature [Jia12]. This small change can be neglected during a permeability calculation. Moreover, in a hydraulic wash column the height of the crystal bed is more or less fixed so that a changing solid content is meaningless in this case. However, it is meaningful to change the crystal size or the efficiency of the separation (see the Chapters 5.4 and 6.4).

6.6 The optimization of the purification of phosphoric acid

In the Chapters 5.3, 5.4, 5.5, 6.3, 6.4 and 6.5 the results and the discussions of the crystal growth, the separation efficiency and the permeability of the crystal bed are discussed, respectively. In each part there is a best condition. However, some parameters have their best results in different directions, for example the purity and the yield. To get a better purity of the product the initial supersaturation of the feed should be low so that the crystals can grow slowly,

but in this case the yield of the product is low. Therefore, all the parameters should be discussed together in order to find the best condition for the process with a high purity and a high yield.

The initial supersaturation of the feed decides the driving force of the crystallization process. By stirring a high initial supersaturation leads to high amounts, small and impure crystals (see Figures 5.3.1.1-4, 5.4.1-1 and 5.5-1). However, on the one hand, an efficient rinsing can significantly increase the purity of the crystals and on the other hand, due to the limitation of a pump and an agitation the solid content in the crystallizer should not be more than 40 wt%. Therefore, according to the results of the crystallization process in the lab scale, if the concentration of the feed is 85 wt%, the maximum initial supersaturation would be 4.4 wt%. In such a case the permeability of the crystal bed will be low.

The time of the crystallization can also influence the purity of the crystals (see Figure 5.4.1-2). In Figures 5.3.2.1-1, 5.3.2.1-2, 5.3.2.2-1 and 5.3.2.2-2 the results from the in-line measurements shows the equilibrium point of the crystallization process. Combined with the purity analysis the retention time of the crystallization process would be best at approx. 90 min.

The agitation speed of most trials is 100 rpm. The speed is fixed at a low value. This is due to the fact that a high speed agitation will break crystals into small pieces. The average size of the crystals will be decreased (see Figure 5.5-1). Small crystals can also decrease the permeability of the crystal bed. Therefore, a vigorous stirring should be avoided.

Rinsing as an efficient post treatment can significantly improve the purity of the crystals. A high amount of rinsing liquid can give a better purity. However, due to the fact that the rinsing liquid is a part of the product, the more rinsing liquid is used the less yield will be achieved. In a wash column in industry no more than 10 wt% of the product is used as a rinsing liquid [Ver09].

Table 6.6-1 summarizes the optimal operation conditions of crystallization and post treatments according to the results which come from the lab trials.

Table 6.6-1: The optimal operation conditions of crystallization and post treatments.

Operation condition	Value
Initial concentration of feed	85 wt%
Maximum supersaturation	4.4 wt%
Time of crystallization	90 min
Stirring speed	100 rpm
Maximum solid content	40 wt%
Maximum amount of rinsing liquid	10 wt% of product
The permeability range of the crystal bed	$2 \times 10^{-11} \sim 8 \times 10^{-10} \text{ m}^2$
Maximum distribution coefficient K_d	0.05

6.7 The mass balance of the pilot plant

All the calculations in the Chapter 5.6.1 are based on the results in the Chapters 5.1, 5.3 and 5.4 and the assumptions which are mentioned in the Chapter 5.6. The assumptions give the simplest conditions of purification. However, during the real operations of the pilot plant a steering flow may be needed to get a sufficient pressure drop in the hydraulic wash column. There are some energy losses during the transportation of the materials. Different impurity contents in feed may have a different K_d . Therefore, the results which are from the calculations only give some predictions on how the quantity and the quality of the flows may look like, but not exact numbers for an industrial use.

During the calculations, for example mother liquor output, recycle and product may have different directions of flows (mother liquor goes out with product, or vice versa). However, in real operations the product loss should be kept zero. The mother liquor should not go out with the product. On the other hand, the solid content in the crystallizer should be controlled to be less than 40 wt% due to the problem of transportation. The temperatures of feed and water input are not as important as the other parameters (may be needed, however, in the energy calculations).

The two examples in the Chapter 5.6.2 show how the results of calculations look like. Example 1 (Figure 5.6.2-1) shows the case of no mother liquor recycle and no water input operations. The concentration of the product is always 91.6 wt% if the product loss is zero. Since the process has no mother liquor recycle the purity of product is not high compared to the one in the Example 2 (Figure 5.6.2-2). For the same solid content in the Example 2 Example 1 cannot reach a low temperature. This is due to the fact that the flow of mother liquor recycle dilutes the solid content in the crystallizer. If a high solid content is required, a lower temperature of

crystallization should be set. However, in a hydraulic wash column the temperature difference at the wash front should be controlled within approx. 10 K for phosphoric acid [Sol14]. It limits the temperature of the crystallization process and the product melt. Example 2 has a mother liquor recycle and a water input. The purity of the product can be improved by the presence of the flow of mother liquor recycle and the concentration of the product can be changed due to the water input. Figure 5.6.3-2 also shows that increasing the flow rate of the mother liquor recycle stream can slightly improve the purity of product. This is because it indirectly increases the retention time in the crystallizer. In addition, the water input does not only change the concentration of the product, but also it decreases the viscosity of the product and further it improves the permeability of the crystal bed during the washing in the hydraulic wash column.

However, all the calculations in the Chapter 5.6.1 do not show any effects of the hydraulic wash column. This is due to the fact that there are no lab trials of phosphoric acid with the hydraulic wash column and it could be a task for future works (see outlook, Chapter 6.8).

6.8 Outlook

Phosphoric acid is purified by melt crystallization. Iron as the key impurity element is studied for the separation efficiency of the crystallization and the post treatments. However, some other elements, for example As, are also important to the crystallization process. In order to study the distribution coefficients of those elements different impurities need to be added into the melt.

Crystal size has been studied under different supersaturations. Based on these results predicting the permeability of a crystal bed will be a part of future works and it needs to be introduced into the calculation of the mass balance of the pilot plant.

The calculation of heat balance of the pilot plant needs to be added to future works. It evaluates the cost of energy of the crystallizer and the melter.

At the end the trial of the pilot plant with a hydraulic wash column needs to be studied in industry. Changing the flow rates and the temperature of crystallization according to the mass balance calculation are the next steps. Due to the fact that ICP-OES can analyze many elements at same time, the separation coefficients of those elements can be analyzed at same time too. The position of the washfront and the ratio of the reflux in the hydraulic wash column need to be studied. Based on all above mentioned future works the purity of phosphoric acid should be even better and the cost should be further reduced.

7. Summary

Crystallization as a low cost, energy saving, environmental friendly and easily to scale up technique can be used for the purification of phosphoric acid. Phosphoric acid hemihydrate crystals ($\text{H}_3\text{PO}_4 \cdot 0.5\text{H}_2\text{O}$) crystallize from the mixture by cooling and most of the impurities are enriched in the mother liquor. Here the question is how to optimize the conditions of crystallization and post treatment process to get high pure crystals (product). All the experiments and the results are discussed.

The solubility study of phosphoric acid in water (Chapters 4.1, 5.1 and 6.1) shows that all the impurities of interest at their respective contents do not change the solubility of phosphoric acid in water. Based on these results the phase diagram of phosphoric acid and water [Jia12b] can be used for the design or the optimization of the crystallization process. The study of vapor pressure of phosphoric acid and water (Chapters 4.2, 5.2 and 6.2) gives a reference that phosphoric acid can be concentrated before crystallization to increase the yield and operation temperature. However, it may also increase the costs of the process.

The study of crystal growth by off-line techniques (Chapters 4.3.1, 5.3.1 and 6.3.1) shows that some impurity elements (B, Fe) can change the morphology of the crystals and slow down crystal growth. In Chapters 4.3.2, 5.3.2 and 6.3.2 two in-line techniques (FBRM and 3D ORM) are used to monitor the crystal growth in the whole crystallization process. The size (chord length or mean diameter) distribution of the crystals in the mixture can be controlled by different supersaturations and stirring speeds. Both off-line and in-line techniques prove that the crystal growth is controlled by diffusion and surface integration ($m = 1.8$).

The study of the distribution coefficient K_d of crystallization and post treatments (Chapters 4.4, 5.4 and 6.4) shows K_d at different conditions. A low supersaturation and a slow growth rate of the crystals lead to a low K_d , but with a low yield of crystals (product). Rinsing with molten crystals or pure melt can increase the purity of crystals further, but it consumes some product. All the results in these Chapters are based on 100 ppm Fe^{3+} addition in feed.

Additionally, some chelating agents were tested concerning the separation efficiency. However, none of them gave a positive result.

Since in the pilot plant an application of a hydraulic wash column is used the porosity and the permeability of crystal bed are studied (Chapters 4.5, 5.5 and 6.5). A high supersaturation makes crystals small and therefore the permeability of the crystal bed is low.

Based on all above mentioned studies optimized operation conditions are summarized and is shown in Table 6.6-1. Further, the mass balance of the pilot plant is calculated according to the results (Chapters 5.6 and 6.7). Two different operation conditions (with and without a mother liquor recycle loop) are compared and the one with mother liquor recycle loop gives a better purity of the product.

At the end, the fundamental background of crystallization of phosphoric acid and water are studied. More than 95 % impurity (based on 100 ppm iron in the feed) can be removed by crystallization and rinsing. The porosity of the crystal bed can be kept at 70 % and the permeability is useful for the application of a hydraulic wash column. It will help to scale up the pilot plant in industry and to be the references of the conditions for an operation.

8. Zusammenfassung

Kristallisation aus der Schmelze ist eine kostengünstige, energiesparende, umweltfreundliche und leicht zu skalierende Technik und wird zur Reinigung von Phosphorsäure eingesetzt. Phosphorsäure-Hemihydrat-Kristalle ($\text{H}_3\text{PO}_4 \cdot 0.5\text{H}_2\text{O}$) kristallisieren aus dem Gemisch durch Kühlung. Dabei werden die meisten Verunreinigungen in der Mutterlauge angereichert.

Die Fragestellung wie die Kristallisationsbedingungen sowie die Nachbehandlung optimiert und wie Experimente durchgeführt und Ergebnisse ausgewertet und genutzt werden können, werden im Rahmen dieser Arbeit diskutiert.

Die Löslichkeitsdaten von Phosphorsäure in Wasser (Kapitel 4.1, 5.1 und 6.1) zeigen, dass alle interessanten Verunreinigungen mit ihren jeweiligen Mengen die Löslichkeit von Phosphorsäure in Wasser nicht verändern. Basierend auf diesen Ergebnissen kann das Phasendiagramm von Phosphorsäure und Wasser [Jia12] für die Kristallisation verwendet werden. Das Studium des Dampfdrucks von Phosphorsäure und Wasser (Kapitel 4.2, 5.2 und 6.2) gibt eine Indikation darüber, wie Phosphorsäure vor der Kristallisation aufkonzentriert werden kann, um die Ausbeute und die Arbeitstemperatur zu erhöhen. Jedoch kann dies auch zur Erhöhung der Prozesskosten führen.

Das Studium von Kristallwachstum durch Offline-Techniken (Kapitel 4.3.1, 5.3.1 und 6.3.1) zeigt, dass einige Verunreinigungselemente (B, Fe) die Morphologie der Kristalle verändern und die Wachstumsgeschwindigkeiten verlangsamen können. In den Kapiteln 4.3.2, 5.3.2 und 6.3.2 werden zwei Inline-Techniken (FBRM und 3D ORM) zur Überwachung des Kristallwachstums im gesamten Kristallisationsprozess eingesetzt. Die Größenverteilung (Sehnenlänge oder mittlerer Durchmesser) der Kristalle in der Suspension kann durch unterschiedliche Übersättigungen und Rührgeschwindigkeiten gesteuert werden. Sowohl die Offline- als auch die Inline-Techniken zeigen, dass das Kristallwachstum nach den Mechanismen der Diffusion und Oberflächenintegration ($m = 1.8$) verläuft.

Studien zum Verteilungskoeffizienten K_d der Kristallisation und Nachbehandlungen (Kapitel 4.4, 5.4 und 6.4) zeigen K_d unter verschiedenen Bedingungen. So führen eine niedrige Übersättigung und eine langsame Kristallwachstumsgeschwindigkeit zu geringen K_d -Werten führen können, jedoch mit einer geringen Ausbeute an Kristallen. Das Spülen mit geschmolzenen Kristallen oder auch reiner Schmelze kann die Reinheit der Kristalle weiter erhöhen, allerdings zu Lasten der Produktausbeute. Alle Ergebnisse in diesem Abschnitt basieren auf der Zugabe von 100 ppm Fe^{3+} im Feed.

Zusätzlich wird der Einfluss einiger komplexbildender Substanzen auf die Trennleistung untersucht, jedoch ohne positives Ergebnis.

Durch den Einsatz einer hydraulischen Waschkolonne im Technikumsmaßstab werden die Porosität und die Durchlässigkeit des Kristallbetts untersucht (Kapitel 4.5, 5.5 und 6.5). Eine hohe Übersättigung führt dabei zu kleinen Kristallen und somit zu einer geringeren Durchlässigkeit des Kristallbetts.

In Bezug auf alle bereits erwähnten Studien werden die optimierten Betriebsbedingungen zusammengefasst und in Tabelle 6.6-1 gezeigt. Ferner wird die Massenbilanz einer Pilotanlage entsprechend der Ergebnisse (Kapitel 5.6 und 6.7) berechnet. Zwei verschiedene Betriebszustände (mit und ohne Mutterlaugenrückführschleife) werden verglichen, wobei der Betriebszustand mit Mutterlaugenrückführung eine bessere Produktreinheit ergibt.

Zum Abschluss werden wichtige fundamentale Daten zur Kristallisation von Phosphorsäure in Wasser gewonnen. Mehr als 95 % der Verunreinigungen (bezogen auf 100 ppm Eisen im Feed) können durch Kristallisation und Spülen entfernt werden. Die Porosität des Kristallbetts kann bei 70 % gehalten werden, und die Durchlässigkeit ermöglicht den Einsatz einer hydraulischen Waschkolonne. Die ermittelten Bedingungen werden bei einem künftigen Scale-up einer industriellen Pilotanlage helfen, die optimalen Bedingungen für einen bestimmten Arbeitsprozess zu ermitteln.

9. List of Symbols and Abbreviations

Notations

A	[a.u.]	Absorbance
A	[m ²]	Cross section area
B	[m ²]	Permeability
B_0	[m ²]	Initial permeability
B_c	[m ²]	Permeability of filter cake
B_m	[m ²]	Permeability of filter medium
c	[mol/L]	Concentration
C	[-]	Constant
C'	[-]	Constant
c_{Fe}	[ppm]	Iron concentration in the sample
D_{10}	[μm]	Ten percent of particles are smaller than this value
D_{50}	[μm]	Fifty percent of particles are smaller than this value
D_{90}	[μm]	Ninety percent of particles are smaller than this value
G	[m/s]	Growth rate
h	[m]	Height
h_c	[m]	Height of filter cake
h_e	[m]	Equivalent height of filter cake
h_m	[m]	Height of filter medium
ΔH	[MJ/kg]	Heat of combustion
$\Delta_{vap}H_m$	[J/mol]	Enthalpy of vaporization
I	[cd]	Intensity of light
k	[m/s]	Growth rate constant
k	[-]	Slope
K	[g s ²]	Measuring cell constant
K_d	[-]	Distribution coefficient
$K(Fe^{3+})$	[-]	Stability constant of iron (III)
L	[cm]	Length
m	[kg]	Mass
m	[-]	Order of crystal growth
m_c	[g]	Mass of measuring cell
p	[Pa]	Pressure

R	[J/mol K]	The ideal gas constant
R^2	[-]	Coefficient of determination
R_c	[1/m]	Resistance of filter cake
R_m	[1/m]	Resistance of filter medium
s	[-]	Compressibility factor
Δs	[wt%]	Supersaturation
t	[s]	Time
T	[s]	Period of oscillation
T	[°C]	Temperature
v	[m/s]	Velocity
V	[m ³]	Volume
x	[wt%]	Concentration
x_A	[wt%]	Concentration of A
$x_{A,eq}$	[wt%]	Solubility of A
$x(Fe)$	[ppm]	Iron concentration in the sample
x_{solid}	[wt%]	Solid content

Greeks

ε	[a.u. L/(mol cm)]	Extinction coefficient
ε	[%]	Porosity
η	[Pa s]	Viscosity
v	[%]	Volume fraction
ρ	[g/cm ³]	Density
ϕ	[cm]	Diameter

Abbreviations

2D	Two dimension
3D	Three dimension
Ac	Acetate
ATMP	Amino tris (methylene phosphoric acid)
DSC	Differential scanning calorimetry
DTPMPA	Diethylenetriamine penta (methylene phosphoric acid)

EDTA	Ethylenediaminetetraacetic acid
FBRM	Focused beam reflectance measurement
HEDP	Etidronic acid
ICP-OES	Inductively coupled plasma-optical emission spectrometry
ML	Mother liquor
MZW	Metastable zone width
ORM	Optical reflection measurement
PA	Phosphoric acid
ppb	Parts per billion
ppm	Parts per million
PVM	Particle vision measurement
rpm	Revolutions per minute
TOC	Total organic carbon
UV-Vis	Ultraviolet or visible light
v/v%	Volume percent
wt%	Weight percent

10. References

- [Ahm07] Ahmed, H., Diamonta, H., Chaker, C., Abdelhamid, R., *Purification of wet process phosphoric acid by solvent extraction with TBP and MIBK mixtures*, Sep. Purif. Technol., 55 (2007) 2, 212-216.
- [Ano85] Anonym, *The nitrophosphates alternative*, Fertilizer International, 209 (1985), 8-11.
- [Ark84] Arkenbout, G., van Kuijk, A., Schneiders, L., *Melt crystallization technology in Industrial crystallization*, eds. Jancic, S. and de Jong, E., Elsevier, Amsterdam, 1984, 137-142.
- [Boh69] Bohn, H., Peech, M., *Phosphatoiron (III) phosphatoaluminium complexes in dilute solutions*, Soil Sci. Soc. Am. J., 33 (1969), 873-876.
- [Bre80] Brennan, E., *Process and apparatus for separating and purifying a crystalline metal*, US 4309878, 1980.
- [Dan07] Dang, L., Wang, Z., Liu, P., *Measurement of the metastable zone width of phosphoric acid hemihydrate in the presence of impurity ions*, J. Chem. Eng. Data, 52 (2007) 5, 1545-1547.
- [Dan10] Dang, L., Wei, H., *Effects of ionic impurities on the crystal morphology of phosphoric acid hemihydrate*, Chem. Eng. Res. Des, 88 (2010) 10, 1372-1376.
- [Dav69] David, M., James, R., *Density, electrical conductivity, and vapor pressure of concentrated phosphoric acid*, J. Chem. Eng. Data, 14 (1969) 3, 380-384.
- [Dia13] Diallo, H., Baudry, M., Khaless, K., Chaufer, B., *On the electrostatic interactions in the transfer mechanisms of iron during nanofiltration in high concentrated phosphoric acid*, J. Membr. Sci., 427 (2013), 37-47.
- [Eag01] Evans Analytical Group, *ICP-OES and ICP-MS detection limit guidance*, 2014.
- [EII06] Elleuch, M., Amor, M., Pourcelly, G., *Phosphoric acid purification by a membrane*

- process: Electrodeionization on ion exchange textiles*, Sep. Purif. Technol., 51 (2006) 3, 285-290.
- [Fil74] Filatova, L., Galochkina, G., *Iron (III) complexes in concentrated orthophosphate solutions*, Russ. J. Inorg. Chem., 19 (1974), 1675-1677.
- [For38] Fortune, W., Mellon, M., *Determination of iron with o-phenanthroline: a spectrophotometric study*, Ind. Eng. Chem., Anal. Ed., 10 (1938) 2, 60-64.
- [Gal63] Galal-Gorchev, H., Stumm, W., *The reaction of ferric iron with ortho-phosphate*, J. Inorg. Nucl. Chem., 25 (1963), 567-574.
- [Gea01] GEA wash column, http://www.gea.com/global/en/binaries/TS04.052012-H%20hydrogen%20peroxide_tcm11-21889.pdf
- [Hei08] Heinrich, J., *Determination of crystallization kinetics using in-situ measurement techniques and model-based experimental design and analysis*, PhD Thesis, Martin-Luther-Universität Halle-Wittenberg, Shaker Verlag, Aachen, 2008.
- [Hel13] Helmdach, L., Schwartz, F., Ulrich, J., *Process control using advanced particle analyzing systems: application from crystallization to fermentation processes*, Chem. Eng. Technol., 36 (2013) 00, 1-9.
- [Hit01] Hitachi High-Technologies GLOBAL, <http://www.hitachi-hightech.com/global/products/science/tech/ana/icp/descriptions/icp-oes.html/>
- [Jan91] Jansen, H., *Examples and opportunities in industrial crystallization*, BIWIC 1991, ed. Ulrich, J., Verlag Mainz, Aachen, 1991, 58.
- [Jan94] Jansens, P., van Rosmalen, G., Chapter 6: *Fractional crystallisation* in *Handbook of crystal growth: 2 Bulk crystal growth*, ed. Hurlle, D., Elsevier Science B.V., Amsterdam, 1994, 287-314.
- [Jia11] Jiang, X., Zhao, Y., Hou, B., Zhang, M., Bao, Y., *Density, viscosity and thermal conductivity of electronic grade phosphoric acid*, J. Chem. Eng. Data, 56 (2011) 2,

205-211.

- [Jia12a] Jiang, X., Hou, B., He, G., Wang, J., *Falling film melt crystallization (I): model development, experimental validation of crystal layer growth and impurity distribution process*, Chem. Eng. Sci., 84 (2012), 120-133.
- [Jia12b] Jiang, X., *Research on melt crystallization preparation process of hyperpure phosphoric acid*. PhD thesis, Tianjin University, Tianjin, 2012.
- [Jon99] Jones, C., Larson, M., *Characterizing growth-rate dispersion of NaNO₃ secondary nuclei*, AIChE J., 45 (1999) 10, 2128-2135.
- [Ken66] Kenneth, W., *Generalized thermodynamic relationships*, Thermodynamics (5th ed.), NY: McGraw-Hill, Inc., New York, 1966.
- [Kim06] Kim, K., *Purification of phosphoric acid from waste acid etchant using layer melt crystallization*, Chem. Eng. Technol., 29 (2006) 2, 271-276.
- [Koo99] Koopman, C., *Removal of heavy metal and lanthanides from industrial phosphoric acid process liquors*, Separ. Sci. Tech., 34 (1999) 15, 2997-3008.
- [Lah90] Lahav, M., Leiserowitz, L., *Tailor-made auxiliaries for the control of nucleation, growth and dissolution of crystals*, in: *Industrial Crystallization*, ed. Mersmann, A., Munich, 1990, 609.
- [Led85] Leder, F., Park, W., Chang, P., Ellis, J., Megy, J., Hard, R., Kyle, H., Mu, J., Shaw, B., *New process for technical grade phosphoric acid*, Ind. Eng. Chem. Process Des. Dev., 24 (1985), 688-697.
- [Ma09a] Ma, Y., Zhu, J., Chen, K., Wu, Y., Chen, A., *Study on growth kinetics of phosphoric acid hemihydrate using FBRM*, J. Cryst. Growth, 312 (2009) 1, 109-113.
- [Ma09b] Ma, Y., Zhu, J., Ren, H., Chen, K., *Effects of Impurity Ions on Solubility and Metastable Zone Width of Phosphoric Acid*, Cryst. Res. Technol, 44 (2009) 12, 1313-1318.

- [Ma10a] Ma, Y., *The basic study of phosphoric acid crystallization purifying process*, PhD thesis, East China University of Science and Technology, Shanghai, 2010.
- [Ma10b] Ma, Y., Chen, K., Wu, Y., Zhu, J., Sheng, Y., *Study of phosphoric acid crystallization using a focused beam reflectance measurement method*, Cryst. Res. Technol., 45 (2010) 10, 1012-1016.
- [Mat86] Matsuoka, M., Fukushima, H., *Determination of solid-liquid equilibrium*, Bunri Gijutsu (Sep. Process Eng.), 16 (1986), 4-10.
- [Met01] METTLER TOLEDO, DE40 operation instructions, 1999.
- [Mig69] Mighell, A., Smith, J., Brown, W., *The crystal structure of phosphoric acid hemihydrate, $H_3PO_4 \cdot 1/2H_2O$* , Acta. Cryst., B25 (1969), 776-781.
- [Mor97] Moritoki, M., Nishiguchi, N., Nishida, S., *Features of the high-pressure crystallization process in industrial use*, Sep. Purif. Cryst., 667 (1997), 136-149.
- [Mos14] Mostafavi, M., Petersen, S., Ulrich, J., *Effect of particle shape on inline particle size measurement techniques*, Chem. Eng. Technol., 37 (2014) 10, 1721-1728.
- [Mul97] Mullin, J., *Crystallization*, Butterworth, Boston, 1997.
- [Nag89] Nagaoka, K., Makita, T., Nishiguchi, N., Moritoki, M., *Effect of pressure on the solid liquid-phase equilibria of binary organic-systems*, Int. J. Thermophys., 10 (1989) 1, 27-34.
- [Ngu08] Nguyen, T., Kim, K., *Kinetic study on hemipenta hydrate risedronate monosodium in batch crystallization by cooling mode*, Int. J. Pharm., 364 (2008), 1-8.
- [Oor00] van Oord-Knol, L., *Hydraulic wash columns solid-liquid separation in melt crystallization*, Ph.D. Thesis, TU Delft, Universal Press Science Publishers, Veenendaal, 2000.
- [Ouy09] Ouyang, Y., Tang, Z., Wang, C., *Progress in preparation and research of electronic*

- grade phosphoric acid*, Mod. Chem. Ind., 29 (2009) 3, 22-26.
- [Pho12] *Phosphoric acid market – Global industry analysis, size, share, growth, trends and forecast, 2013 – 2019*, Transparency Market Research, 2012.
- [Pho83] *Phosphoric acid manufacture using hydrochloric acid: An examination of the IMI process*, Phosphorous and Potassium, 125 (1983), 29-33.
- [Pos96] Poschmann, M., Ulrich, J., *Fractional suspension crystallization with additional purification steps*, J. Cryst. Growth, 167 (1996) 1-2, 248-252.
- [Ram54] Ram, A., Bose, A., Kumar, K., *Polarographic studies on ferriphosphate complexes in solution*, J. Sci. Ind. Res., 13B (1954), 217-219.
- [Rin67] Ringbom, A., *Les Complexes en Chimie Analytique*, Dunod, Paris, 1967.
- [Roh01] RoHS C-MET, ICP-OES instruction, <http://www.rohs-cmet.in/content/icp-oes>.
- [Ros25] Ross, W., Jones, R., Durgin, C., *The purification of phosphoric acid by crystallization*, Ind. Eng. Chem., 17 (1925) 10, 1081-1083.
- [San10] Sangwal, K., *On the effect of impurities on the metastable zone width of phosphoric acid*, J. Cryst. Growth, 312 (2010) 22, 3316-3325.
- [Sch02] Scholz, R., Ruemekorf, R., Verdoes, D., Niendoord, M., *Wash columns – state of the art and future developments*, Chem. Eng. Trans., 1 (2002), 1425-1430.
- [Sch08] Schrödter, K., Bettermann, G., Staffel, T., Wahl, F., Klein, T., Hofmann, T., *Phosphoric Acid and Phosphates*, Ullmann's Encyclopedia of Industrial Chemistry, Berlin, 2008
- [Sid73] Sidorenko, V., Zhuralev, E., Gordienko, V., Grineva, N., *Amperometric investigation of the complex formation by Fe (III) ions with phosphoric acid in perchloric acid solutions*, Russ. J. Inorg. Chem., 18 (1973), 670-672.

- [Sko03] Skoog, D., West, D., Holler, F., *Fundamentals of analytical chemistry* 8th ed., Brooks/Cole, Belmont, United States, 2003.
- [Slu87] van der Sluis, S., *A clean technology phosphoric acid process*, Ph.D. Thesis, University of Delft, Delft, 1987.
- [Smi09] Smith, A., Menzies, A. W.C., *The Solubilities of orthophosphoric acid and its hydrates. A new hydrate*, J. Am. Chem. Soc., 31 (1909) 2, 1183-1191.
- [Sol01] Solvay Fluor GmbH, Electronic wet chemicals.
- [Sol02] Solvay Fluor GmbH, <http://www.solvay.com/en/markets-and-products/featured-products/Electronic-Grade-Phosphoric-Acid.html>
- [Sol13] H₃PO₄-water vapor pressure data from Hirschberg and Innophos, personal information, Solvay Fluor GmbH, 2013.
- [Sol14] Personal information, Solvay Fluor GmbH, 2014.
- [Sul01] Sulzer wash column, <http://www.sulzer.com/en/Products-and-Services/Separation-Technology/Crystallization/Suspension-Crystallization>
- [Sun10] Sun, K., Minshull, T., *How to choose chelating agents in different areas*, The 30th China Cleaning Industry Association (CCIA) Annual Meeting, Beijing, 2010.
- [Tak83] Takegami, K., Morita, M., Nakamaru, K., Miwa, K., *Countercurrent, cooling crystallization and purification method for multi-component molten mixture*, EP 0105524 B1, 1983.
- [Tak84] Takegami, K., Nakamaru, N., Morita, M., *Industrial molten fractional crystallization*, in: *Industrial crystallization*, eds. Jancic S. and de Jong, E., Elsevier, Amsterdam, 1984, 143-146.
- [Thi83] Thijssen, H., Arkenbout, G., *Process for the continuous partial crystallization and the*

- separation of a liquid mixture*, US 4666456, 1983.
- [Thi85] Thijssen, H., Arkenbout, G., *Apparatus for concentrating a suspension*, US 4735781, 1985.
- [Til37] Tilton, L., Taylor, J., *The accurate representation of the refractivity and density of distilled water as a function of temperature*, J. Res. Natl Bur. Stand. Wash. 18 (1937), 205-214.
- [Tno01] TNO-Thijssen hydraulic wash column, <https://www.tno.nl/en/focus-area/industry/sustainable-chemical-industry/efficient-processing/ultrapurification/>
- [Toy94] Toyokura, K., Fukuda, M., Nishiguchi, N., Moritoki, M., *Effect of pressure on solubility of DL-mandelic acid in water*, Kagaku Kogaku Ronbunshu, 20 (1994) 2, 156-161.
- [Ulr02] Ulrich, J., Bülau, H., *Melt crystallization*, in: *Handbook of Industrial Crystallization*, eds. Myerson, A., Butterworth-Heinemann, Boston, 2002, 161-179.
- [Ulr89] Ulrich, J., *Growth rate dispersion – A review*, Cryst. Res. Technol., 24 (1989) 3, 249-257.
- [Ver02] Verdoes, D., Schneiders, L., Nienoord, M., Fokker, P., *Efficient separation and washing of crystals and other solids*, Chem. Eng. Trans. 1 (2002), 1431-1436.
- [Ver09] Verdoes, D., Bassett, J., *The TNO hydraulic wash column: high purity products by crystallization*. Speciality Chemicals Magazine, 29 (2009) 9, 32-35.
- [Vor72] Vorstman, M., Thijssen, H., *Stability of displacement of viscous aqueous solutions by water in a packed bed of ice crystals*, Proc. Int. Symp. on Heat and mass transfer problems in food engineering, Wageningen, 1972, D4-1-22.
- [Wah80] Wahba, C., Hill, K., More, A., *Phosphoric acid: outline of the industry*, The British Sulphur Corporation, London, 1980.
- [Wan12] Wang, B., Li, J., Qi, Y., Jia, X., Luo, J., *Phosphoric acid purification by suspension*

- melt crystallization: parametric study of the crystallization and sweating steps*, Cryst. Res. Technol., 47 (2012) 10, 1113-1120.
- [Wil85] Wilhelmy, R., Patel, R., Matijevic, E., *Thermodynamics and kinetics of aqueous ferric phosphate complex formation*, J. Inorg. Chem., 24 (1985), 3290-3297.
- [Wyn03] Wynn, E., *Relationship between particle-size and chord-length distributions in focused beam reflectance measurement: stability of direct inversion and weighting*. Powder Technol., 133 (2003) 1, 125–133.
- [Yu06] Yu, Z., Jiang, G., *Analytical chemistry experiment*, Chemical Industry Press, Beijing 2006.

Statement of Authorship

I declare that I have written this document on my own. It is a compilation of the results of work carried out by my own or by students under my supervision. The used resources and tools or previously cited information have been distinguished by quotation marks.

Halle (Saale), 19.05.2016

Haihao Tang

Curriculum Vitae

Haihao Tang

Date of birth: 14.04.1988 in Wenzhou, China

Nationality: Chinese

Education

10/2012-now	PhD candidate at Martin Luther University Halle-Wittenberg Halle (Salle), Germany
04/2011-10/2012	Master of Biomedical Engineering at Martin Luther University Halle-Wittenberg Halle (Saale), Germany
10/2010-04/2011	Master of Biomedical Engineering at FH Anhalt Köthen, Germany
09/2006-06/2010	Bachelor of Chemical Engineering and Technology at Ocean University of China Qingdao, China

Publications

H. Tang, J. Ulrich: *Permeability, purity and yield in crystal beds*: proceeding in the journal of Chemical Engineering and Technology, 2016.

H. Tang, J. Ulrich: *Permeability of the crystal bed*: in BIWIC 2015, 22nd International Workshop on Industrial Crystallization, Daejeon, South Korea, eds.: K. Kim and K. Lee, Hanbat National University, South Korea, 9.-11.9.2015, 182-189.

H. Tang, J. Ulrich: *Phosphoric acid purification by suspension crystallization*: presentation in the conference of Fachausschuss Kristallization, Magdeburg, 18.-20.03.2015.